Summer 2011

The effects of quasi-steady loading on a virtual spur gear model

Michael Patrick Kelso
University of Iowa

THE EFFECTS OF QUASI-STEADY LOADING ON A VIRTUAL SPUR GEAR MODEL

by

Michael Patrick Kelso

A thesis submitted in partial fulfillment
of the requirements for the Master of
Science degree in Mechanical Engineering
in the Graduate College of
The University of Iowa

July 2011
Thesis Supervisors: Professor Emeritus Lea-Der Chen
Professor Patrick Barry Butler

Graduate College
The University of Iowa
Iowa City, Iowa

CERTIFICATE OF APPROVAL

_____

MASTER'S THESIS

_____

This is to certify that the Master's thesis of

Michael Patrick Kelso

has been approved by the Examining Committee
for the thesis requirement for the Master of Science
degree in Mechanical Engineering at the July 2011 graduation.

Thesis Committee: _____
Lea-Der Chen, Thesis Supervisor

_____
Patrick Barry Butler, Thesis Supervisor

_____
Shaoping Xiao

To my beautiful wife Jennifer whose support has been unwavering and to my son Jack for making life far more interesting and enjoyable

ACKNOWLEDGMENTS

The author would like to thank a number of people for their assistance with this thesis. First, thanks must be given to Professors Lea-Der Chen and Patrick Barry Butler for their guidance and support as co-advisors. Additional thanks must be given to Professor Chen for his help in translating Yurong Cai's Japanese dissertation work, which was generously lent to the author. Also, the author would like to thank the thesis defense committee, consisting of the two aforementioned professors as well as Professor Shaoping Xaio, for taking the time to attend and evaluate the thesis and defense.

The author would also like to extend thanks to his friends and family for their unwavering support and critiques of the thesis, especially Benjamin Feltz, Tim Kallaus, and Jonathan Sticther. Also, a much needed thanks is extended to Marcio Tokita at LMS International for providing critical modeling support and additional translations of Japanese technical literature. Lastly, the author would like to extend thanks to the late scientist Carl Sagan for providing him with continuous inspiration and reminding him that the pursuit of knowledge is the key to understanding.

ABSTRACT

With the projected growth of wind energy in the United States expected to account for 20% of the energy portfolio by 2030, it can be expected that wind turbines will not only increase in number, but also in size. This increase in size implies that internal components, such as the gearbox, will also increase to handle the higher loads. And given the high failure rates for gearbox components already in existence, one could expect more failure if nothing is done to improve reliability. It is well known that wind loading is not constant, rather it is random and ultimately causes fatigue loading. This thesis is concerned with studying what the effects of dynamic loading are on a smaller gear system. It is assumed the findings of this study can be scaled to a larger wind turbine system. A simple spur gear pair is first simulated at constant loading to establish a baseline and then run with a sinusoidal input with differing amplitudes and frequencies. The hypothesis is that by varying the amplitude and frequency, the responses for gear contact force and input and output shaft torques will also vary. And if these variations are noted, then conclusions may be drawn as how the frequency and amplitude influence the system. After which, it may then be correlated to a wind turbine system. Knowing what affects the frequency and amplitude have on a smaller system may help to establish guidelines.

For this model, mechanical simulation software is used to build a multibody dynamics model of a spur gear system with flexible shafts. Using known wind data obtained near Amarillo, TX, a matrix of possible frequencies and amplitudes for a sinusoidal input are implemented and the solutions compared to those at constant loading. It was found that the system responded similarly regardless of input, showing RMS values for accelerations of approximately 50 m/s^2, gear contact forces of 520 N, input shaft torques of 42 Nm, and output shaft torques of 78 Nm. This behavior is not expected is most likely due to insufficiencies in the assumptions made to construct the model.

TABLE OF CONTENTS

LIST OF TABLES

LIST OF FIGURES

LIST OF ABBREVIATIONS

MW—megawatt

MWh—megawatt-hours

DOE—Department of Energy

MBD—multibody dynamics

LSS—low speed shaft

WTAMU—West Texas A&M University

RPM—rotations per minute

MBS—multibody system

DOF—degree of freedom

2D/3D—two and three dimensional

CG—center of gravity

MOI—moment of inertia

EOM—equation of motion

FEA—finite element analysis

RSDA—rotational spring-damper-actuator

DAE—differentiable algebraic equation

VL—Virtual.Lab

GUI—graphical user interface

ODE—ordinary differential equation

PECE—predict-evaluate correct-evaluate

CAD—computer aided design

brk—bracket joint

rev—revolute joint

RMS—root-mean square

FFT—fast Fourier transform

LIST OF SYMBOLS

A [RPM]: Sinusoidal input function amplitude

A_b [m^2]: Swept area of blades

a_{rms} [RPM]: Calculated RMS values for acceleration, force, and torque

c [kg/s]: Damping constant

$\boldsymbol{c(q,t)}$: Constraints vector as a function of generalized coordinates and time

$\boldsymbol{C}_g$: Generic damping matrix for a second-order differential equation

$\boldsymbol{C}_q$: Jacobian matrix

d [m]: Shaft diameter

E [J]: Energy in wind

$\boldsymbol{F(t)}$: Generic forcing function

G [N/m2]: Modulus of rigidity

h: Discrete number of divisions for PECE method

I_x, I_y, I_x [kg m^2]: Mass moment of inertias for Cartesian space

I_u: Turbulence intensity factor

J [kg m^2]: Polar mass moment of inertia

k [N/m]: Stiffness constant

$\boldsymbol{K}_g$: Generic stiffness matrix for a second-order differential equation

L [m]: Shaft length

m: Mobility, number of degrees of freedom in system

$\boldsymbol{M}$ [kg, kg m^2]: Mass matrix composed of acceleration coefficients (mass and inertia)

$\boldsymbol{M}_g$: Generic mass matrix for a second-order differential equation

n: Number of bodies in system

n_c: Summed number of constraints in system

n_t: Number of data points used in RMS calculation

P_{wind} [W]: Power available in the wind

$\boldsymbol{q}$: Generalized coordinates vector

$\boldsymbol{q}_c$: Constraint forces vector

$\boldsymbol{q}_d$: Second derivative of the constraints equation

$\boldsymbol{q}_e$: External forces vector

$\boldsymbol{q}^i$: Generalized coordinates vector for the ith body

r_1, r_2 [m]: Radii of gears

$\boldsymbol{r}^i$ [m]: Position vector from global origin to ith body origin

$\boldsymbol{r}_x^i$, $\boldsymbol{r}_y^i$, $\boldsymbol{r}_z^i$ [m]: Cartesian coordinate vectors for the ith body

t [s]: Time

T [N m]: Shaft torque

t_o [s]: Offset time used for normalization

t_z [s]: Period of vibratory response

U [m/s]: Longitudinal wind velocity

$\bar{U}$ [m/s]: Average longitudinal wind velocity

$\bar{U}(z_{ref})$ [m/s]: Average longitudinal wind velocity at a reference height above ground

$\bar{U}(z)$ [m/s]: Average longitudinal wind velocity at a specified height above ground

x: PECE method independent variable

$\boldsymbol{x}$: Generic position vector

$\dot{\boldsymbol{x}}$: Generic velocity vector

$\ddot{\boldsymbol{x}}$: Generic acceleration vector

X [RPM]: Mean shaft angular velocity

x^i [m]: global x-coordinate on the ith body

x': Normal distribution random variable

y: PECE method dependent variable

y^i [m]: global y-coordinate on the i^{th} body

z [m]: Height above ground

z_{ref} [m]: Reference height above ground

z_0 [m]: Surface roughness factor

ε: Generic variable of calculated acceleration, force, and torque quantities

θ^i [rad]: Local rotation of the i^{th} body

θ_x^i, θ_y^i, θ_x^i [rad]: Rotation angles for the i^{th} body

$\boldsymbol{\lambda}$: Lagrange multiplier vector

μ': Normal distribution mean

π: Ratio of circle circumference to diameter (3.14159)

ρ [kg/m^3]: Density of air

σ_a [N/m^2]: Amplitude stress for cyclic loading

σ_m [N/m^2]: Mean stress for cyclic loading

σ_{max} [N/m^2]: Maximum stress for cyclic loading

σ_{min} [N/m^2]: Minimum stress for cyclic loading

σ_u [m/s]: Standard deviation of wind velocity

σ': Normal distribution standard deviation

ϕ [rad]: Shaft angle of twist

ω [rad/s]: Sinusoidal angular frequency

ω_1, ω_2 [rad/s]: Angular velocity

Ω [RPM]: Angular velocity of input shaft

CHAPTER 1

INTRODUCTION

1.1 Background

The purpose of this study is to analyze the effects of dynamic input to a simple gear train system and then correlate those findings to a typical wind turbine gear train system. The study of wind turbine gearbox dynamics is currently of great importance for a couple of reasons: 1) increased turbine component sizes and production to meet demand, and 2) durability of the system as a result of dynamic loading (Sheng et al., 2009). The compounded effect of higher and more variant loading on internal components of a wind turbine, such as the gear train, will therefore become a topic of increased significance as an increased number of turbines are deployed in areas of higher turbulence wind.

An increase in demand is instigated from a national push from the US government to have 20% of domestic energy generated come from wind power alone. This translates to having an installed capacity of 300,000 megawatts (MW) for a projected annual consumption of 5.8 billion megawatt-hours (MWh) in only nineteen years (DOE, 2008). And, as of December 31, 2010, there are only 40,180 MW of installed capacity (DOE, 2010). This will require a surge in turbine production and innovation to meet the demand accordingly. The innovation will come into play by designing larger turbines as it is well established that the power extracted by a turbine is proportional to the square of rotor diameter. Therefore, to get the most out of a single turbine, the overall size of, and the components within, will most likely increase to accommodate the increased loads.

Dynamic loading is known to be detrimental in mechanical systems because it tends to introduce vibratory responses and initiate fatigue, both of which can significantly reduce the life expectancy of the system. There is much variation in wind velocity in any given time domain and this variation provides the dynamic loading input for the system. And since the power available in the wind is proportional to the cube of its velocity, it

can be expected that turbines will be located in areas of higher velocities to maximize power generation and return on investment.

Because dynamic loading is prevalent in a wind turbine system, and because the negative effects are sometimes severe, it is of great importance to understand how they are developed and distributed throughout the system. For this study, multibody dynamics (MBD) is used to construct a reduced model of relatively low complexity and subjected to both constant and quasi-steady. The effects of steady state are used to validate experimental results with a virtual model.

1.2 Brief History of Gears

There are many historical references to tools and machines being used in early civilizations to enhance the quality of life for the inhabitants of each contemporary period. The span ranges from crude to sophisticated, sticks and stones to modern electronics. And although there are many inventions which have had a great impact, only a few have the honor of standing out among the rest. One such invention was the gear because it, in one form or another, is still in use today. In the simplest of terms, two gears mesh together and form a gear pair, which is a system that transmits mechanical motion from one axis of revolution to another. It can be said that gears are simple in concept and design, but powerful and versatile in application. They have effectively altered the existence of mankind and helped to usher in the dawn of mechanical engineering many centuries ago. And although not much has changed in the concept of gear transmission, the methods used today employ greater sophistication and more intimate knowledge of gear dynamics than they did long ago.

The first gears were nothing more than wooden wheels with pegs extending out from the circumference. The pegs would come into contact with another wooden when which had internal dowels and were perpendicular to the pegs in the other gear when enmeshed as shown in Figure 1-1. This type of arrangement allowed for motion to be

transmitted from perpendicular or parallel arrangements. For example, they worked particularly well in early waterwheel applications.

These early gears were put to great use in grain mills because wind and water power could now be effectively harnessed and transmitted. The wind or water would drive an input shaft, and gears would transmit the power to the grinding stones as shown in Figure 1-2. And because of the fundamental law of gears, shown in Equation (1-1), the proper speed ratios could easily be reached by appropriately sizing the gears, thus allowing mills to be effectively used in a variety of locations around the world.

$$r_1\omega_1 = r_2\omega_2 \tag{1-1}$$

In Equation (1-1), r_1 and r_2 are the radii of the first and second gears, and ω_1 and ω_2 are their respective angular velocities.

The first great impact on civilization is realized when one considers that grain could now be easily processed without human or animal power. Up until gears, grain mills had relied mostly on animal power as it was the most reliable method (Rosenberg, 1992). Reducing the amount of labor it took to make flour from grinding grain allowed for greater advancement because humans were now free to engage in other studies and laid the foundation for the commencement of the industrial revolution. It was in this period that mechanization occurred on a scale not seen before and introduced far more complexities in gear design due to the increased loads of steam engines. These were far more powerful than anything yet experienced and the gears needed to withstand the punishment.

To accommodate the increase in power, gear design became better and more complex. The steady improvement in gear design came as a result of the need to have cheaper, quieter, lighter, and more powerful machinery (Dudley, 1954). This cause and effect relationship between machine power and gear advancement continues today. Complexly designed steel gears are used in all types of application from simple pocket

watches to vehicle drive trains to wind turbine gearboxes. And today, just as it was back then, loads have driven the need to develop better, more reliable gears. This is especially true in most modern wind turbine where there are many gear failures (Musical, 2000). However, this is not due only to the increase in magnitude, but also from transient wind loads (Mucke, 2011). As will be discussed in the following section, variability in loading affects the system in a way which constant loading does not.

1.3 Constant and Variable Loading

On a fundamental level, there are two basic types of loads in engineering mechanics; those that are constant (static) and those that vary with time (dynamic). Knowing what type of load a mechanical apparatus will be subjected to is of the utmost importance for design consideration. This is because static loads pose little to no design challenges because mechanical systems respond well to this type of load, if appropriately designed, because once the load is applied, the system only has to bear it. Dynamic loads, on the other hand, are of great importance because these types of loads cause vibratory responses and induce fatigue within the system which may cause premature failure.

Fundamentally, dynamic loading subjects mechanical members to stresses which vary, either periodically or randomly, with time. This is referred to as cyclic loading and is defined by calculating the maximum and minimum stresses (σ_{max} and σ_{min}). These are the stress limits of what a member is subjected to during the loading cycle and are usually some combination of axial, bending, and torsional stresses. Figure 1-3 shows a simplified diagram of the stresses present for one cycle. σ_m and σ_a are the mean and amplitude stresses, respectively, and are calculated using the max and minimum stresses with Equations (1-2) and (1-3).

$$\sigma_m = \frac{\sigma_{max}+\sigma_{min}}{2} \tag{1-2}$$

$$\sigma_a = \left|\frac{\sigma_{max} - \sigma_{min}}{2}\right| \quad (1\text{-}3)$$

A simple example which illustrates the devastating effects of cyclic loading is the back and forth bending of a common paper clip. After only a few cycles, the paperclip fractures into two pieces. This phenomenon can be analogous to larger, more complex mechanical systems and needs to be considered in the design.

1.4 Wind Speed and Variability

On a basic level, wind is generated by the sun. As the Earth rotates, only one hemisphere is exposed to the incoming solar radiation, leaving the other hemisphere exposed to darkness. In addition, the earth is differentially heated due to the angle of incidence, atmospheric variability, and terrain differences. These create a difference in temperature and pressure, and, like any other natural system, equilibrium is sought. Thus, the wind blows around the world in a quite predictable pattern, like the trade winds. Of course, there are other influences such as the Coriolis Effect and surface roughness, but wind can be essentially thought of as an indirect form of solar energy (Burton et al., 2001).

But, unlike solar energy, which is moderately predictable depending on the region, wind energy has more variability. What is perhaps most interesting is that wind varies in both space and time and over a wide variety of ranges. Depending on the region, wind typically ebbs and flows in a chaotic fashion fitting well to a Weibull distribution for annual data samples. This fluctuation in wind speed and direction directly correlates to the dynamic loads experienced by the gear train of a wind turbine. Although there are many control systems which seek to negate some of the dynamic effects, they cannot eliminate all as illustrated in Figure 1-4. Therefore, understanding what the mechanical responses are to variable input is paramount when considering wind turbine gearbox design.

What compounds the issue of wind speed variability is that the power available in the wind is proportional to the cube of wind velocity. This relationship is shown in Equation (1-4).

$$P_{wind} = \frac{1}{2}\rho A U^3 \tag{1-4}$$

where, ρ is the density of air, A is the swept area of the blades, and U is the instantaneous wind velocity. Thus, it can be seen that it is more advantageous to place a turbine in an area which sees higher magnitudes of wind velocity to maximize power output. However, the trade off is that now there are higher loads and it is subject to greater variation. And, as discussed earlier, it is this variation in wind loading that initiates cyclic loading on the internal components.

Energy from wind loading on the blades is transferred all the way through the system to the generator. The loads which are transferred are based on fundamental aerodynamics and mechanical system analyses. As wind flows over the blades, which act as airfoils, lift and drag forces are created. These forces induce torque and bending moments on the shaft as well as transverse and longitudinal forces. The loads are then transferred to the gear train which turns the generator. If wind velocities were relatively constant, the variation in loading would be minimal. However, wind is not always steady and as such produces fluctuating loads.

Wind speed and variation depend on a number of factors which include, but are not limited to: height above ground, terrain topology, geographic location, vegetation type and coverage, and urban or rural environments (Burton et al., 2001). These influences cause the wind to behave in a manner similar to fluid flowing over a flat plate. At the boundary layer, there is a no slip condition and the result is a velocity profile which grows logarithmically as seen in Figure 1-5. As the height above the plate (ground) increases, wind velocity increases until it reaches the free stream velocity. This is an experimentally derived gradient and all fluids satisfy this condition (Munson et al. 2006).

The slope of the profile depends on the roughness of the surface over which the fluid is flowing and is described by Equation (1-5).

$$\bar{U}(z) = \bar{U}(z_{ref}) \left[\frac{\ln(z/z_0)}{\ln(z_{ref}/z_0)} \right] \quad (1\text{-}5)$$

where $\bar{U}(z_{ref})$ is the average velocity at a specified point from the ground, z is the height above ground for which the speed is desired, z_{ref} is the reference height for the $\bar{U}(z_{ref})$, and z_0 is the surface roughness length. This is an experimentally derived value and some typical values are shown in Table 1-1.

Due to surface roughness and other predominant atmospheric conditions present, typical wind profiles are not laminar. Instead, they are more likely to be turbulent. This is illustrated in Figure 1-6 where the flow is laminar at first and then transitions into turbulent. Turbulent wind flow, or atmospheric turbulence, is on a very fast time scale, which is usually less than 10 minutes (Burton et al., 2001). And it is atmospheric turbulence which specifically introduces cyclic loading into a turbine system.

To illustrate that wind variation is an actual phenomenon, data are needed to build curves which show the wind speed versus time. One such data collection site is a 50 meter high tower near Amarillo, Texas. It records an assortment of data, including wind speed, in 10 minute increments. Using the data collected, one can construct a curve for the wind speed variation over any period of time greater than 10 minutes. Figure 1-7 shows the variation in wind speed over the period of one day. It can be seen that the average velocity for that day was around 9.77 m/s with a variation from 2 m/s to 20 m/s. This is a powerful illustration because it shows that a wind turbine gearbox, like the one pictured in Figure 1-8, is indeed subject to a fluctuating input and thus cyclic loading.

Table 1-1: Typical Surface Roughness Lengths.

Type of terrain	**Roughness length z_0 (m)**
Cities, forests	0.7
Suburbs, wooded countryside	0.3
Villages, countryside with trees and hedges	0.1
Open farmland, few trees and buildings	0.03
Flat grassy plains	0.01
Flat desert, rough sea	0.001

Source: Burton, T., Sharpe, D., Jenkins, N., and Bossanyi, E. (2001) *Fundamentals of Wind Turbines*, John Wiley and Sons Ltd. West Sussex, England.

Figure 1-1: Model of basic, early gears.

Source: Williams, R. "Solar One, to International Space Station; Move over I'm coming into Near Orbit." Engineering.com, June 6, <http://www.engineering.com/Library/ArticlesPage/tabid/85/articleType/ArticleView/articleId/704/Solar-One-to-International-Space-Station-Move-over-Im-coming-into-Near-Orbit.aspx>

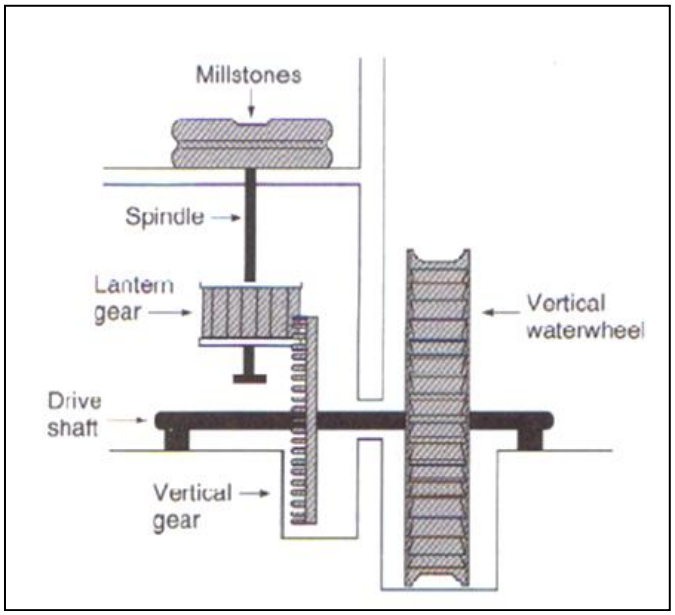

Figure 1-2: Illustration of a gristmill waterwheel system.

Source: Schobert, H. H., (2002) *Energy and Society: An Introduction*. Tayor & Francis. New York, NY.

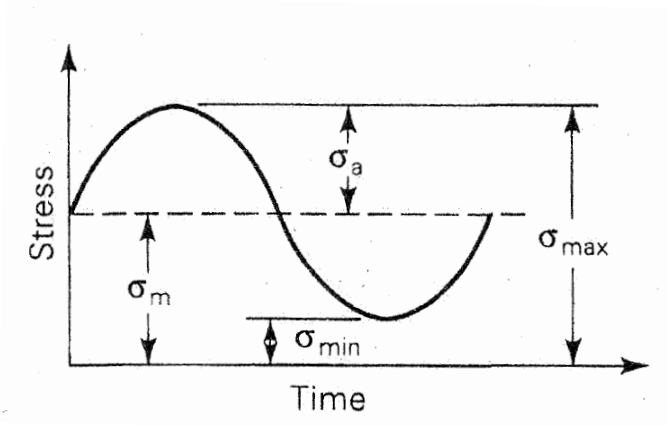

Figure 1-3: Generic plot of stress vs. time for a fluctuating load.

Source: Ugural, A. C., Fenster, S. K., (2003) *Advanced Strength and Applied Elasticity: Fourth Edition.* Pearson Education Inc. Castleton, New York

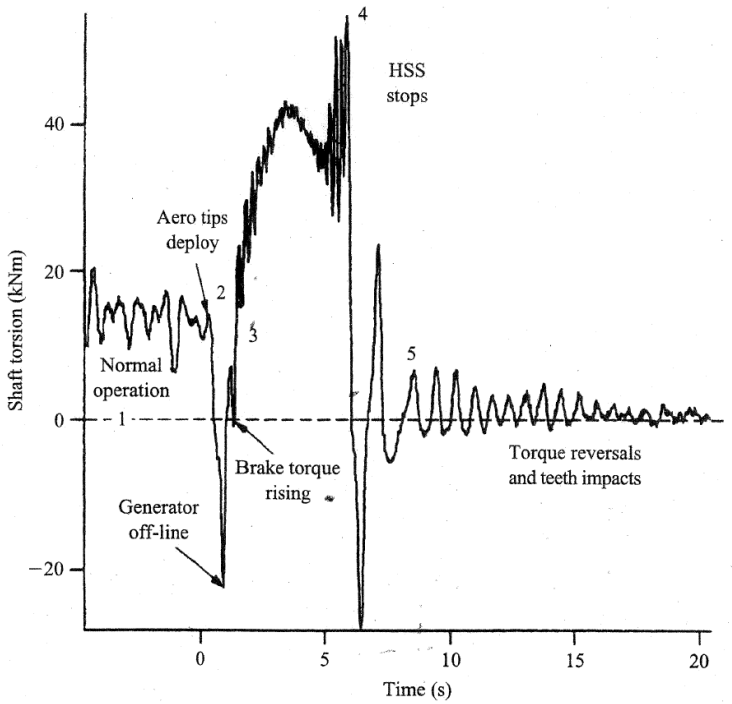

Figure 1-4: Plot of low-speed shaft (LSS) during breaking on a normal shut down.

Source: Burton, T., Sharpe, D., Jenkins, N., and Bossanyi, E. (2001) *Fundamentals of Wind Turbines*. John Wiley and Sons Ltd. West Sussex, England.

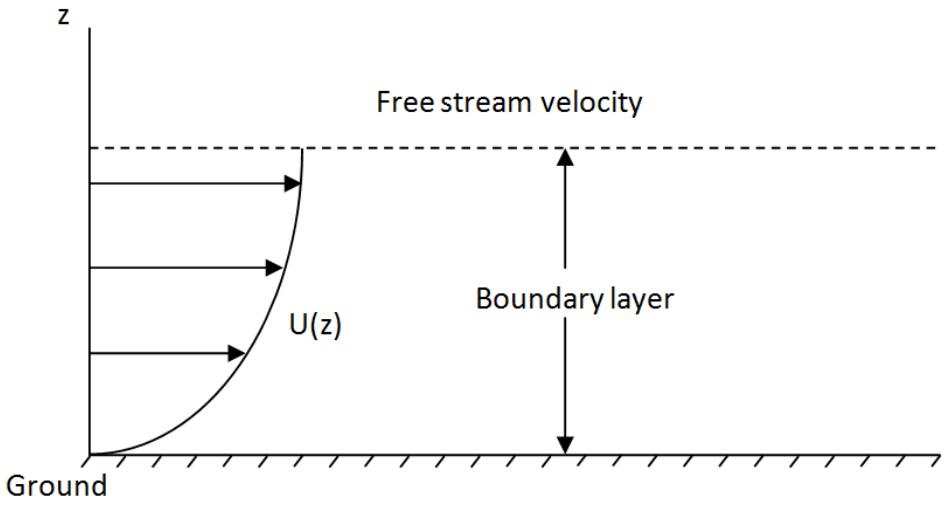

Figure 1-5: Logarithmic wind velocity profile of wind flowing over a flat surface.

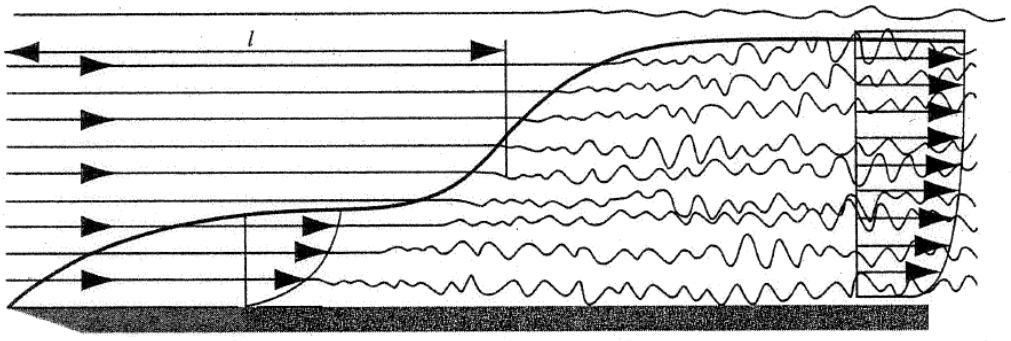

Figure 1-6: Laminar and turbulent boundary layers.

Source: Burton, T., Sharpe, D., Jenkins, N., and Bossanyi, E. (2001) *Fundamentals of Wind Turbines*. John Wiley and Sons Ltd. West Sussex, England.

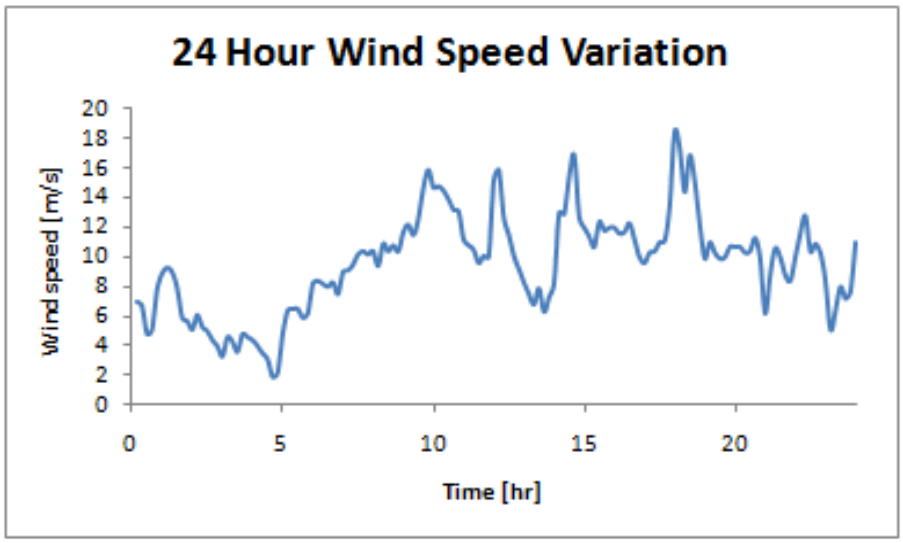

Figure 1-7: Plot of wind speed vs. time over a 24 hour period. Data taken from anemometer tower located near Amarillo, TX.

Source: West Texas A&M University (WTAMU), Killgore Research Center. 2010. Alternative Energy Institute. <http://www.windenergy.org/datasites/>

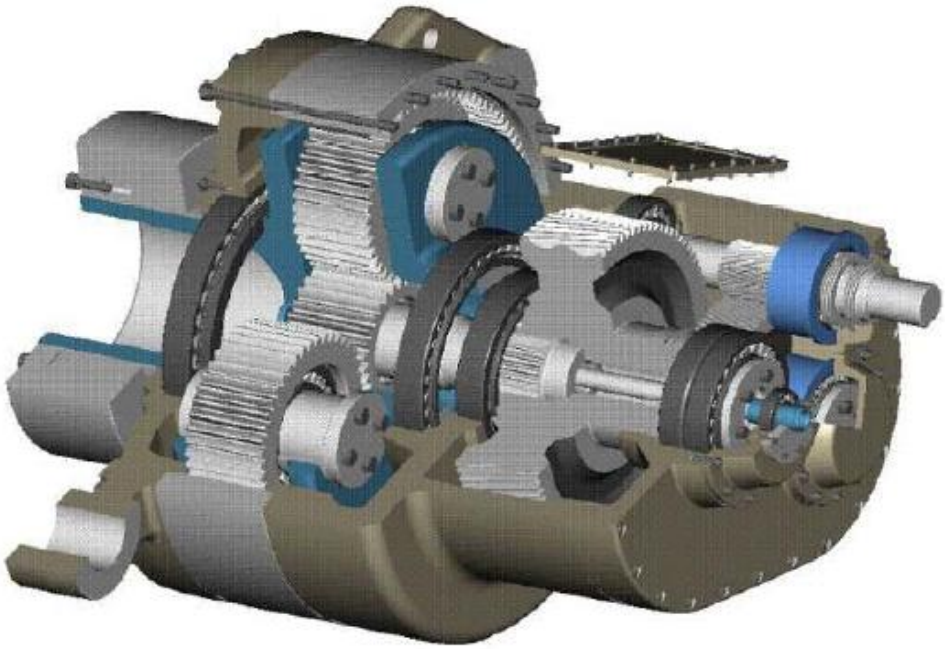

Figure 1-8: Picture of a planetary gearbox for a wind turbine.

Source: Musical, W., Butterfield, S., McNiff, B. May 2007. "Improving Wind Turbine Gearbox Reliability." Conference Paper, NREL/CP-500-41548.

CHAPTER 2

METHODOLOGY

Model building consists of several parts and is by its very nature an iterative process. Methodology is needed to make clear some assumptions made as well as provide an outline of model construction. The reason is two-fold as it helps the builder to establish correlations when constructing the model and helps convey the necessary information to those using the model. Without such a road map, much ambiguity and misinformation could result.

2.1 Modular Approach

A wind turbine is a large structure composed of many different systems and it is convenient to break it down into smaller pieces for the purpose of analysis. For mechanical motion analysis, a turbine can be segmented into three constituent parts: blade aerodynamics, mechanical power transmission, and electrical generation. All three affect, in some manner, the internal dynamics of the overall system. For this thesis, mechanical power transmission, specifically gearbox dynamics, will be studied. However, the gear system is not that of an actual wind turbine. Instead, a smaller system consisting of two spur gears will be used. The intention is that the response of varying the input load to the smaller system will be analogous to a larger, more complex gear system, such as those found in most commercial wind turbines.

There are a few reasons for pursuing this method. First, obtaining accurate data for real wind turbine systems is difficult and sometimes impossible for proprietary reasons. Secondly, having a larger system implies that the virtual model is more involved and far more complicated, which is more computationally expensive. And lastly, using a simpler model is a more logical first step to take when attempting to validate experimental results virtually.

Having noted this, it must be said that by breaking the system into smaller pieces, to maintain continuity, the inputs and outputs of the gear system need consideration. During operation, the three subsystems all work in unison to efficiently extract energy from the wind, and more importantly, they all share feedback with one another. For example, blades can pitch to reduce generator output, or a generator can increase magnetic flux and so create a higher torque load on the gearbox. Therefore, to establish and maintain a correlation to a larger gear system, the input and output to the simple spur gear model will stay within a set range of values to be defined in later chapters.

2.2 Experimental Model and Model Validation

The simple spur gear system comes from an experiment done at Tokyo Institute of Technology by researcher Cai. In his experiment, two spur gears are enmeshed and have flexible shafts which connect the gears to an AC motor for input, and a powder brake to provide counter torque. A schematic of this experimental set up is shown in Figure 2-1 (Cai, 1992). The wind turbine analogy is that the motor represents system input from the blades responding to wind flow and the powder brake represents the counter torque provided by a permanent magnet generator.

For the experiment, the motor was driven at constant angular velocities of 200 rotations per minute (RPM) and 300 RPM for two distinct runs. In each experiment, the brake provides a counter torque of 49 Nm. Accelerometers are attached to the peripheries of the drive and driven gears and measure the torsional vibrations of the system during operation. Figure 2-2 shows the results of the experiments as well as the predicted responses according to a linear and nonlinear gear contact equations. These are the results that the virtual model seeks to reproduce. Once the virtual results approximately resemble the experimental results, model validation is complete.

2.3 Dynamic Loading

Once model validation is established, simulations with dynamic input can be computed. Dynamic loads in wind turbine systems arise from the blades responding to atmospheric turbulence. For the virtual model to read this type of input would entail generating a wind load profile based on the data gathered from a wind site. However, building such an input curve creates another path of exploration and is not within the scope of this thesis.

Instead, to represent this variation in loading, a quasi-steady, sinusoidal input for shaft RPM is used. The sine wave provides a mathematical relationship which links the mean value (X), amplitude (A) and frequency (ω) of the wave, which are considered the control variables. By changing each of these variables slightly, the behavior of the system will change. And, by noting the different states of the control variables, the corresponding changes to the system's response can be attributed accordingly. This is represented by Equation 2-1 (Sheinman, 1992).

$$\Omega = A\sin(\omega t) + X \tag{2-1}$$

To liken the quasi-steady input to true transient input, a set of wind turbulence parameters is needed. The turbulence intensity factor, which is a measure of the overall turbulence of the wind, relates the longitudinal mean wind speed to the standard deviation of the variation in that wind speed, and is given in Equation 2-2.

$$I_u = \frac{\sigma_u}{\bar{U}} \tag{2-2}$$

where $\bar{U}$ is the mean wind velocity, σ_u is the standard deviation, which is roughly Gaussian, and the subscript u represents the longitudinal direction. Therefore, if the mean velocity and turbulence intensity factors are known, standard deviation of the wind profile can be approximated. It must be noted that there is much variation in turbulence intensity depending on what standard is used. Using the value of 9.77 m/s for average velocity (from chapter 1.4) and an approximated range of 0.16 to 0.18 for turbulence

intensity, the corresponding standard deviations from that mean are approximately in the range of 1.56 m/s to 1.77 m/s, respectively (Burton et al., 2001). And recalling that the power available in the wind is proportional to the cube of velocity, these variations correlate to a power multiplication factor range of 3.8 to 5.5.

This can be made analogous to the amplitude of the sine wave. If it is assumed that the fluctuation in wind speed creates torque loads which are present in the system, the change in amplitude for the sine wave will replicate this response. Therefore, using a correlation to turbulence intensity of 16, 17, and 18%, the amplitude will change at 3.8, 4.6, and 5.5% from the mean for three different tests. See Figure 2-3 for a flow chart depicting the process of correlating wind turbulence intensities to sinusoidal amplitude inputs.

To replicate the frequency of turbulence, it is necessary to look at the frequency content of the wind speed, which is known as the turbulence spectrum and is shown in Figure 2-4 (Burton et al., 2001). The range roughly consists of 0.001 to 1 Hz, depending on which standard is used. Since the range is quite broad, and since it is desired to have at least one cycle for the input, the frequencies chosen for this thesis are 0.5, 0.1, and 1 Hz.

Now that two of the three control parameters have been related, the third must follow. The above ranges for frequency and amplitude have direct correlations to wind speed. Therefore, it should follow that the mean wind speed of 9.77 m/s used in the above calculations be used to represent a constant shaft speed. And since the model responds well to an input of 200 RPM, this value can be taken as the mean angular velocity for the input.

It should be noted that the assumptions made in this section are done to simplify very complex phenomena and cannot truly represent the actual physics of wind turbine systems. However, doing so does allow for conclusions to be drawn which may be useful if the assumptions are within realistic boundaries.

2.4 Multibody Dynamics

Dynamics is a branch of engineering which deals with the physics of bodies in motion, where a body is loosely defined as a collection of particles which has mass and occupies space (Ohanian, 1989). According to Shabana (2010), modern mechanical systems of interest are linked together via joints and forces and are referred to as multibody systems (MBS). These joints eliminate various degrees of freedom (DOF) from the system depending on the type of joint. The DOF for a system are defined as the number of independent coordinates needed to drive the system (Shabana, 2010). They, in essence, describe the possible path, or paths, of motion for a body which is in either two or three dimensional (2D, 3D) space.

A MBD approach is useful for determining variables of interest like positions, velocities, accelerations, forces, and moments for the bodies which comprise the MBS. For many dynamic systems, a body is thought to be rigid, meaning that there is no deformation or, more specifically, there are no changes in position of any two points located on that body when forces are applied (Beer, et al., 1988). Furthermore, this collection of particles which makes up the body behaves in such a manner as to have a single point of concentrated mass where the action may take place and is called the center of gravity (CG). It is also about this point that the principal moments of inertia (MOI) act.

These three quantities are important because they are the parameters needed to describe the physics of motion for rigid bodies. If these parameters are known, then the dynamic equations of motion (EOM) may be constructed and assembled so that a solution may be computed, regardless of part geometry. However, it should be noted that it is possible to leave the realm of rigid body mechanics and instead use flexible bodies. This requires more intense formulation and the addition of finite element analysis (FEA) and is beyond the scope of this thesis.

To construct a kinematically constrained MBS, bodies must be combined with joints. When two or more bodies are linked together, the joint type takes away specific

DOF so that the appropriate motion is achieved. Consider two bodies linked together using a revolute joint, which removes all DOF but the rotation around one axis. Assume that the first body is fixed and cannot move at all. The second body, which is connected with a revolute, would be free to only rotate around the first body. Now replace the revolute with a translational joint, which eliminates all but one translation along a specified axis. The motion of the second body now will only move in a straight line along the chosen axis relative to the first body.

As more bodies are added, more joints are required to build the system. To get the desired motion for a system, the appropriate joints must be used. This brings up the issue that for a kinematically constrained rigid body model, the joint topology becomes important, especially depending on whether the model is in 2D or 3D space. This is covered in greater detail in the following section.

It should also be noted that one need not use joints to describe the system as joints create a model which is entirely ideal. Instead, force elements, such as bushings and radial spring damper actuators (RSDA) may be used. Using these elements adds compliance to the system, making it a more accurate model, but one which requires more parameters to build. Since there is a sufficient lack of such parameters, the MBS for this thesis is kinematically constrained. However, force elements will be introduced to make the system behave more realistically.

2.5 Planar and Spatial Dynamics

As mentioned in the preceding chapter, there are two distinct vector spaces to consider in dynamics as they influence the joint topology of the system and the final solution. This is best illustrated with an example, but first, a basic understanding of planar and spatial is needed. In dynamics, planar refers to 2D space as defined by x and y-axes. A body in this space may only translate along these axes. Rotation occurs, but around the z-axis, which is normal to the plane. Therefore, at most, there are three DOF

for any body. Spatial refers to 3D space and is defined by x, y, and z-axes. A body may either translate along or rotate about any axis. Thus, a body has at most six DOF. Refer to Figure 2-5 for a representation of planar and spatial axis systems.

To illustrate the difference in joint topology for planar and spatial cases, a simple four-bar mechanism, called a slider-crank, is used. This mechanism is composed of four bodies: ground, crank, connecting rod, and slider, and is shown in Figure 2-6.

In the planar case, the joint topology calls for three revolute joints and one translational joint as depicted in Figure 2-7. To calculate the mobility, or DOF, of the system, Equation 2-2 is used

$$DOF = 3n - n_c \tag{2-2}$$

where n is the number of bodies in the system and n_c is the number of constraints removed from all the joints. Evaluation of the above equation yields a single DOF and is shown below.

$$DOF = 3x4 - (3x2\ \{rev\} + 1x2\ \{trans\} + 3\ \{grnd\}) = 1$$

This single DOF for the system means that there is one constraint needed to drive the system such that the kinematic and dynamic information can be found.

For the spatial case, using three revolute joints and one translational joint will no longer work because it will be over constrained according to the spatial mobility equation as shown in Equation 2-3.

$$DOF = 6n - n_c \tag{2-3}$$

Evaluation of this equation with improper joint topology yields a negative number for DOF, thus implying that the system is over constrained and needs attention.

$$DOF = 6x4 - (3x5\ \{rev\} + 1x5\ \{trans\} + 6\ \{grnd\}) = -2$$

Figure 2-8 shows the correct joint topology for the slider-crank in spatial coordinates. Here, a revolute, a spherical, a cylindrical, and a translational joint are used. It may seem counterintuitive, but a quick analysis reveals the opposite. The revolute

between ground and the crank allows only one rotation about the in-plane axis. Connecting the crank together with a spherical joint would normally allow rotation about any axis, but the revolute joint at ground limits the rotation to only one axis (i.e. the motion of the crank is fixed to the plane perpendicular to the rotational axis). Therefore, the spherical joint will only rotate about the same axis as the revolute joint, but will remove only three DOF instead of five. The cylindrical joint, which removes four DOF, between the connecting rod and slider would normally rotate and translate on the chosen axis, but the translational joint between ground and the slider ensures that the only motion it has is rotation about the in-plane axis. And an evaluation of the mobility equation with this joint topology now yields a single DOF.

$$DOF = 6x4 - (5\{rev\} + 3\{sph\} + 4\{cyl\} + 5\{trans\} + 6\{grnd\}) = 1$$

It should be noted that spatial analyses predominate real MBS as life unfolds in 3D space. However, planar mechanics is not entirely useless. It serves as a way to learn about dynamic systems, as they are easier to comprehend. Once the basic planar concepts are cemented, one only has to use analytical and algebraic extensions to understand spatial mechanics (Haug, 1989).

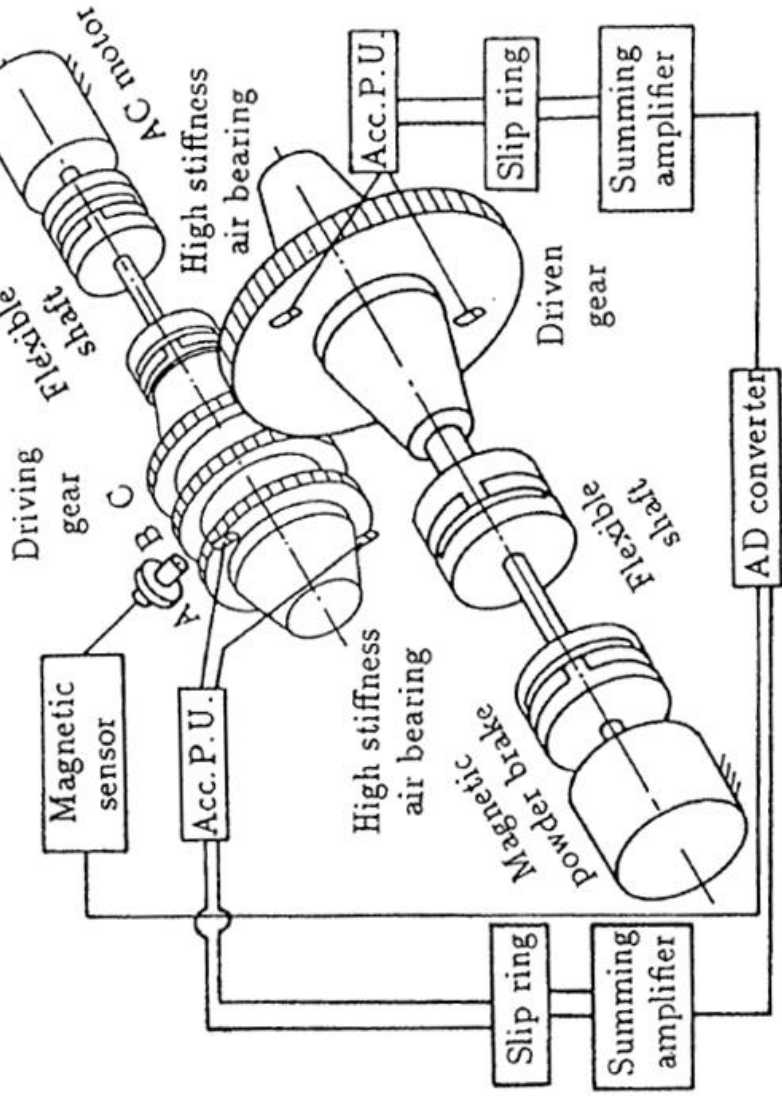

Figure 2-1: Cai's diagram of the experimental model complete with instrumentation.

Source: Cai, Y. The Linear Approximated Equation of Vibration of a Pair of Spur Gears (Theory and Experiment). Ph.D. Dissertation, Precision and Intelligence Laboratory, Tokyo Institute of Technology, Tokyo, Japan, 1991.

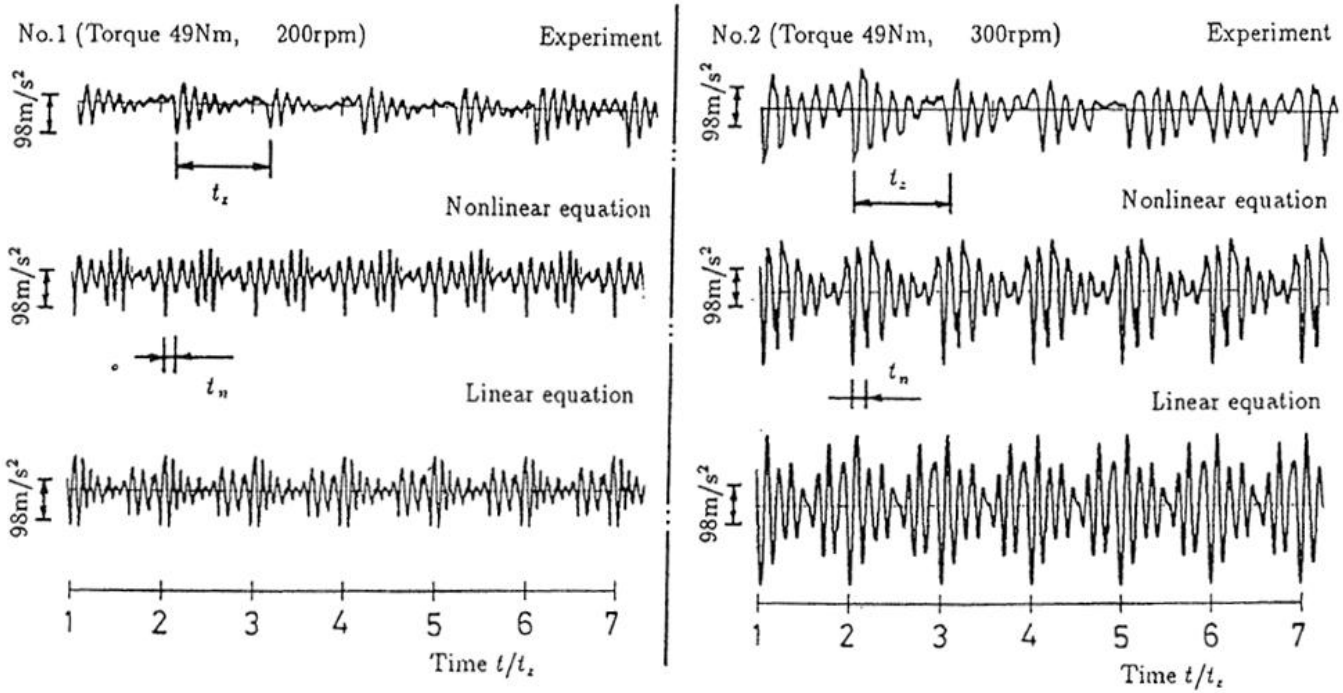

Figure 2-2: Cai's experimental results.

Source: Cai, Y. The Linear Approximated Equation of Vibration of a Pair of Spur Gears (Theory and Experiment). Ph.D. Dissertation, Precision and Intelligence Laboratory, Tokyo Institute of Technology, Tokyo, Japan, 1991.

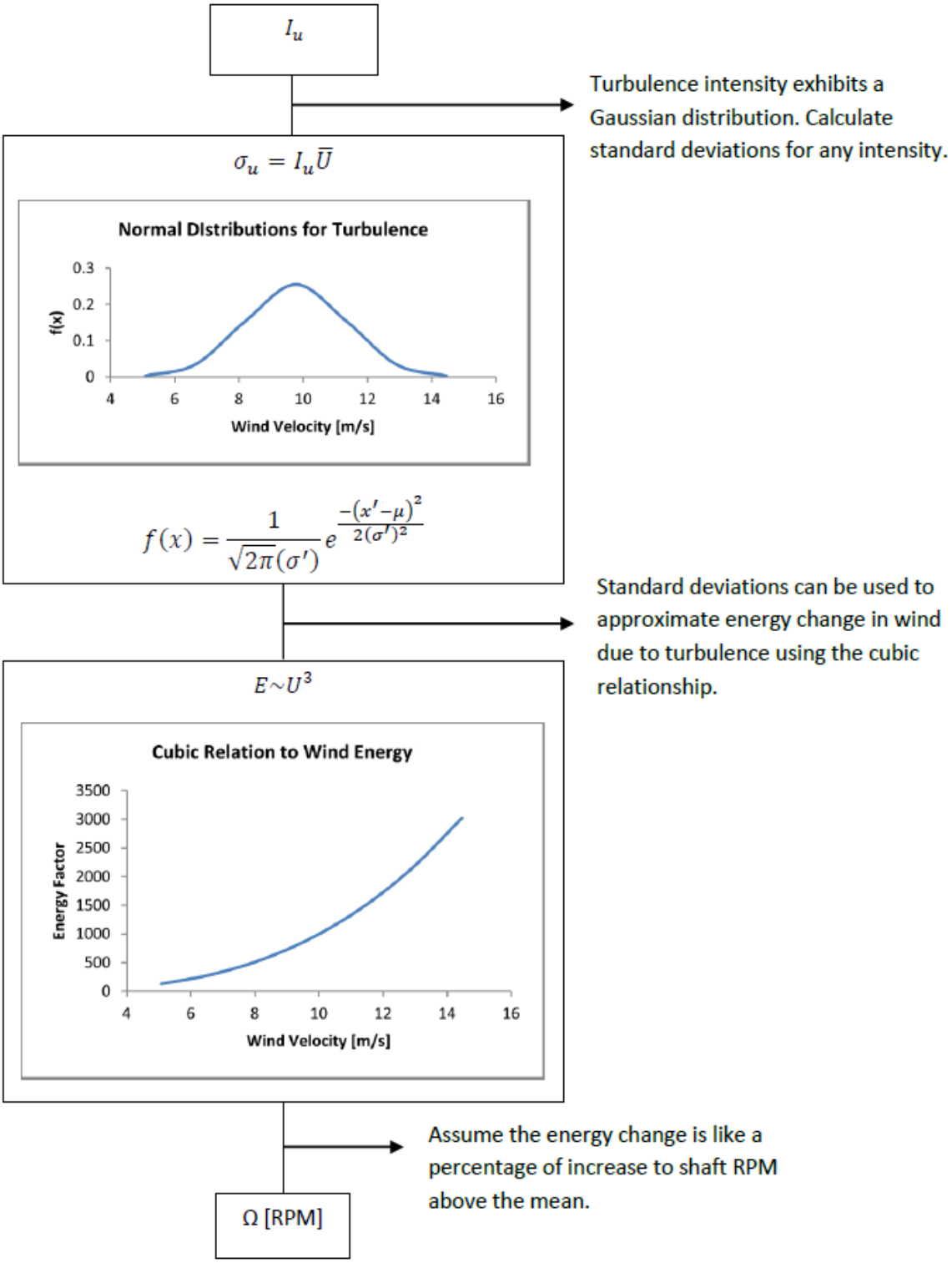

Figure 2-3: Flow chart relating the turbulence intensity factor to shaft rotation.

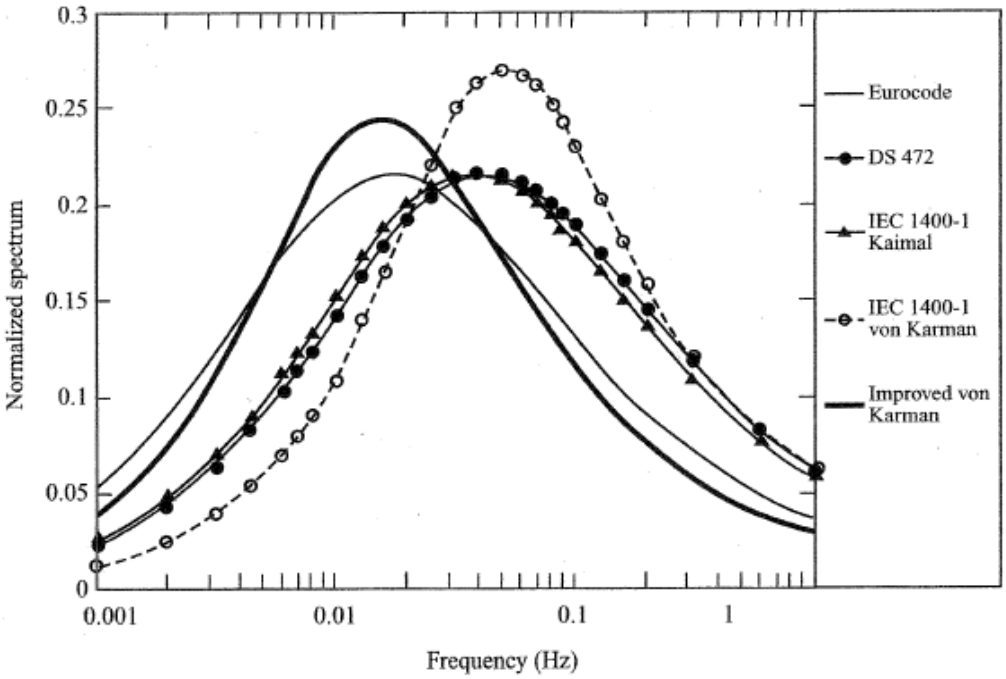

Figure 2-4: Frequency spectra.

Source: Burton, T., Sharpe, D., Jenkins, N., and Bossanyi, E. (2001) *Fundamentals of Wind Turbines.* John Wiley and Sons Ltd. West Sussex, England.

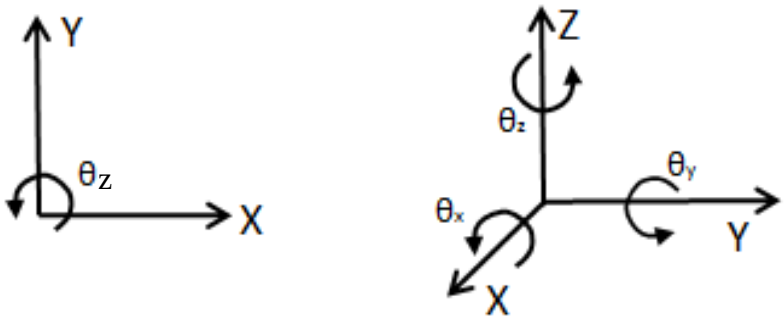

Figure 2-5: Planar and spatial axis systems showing the possible DOF.

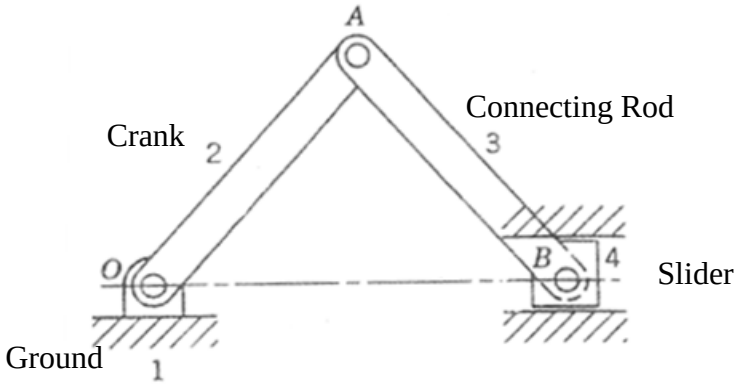

Figure 2-6: Slider-crank mechanism showing bodies.

Source: Shabana, A. A., (2010) *Computational Dynamics: Third Edition, pp. 1, 112*. John Wiley & Sons Ltd. West Sussex, England.

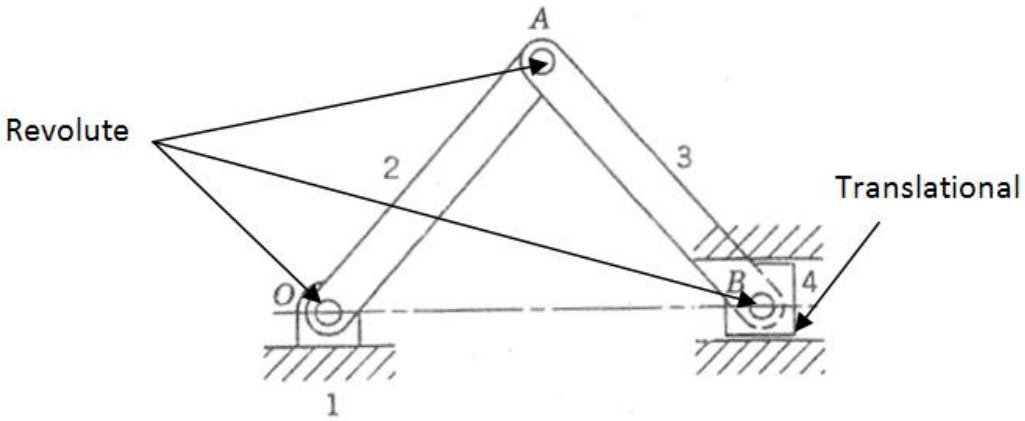

Figure 2-7: Slider-crank with planar joint topology.

Source: Shabana, A. A., (2010) *Computational Dynamics: Third Edition, pp. 1, 112*. John Wiley & Sons Ltd. West Sussex, England.

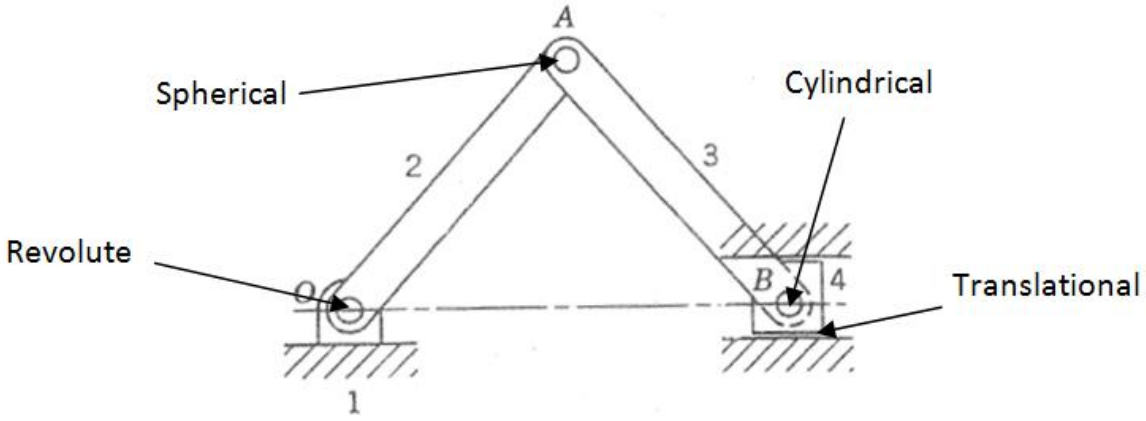

Figure 2-8: Slider-crank with spatial joint topology.

Source: Shabana, A. A., (2010) *Computational Dynamics: Third Edition, pp. 1, 112*. John Wiley & Sons Ltd. West Sussex, England.

CHAPTER 3

COMPUTER SIMULATION

The complexity of MBD systems lends itself well to computer simulation. To facilitate this, the dynamic EOM, which are differentiable algebraic equations (DAE), are put into matrix form. The Lagrange formulation is a classical mechanics method and is used here (Haug, 1989).

3.1 Computational Approach

To begin the analysis, a generalized coordinates vector, $\boldsymbol{q}^i$, is formed by listing the DOF for each body in Cartesian coordinates, for n number of bodies and is shown in Equation 3-1

$$\boldsymbol{q}^i = \left[\boldsymbol{r}_x^i \; \boldsymbol{r}_y^i \; \boldsymbol{r}_z^i \; \theta_x^i \; \theta_y^i \; \theta_z^i\right]^T \tag{3-1}$$

where $\boldsymbol{r}_x^i,\ \boldsymbol{r}_y^i,\ \boldsymbol{r}_z^i$ and $\theta_x^i, \theta_y^i, \theta_z^i$ are position vectors and angles, respectively, from the global origin to a point on the next body, see Figure 3-1 for an illustration.

According to Shabana, the number of constraint equations, n_c, is equal to the number of active system coordinates for a kinematically driven system. Therefore, the constraint equations are given in Equations 3-2 through 3-6,

$$\boldsymbol{c}(\boldsymbol{q}, t) = [c_1(\boldsymbol{q}, t) + c_2(\boldsymbol{q}, t) + \cdots + c_n(\boldsymbol{q}, t)]^T = \boldsymbol{0} \tag{3-2}$$

$$\boldsymbol{C_q}\dot{\boldsymbol{q}} + \boldsymbol{c_t} = \boldsymbol{0} \tag{3-3}$$

$$\boldsymbol{C_q}\ddot{\boldsymbol{q}} = \boldsymbol{q_d} \tag{3-4}$$

where,

$$\boldsymbol{c_t} = \left[\frac{\partial C_1}{\partial t} \quad \frac{\partial C_2}{\partial t} \quad \cdots \quad \frac{\partial C_n}{\partial t}\right] \tag{3-5}$$

$$\boldsymbol{q_d} = -\left(\boldsymbol{C_q}\dot{\boldsymbol{q}}\right)_{\boldsymbol{q}} - \boldsymbol{2C_{q_t}}\dot{\boldsymbol{q}} - \boldsymbol{C_{tt}} = \boldsymbol{0} \tag{3-6}$$

Due to the large nature of the equations, it is often best to use matrix notation. In this thesis, bold upper case letters represent matrices and lower case bold letter represent vectors unless otherwise noted. Equation 3-7 shows the Euler-Lagrange EOM in matrix form,

$$\begin{bmatrix} \boldsymbol{M} & \boldsymbol{C_q^T} \\ \boldsymbol{C_q} & \boldsymbol{0} \end{bmatrix} \begin{bmatrix} \ddot{\boldsymbol{q}} \\ \boldsymbol{\lambda} \end{bmatrix} = \begin{bmatrix} \boldsymbol{q_e} \\ \boldsymbol{q_d} \end{bmatrix} \tag{3-7}$$

where $\boldsymbol{M}$ is the mass matrix, $\boldsymbol{C_q}$ is the first derivative of the constraints matrix with respect to the generalized coordinates vector and is known as the Jacobian constraints matrix, $\boldsymbol{C_q^T}$ is the transpose of the Jacobian constraints matrix, $\ddot{\boldsymbol{q}}$ is the second derivative of the generalized coordinates vector, $\boldsymbol{\lambda}$ is the Lagrange multiplier vector, $\boldsymbol{q_e}$ is the external forces vector, and $\boldsymbol{q_d}$ is the second derivative of the constraints equations.

These are shown in more detail in Equations 3-8 through 3-12,

$$\boldsymbol{M} = \begin{bmatrix} m^i & 0 & 0 & 0 & 0 & 0 \\ 0 & m^i & 0 & 0 & 0 & 0 \\ 0 & 0 & m^i & 0 & 0 & 0 \\ 0 & 0 & 0 & I_x^i & 0 & 0 \\ 0 & 0 & 0 & 0 & I_y^i & 0 \\ 0 & 0 & 0 & 0 & 0 & I_z^i \end{bmatrix} \tag{3-8}$$

$$\boldsymbol{C_q} = \begin{bmatrix} \frac{\partial C_1}{\partial q_1} & \frac{\partial C_1}{\partial q_2} & \cdots & \frac{\partial C_1}{\partial q_n} \\ \frac{\partial C_2}{\partial q_1} & \frac{\partial C_2}{\partial q_2} & & \frac{\partial C_2}{\partial q_n} \\ \vdots & & \ddots & \vdots \\ \frac{\partial C_n}{\partial q_1} & \frac{\partial C_n}{\partial q_2} & \cdots & \frac{\partial C_n}{\partial q_n} \end{bmatrix} \tag{3-9}$$

$$\ddot{\boldsymbol{q}}^i = \begin{bmatrix} \ddot{\boldsymbol{r}}_x^i & \ddot{\boldsymbol{r}}_y^i & \ddot{\boldsymbol{r}}_z^i & \ddot{\theta}_x^i & \ddot{\theta}_y^i & \ddot{\theta}_z^i \end{bmatrix}^T \tag{3-10}$$

$$\boldsymbol{q_c} = -\boldsymbol{C_q^T}\boldsymbol{\lambda} \tag{3-11}$$

$$\boldsymbol{q_e} = \begin{bmatrix} f_{xj}^i & f_{yj}^i & f_{zj}^i & M_{xj}^i & M_{yj}^i & M_{zj}^i \end{bmatrix} \tag{3-12}$$

where $\boldsymbol{q_c}$ is constraint forces vector, the subscript *j* refers to the nomenclature forces and moments (i.e. f^1_{x1}, M^3_{z2}, etc.) and the superscript *i* refers to the body number.

3.2 LMS Virtual.Lab Software

LMS Virtual.Lab (VL) is a MBD software which allows the user to logically assemble rigid bodies together, with kinematic constraints or force elements, in a graphical user interface (GUI) window (Zemen, 2009). By default, when building a MBS, the first body is automatically present and is called the ground body. This is the body in which the global coordinate system is normally located and from which all other body coordinates are referenced. To build a MBS, new bodies are inserted and axis systems are placed on these bodies. They are then linked together via joints or force elements. Once a model is appropriately constrained with the correct joint topology, and a driving function is implemented on the remaining DOF, it is fully defined and can be solved.

To solve the analysis case, VL writes a solver input file, which contains the necessary information such as mass, CG, MOI, and initial conditions (Zemen, 2009). The solver, which is run as a different process from the user interface, sets up and solves the EOM and computes the results for position, velocity, acceleration, and reaction forces on a time-domain (LMS International, 2010). These results can be either viewed as plots within VL or written to Excel for data reduction. Also, the user may animate the model to get a visual on how the system operates, which is a useful tool.

Before the solver may compute the solution, the user has the option of selecting some advanced solution techniques, which include integration step size, solution tolerance, integration methods, assembly algorithms, and matrix operations. These advanced options allow the user to define what numerical scheme will be employed to obtain the solution. For this simulation, the time step was reduced until a smooth curve resulted. Reduction beyond this increment did not result in more accuracy. This time step was 0.0005 s. The solution tolerances were set to 0.00001 m to ensure good convergence without being to computationally expensive.

3.3 Numerical Scheme

Many problems in engineering exhibit behavior which can be approximated by second order, ordinary differentiable equations (ODE). Numerical methods are needed because these ODE are often either too difficult or impossible to obtain exact solutions. Numerical methods offer a way to iterate until a convergence, either implicitly or explicitly, to a solution given a specified tolerance. This solution is, of course, only an approximation, but the approximation can be quite accurate depending on the numerical method used.

The numerical scheme chosen for the simulation of the simple spur gear model is the Predict, Evaluate, Correct, Evaluate (PECE) method, which is an explicit Adams-Moulton-Bashforth predictor-corrector method (LMS International, 2010). Figure 3-2 shows that this is a fourth-order method, meaning it uses four points (three previous and one current) to predict the next point, which makes it more stable and less prone to error propagation than second-order methods, however, it is not self-starting and requires a method to initiate the first four points. Predictor-corrector methods generally use information from several known points of a previous iteration to compute the next point. The disadvantage of such a technique is that it is not always self-starting and may take another method to provide the first step. However, the advantage is that they are more efficient at using existing information to continue through the iterations. Figure 3-3 shows a typical predictor-corrector flow chart (Griffiths, et al., 1991).

There are two formulae which form the iteration process, the predictor and corrector. The predictor formula (Adams-Bashforth predictor) uses existing information to extrapolate an estimate of a new point and the corrector formula (Adams-Moulton corrector) improves the estimate. The basic algorithm, shown in Equations 3-1 and 3-2, is repeated until convergence is met.

$$y_{i+1}^{(0)} = y_i + \frac{h}{24}[55f(x_i, y_i) - 59f(x_{i-1}, y_{i-1}) + 37f(x_{i-2}, y_{i-2}) - 9f(x_{i-3}, y_{i-3})] \qquad (3\text{-}1)$$

$$y_{i+1}^{(1)} = y_i + \frac{h}{24}\left[f(x_{i-2}, y_{i-2}) - 5f(x_{i-1}, y_{i-1}) + 19f(x_i, y_i) - 9f\left(x_{i+1}, y_{i+1}^{(0)}\right)\right] \quad (3\text{-}2)$$

The equations which the PECE method will solve are second-order ODE which are of the form shown in Equation 3-3.

$$\boldsymbol{M\ddot{x} + C\dot{x} + Kx = F}(t) \quad (3\text{-}3)$$

where $\boldsymbol{M}$, $\boldsymbol{C}$ and $\boldsymbol{K}$ are generic mass, damping, and stiffness matrices, respectively, $\boldsymbol{\ddot{x}}$, $\boldsymbol{\dot{x}}$, and $\boldsymbol{x}$ are generic acceleration, velocity, and position vectors, respectively, and $\boldsymbol{F}(t)$ is a generic forcing function vector.

3.4 Virtual Model

The virtual model tries to replicate the physical model as closely as possible while remaining relatively low in complexity. This is because it is more beneficial to first validate a simpler model and then layer in more complexity and sophistication later. The model, shown in Figures 3-4 through 3-6, consists of 11 bodies (ground, two gears, four shafts, and four accelerometers), 10 joints (six bracket and four revolute), four force elements (gear contact and three RSDA), and one driver (joint velocity driver).

The bodies have two sets of axis systems. One set is the CG axes, which are the points about which all kinematic information is calculated. The other set acts as points to make joint connections. These axis systems are a way to describe the geometric attributes of the bodies independent of computer-aided design (CAD) models. The CAD geometry is later overlain on these axis systems to reduce confusion, but do not directly affect the simulations. For visualization reasons, these axis systems are hidden during simulation, but are shown in Figure 3-7 for illustration purposes.

When the bodies have the appropriate axis systems, joints can be applied. The joint topology had to be carefully chosen so as not to over constrain the model. There are six bracket joints which connect the accelerometers to the gears and the gears to the input and output shafts. They remove all DOF, rigidly fixing one body to the other. Four revolute joints were used to allow rotation around the z-axis and are placed in the middle

of the split shafts and at the motor and brake locations. Performing the calculation for mobility leaves four DOF for the system. Refer back to Figure 3-5 for layout of the joint topology.

A joint velocity driver is added at the revolute joint between shaft 1 and the motor, which is considered ground. It is this joint which will be kinematically driven for all analysis cases. The addition of the driver takes one more DOF away from the system leaving only 3 DOF. These will allow vibratory responses to occur in three bodies: the drive gear, driven gear, and output shaft.

3.5 Model Parameterization

Once the system is built and properly constrained, it is possible to parameterize the model. Doing so allows for the user to expedite model updates by creating links with variables of interest to a list of parameter values. As mentioned in preceeding chapters, some of the parameters of interest for rigid body dynamics are the mass, CG, and MOI. Therefore, for each shaft and gear body, a set of mass and inertia parameters were made and are shown is Table 3-1.

It should be noted that the CG location and mass and inertia values for the shafts and gears are approximations. Since there was no existing data to use, values had to be calculated using material properties and geometry in VL. By choosing the material to be steel, and working with the known geometry, the masses associated with each part were calculated. However, some estimation was required as there was no information on the conical connectors linking the gears to the shafts. These too were calculated in VL, as solid parts, and the mass and inertia terms distributed between the gears and shafts. This assumption helped generate a better response curve than existed otherwise, but may also be a significant source of error.

This was also the case for shaft flexibility. The approach taken to model this flexibility was to split the input and output shafts into two pieces, and insert an RSDA

element in the middle. An RSDA element is a rotational spring which can be described with stiffness, damping, or torque values. Thus, each of the two shaft halves acted as one shaft once connected with an RSDA, provided stiffness values were given. The stiffness was obtained by using the shaft geometry and rearranging the equation for angle of twist for circular shafts given in Equations 3-4 and 3-5,

$$\phi = \frac{TL}{JG} \tag{3-4}$$

$$k = \frac{T}{\phi} = \frac{JG}{L} = \frac{\pi d^4}{32L} \tag{3-5}$$

where ϕ is the angle of twist, T is the torque applied, L is the length of the shaft, J is the polar moment of inertia, G is the modulus of rigidity, k is stiffness, and d is shaft diameter. With the shafts both having lengths and diameters of 70 mm and 8 mm, respectively, the associated stiffness was calculated to be 422.3 Nm/rad (Cai, 1992).

The third RSDA element represents the counter torque applied to the system by the power brake mechanism. Since this element can take a torque value as input, a constant 49 Nm was assigned and thus applied for all analysis cases. And since the model is kinematically driven, the counter torque is always overcome by the driver, which runs the system at the set angular velocity regardless of the forces and moments counteracting it. This allowed for the overall system response to closely resemble that of the experimental test.

The final force placed in the model is a gear contact element, which is used to provide a method to transfer motion from the drive gear to the driven gear via contact properties. The theory for basic gear contact revolves around the idea that gear teeth are flexible and can as such be modeled as an equivalent mass-spring-damper system where the forces act along the line of action from one gear to the other, and is shown in Figure 3-8 (Bonori et al., 2008).

VL has a built-in tool to facilitate the construction of the gear contact element. When selected, the user must choose from a variety of gear mesh options which describe the physical gears, such as gear type, module, number of teeth, pressure angle, etc. After these physical attributes are filled in, the contact properties can be populated but vary depending on what stiffness method is chosen: Cai, ISO, and Linear. The Cai stiffness method is used in this model and includes the contact parameters of rim and web thickness, backlash, modulus of elasticity, time-varying stiffness, and damping constant. See Figures 3-9 and 3-10 for the completed dialog boxes which are used in the model. The data used to build the gears are provided by Cai and are shown in Table 3-2.

Other key assumptions for this model are that damping is neglected, backlash is approximated from the given tooth profile errors, and time-varying stiffness is used. Damping is a value which is generally measured for the overall system in terms of a damping ratio. For his experiment, Cai (Cai, 1992) found an overall system damping ratio of 0.068. However, applying the proper damping constants to each RSDA and gear contact element is impractical since there is no way to know for certain how it is distributed among the elements. This could be improved by running a design of experiments (DOE) for which the damping ratios for each element are assigned values and iterated on until the system falls within a predetermined tolerance. But since this is quite computationally expensive, the assumption that there is no damping is justified.

Gear backlash is loosely defined as the gap between teeth as one tooth comes into contact with the other and is generally set at a value which is higher than the total error of the gear pair (Bosch, 2007). Since the errors in tooth profile for the gears were around five microns, a value of 0.1 mm was used for the simulation. It should be noted that this assumption is necessary since a backlash value could not be obtained and the simulation results were not sufficient with zero backlash.

The last option to review is the equivalent stiffness. Time varying stiffness is used in gear mesh equations because it provides a more accurate way to model. A gear tooth

can be simply thought of as a cantilevered beam of varying cross-section. As such, it will have stiffness values which change depending on the cross-sectional location. And, as the gear contact point sweeps along the involute path, it applies a force at different locations along the beam (gear tooth). Therefore, as the gears rotate, the stiffness varies with time.

3.6 Virtual Model Validation

As with any virtual model, validation is paramount. Without having a valid model, further analyses will most likely not yield any usable data. The approach to validate this model was to compare the response of two simulations, run at the constant angular velocities of 200 and 300 RPM, respectively, to the responses documented by Cai. Just as in the experiment, the virtual response was measured by accelerometers for each gear and shows the torsional vibration accelerations within the model. Therefore, the virtual model, if accurately built, should replicate the vibratory response of the system. See section 4-1 for plots.

3.7 Quasi-steady Input

Recall that the input for quasi-steady loading is correlated to actual wind load limits as discussed in section 2.3. It was decided that the change in sinusoidal amplitude should correlate to the turbulence intensity factors of 16, 17, and 18%. When adjusted to correlate the cubic relationship for wind power, the amplitude then becomes 3.8, 4.6, and 5.5% of the mean RPM value, which was taken to be 200 RPM. Therefore, the three amplitudes are 7.6, 9.2, and 11 RPM. And with the frequencies being 0.05, 0.1, and 1 Hz, there are now nine different combinations (i.e. each amplitude run at all frequencies). This creates a matrix of solution combinations and is shown in Table 3-3.

The sine wave profile changes depending on the two input parameters of amplitude and frequency. Therefore, to better visualize what the input to the system looks like, each of the frequencies are plotted with amplitude of unit magnitude and is shown in Figure 3-11.

Table 3-1: List of model parameters.

Model Parameters		
Parameter	**Value**	**Location**
Shaft Mass	3.858 kg	Half Shaft CG
Shaft Inertia	0.001 kg m^2	Half Shaft CG
Shaft Stiffness	442.3 Nm/rad	Shaft RSDA
Gear 1 Mass	1.333 kg	Driving Gear
Gear 1 Inertia	0.002 kg m2	Driving Gear
Gear 2 Mass	10.667 Kg	Driven Gear
Gear 2 Inertia	0.002 kg m2	Driven Gear
Brake Torque	49 Nm	Brake RSDA

Table 3-2: List of Cai's gear parameters.

Gear Parameters		
Parameter	**Driving Gear**	**Driven Gear**
Module	3	3
Number of Teeth	40	80
Facewidth [mm]	15	30
Pressure Angle [Deg]	20	20
Helix Angle [Deg]	0	0
Addendum Modification Factor	0	0
Pitch Diameter [mm]	120	240

Source: Cai, Y., Hayashi, T. "Linear approximated equation of vibration for a pair of spur gears: theory and experiment." *American Society of Mechanical Engineers, Design Engineering Division (Publication) DE,* v 43 pt 2 , *Advancing Power Transmission into the 21st Century*.

Table 3-3: Simulation Table for Quasi-steady Loading

	Amplitude [RPM]		
Frequency [Hz]	**7.6**	**9.2**	**11**
0.05	Run 1	Run 2	Run 3
0.1	Run 4	Run 5	Run 6
1	Run 7	Run 8	Run 9

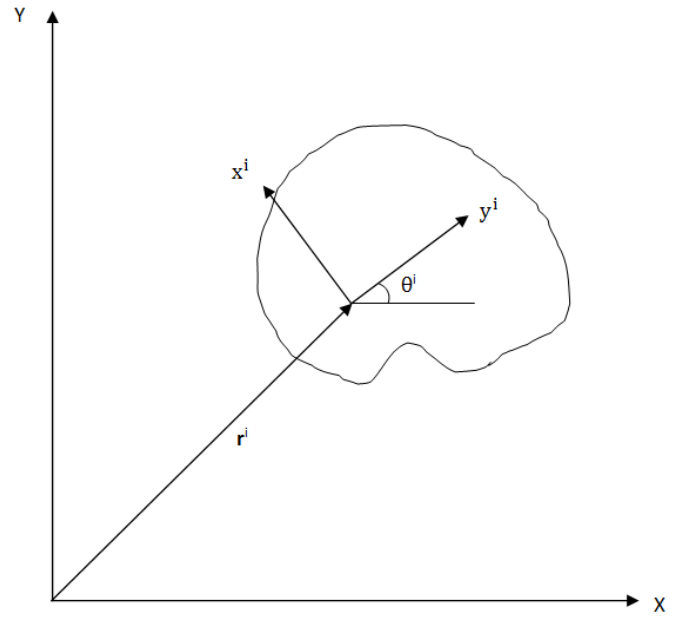

Figure 3-1: MBD global and local coordinate systems.

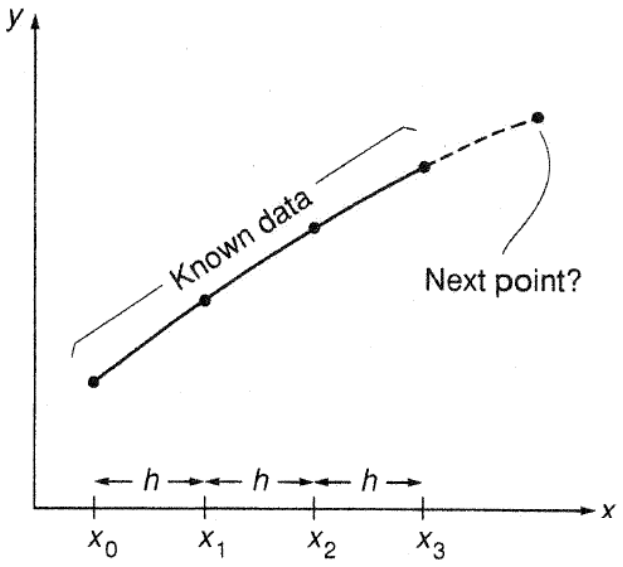

Figure 3-2: Predictor-corrector methods.

Griffiths, D. V., and Smith, I. M. (1991) *Numerical Methods for Engineers*. Blackwell Scientific Publications. Oxford, England.

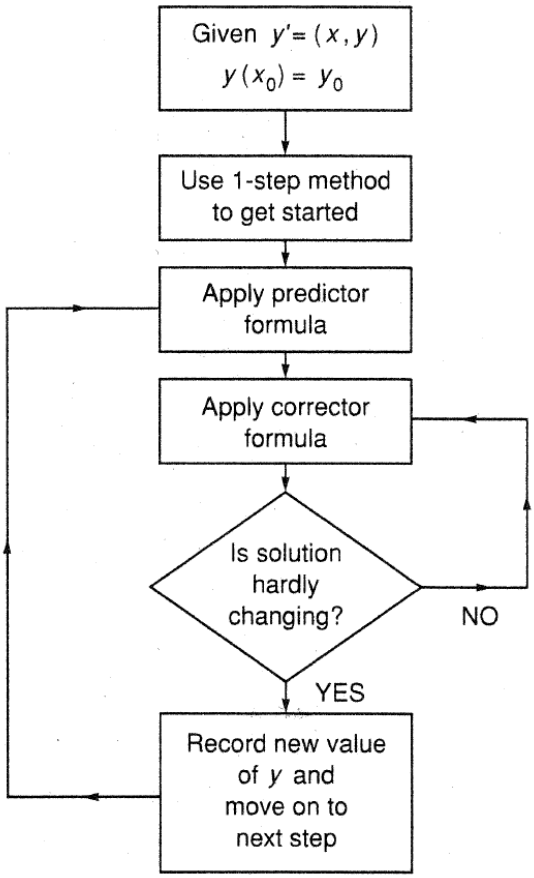

Figure 3-3: Numerical scheme flow chart.

Griffiths, D. V., and Smith, I. M. (1991) *Numerical Methods for Engineers*. Blackwell Scientific Publications. Oxford, England.

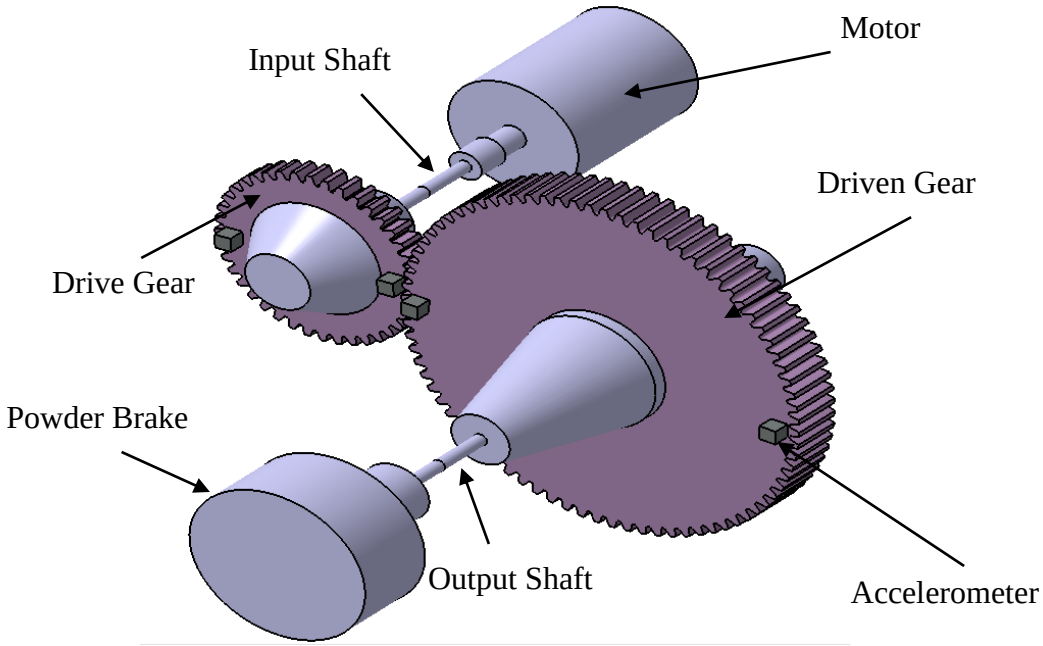

Figure 3-4: MBD model of simple spur gears.

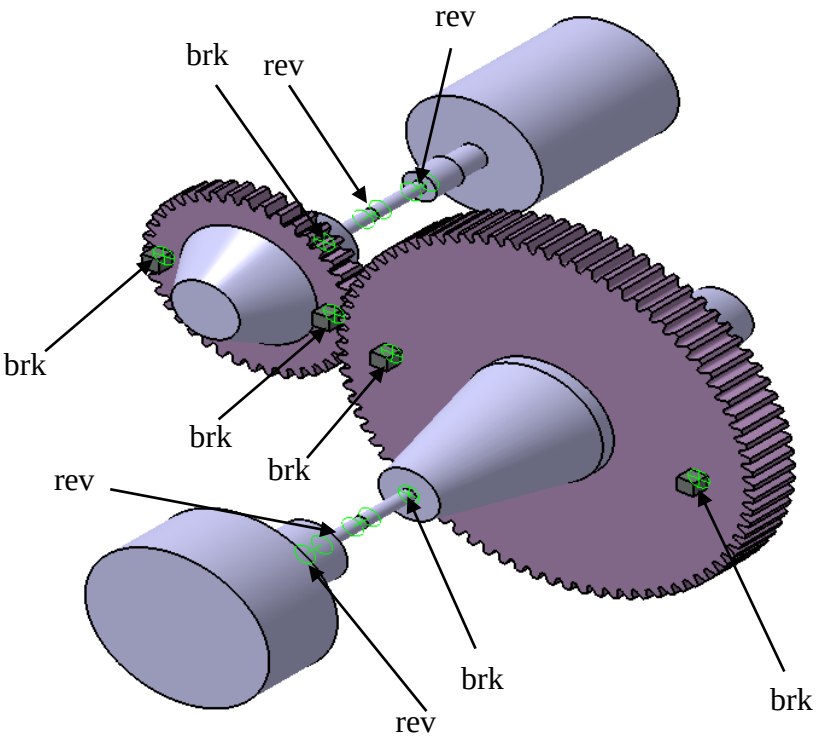

(a)

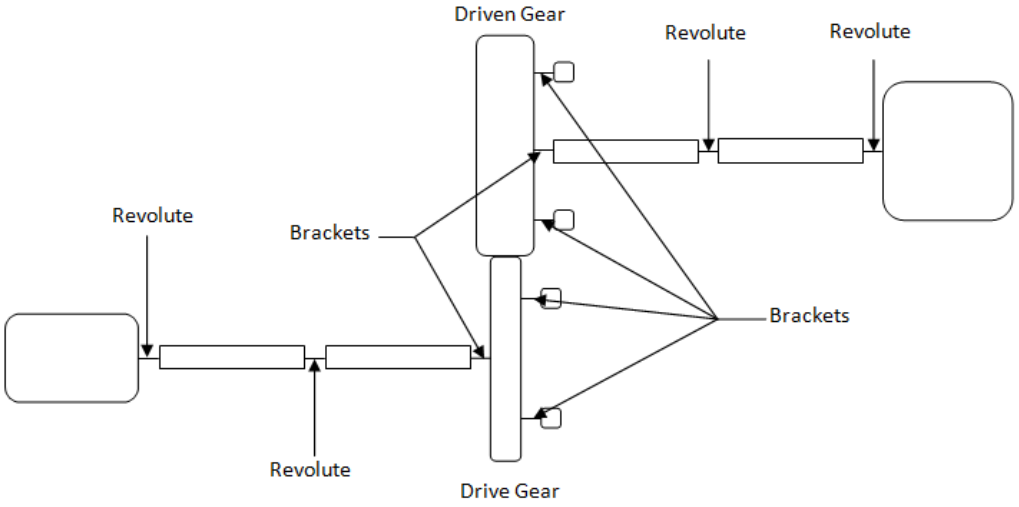

(b)

Figure 3-5: Joint topology with 6 bracket (brk) and 4 revolute (rev) joints.
(a) Model view
(b) Top-view joint topology diagram.

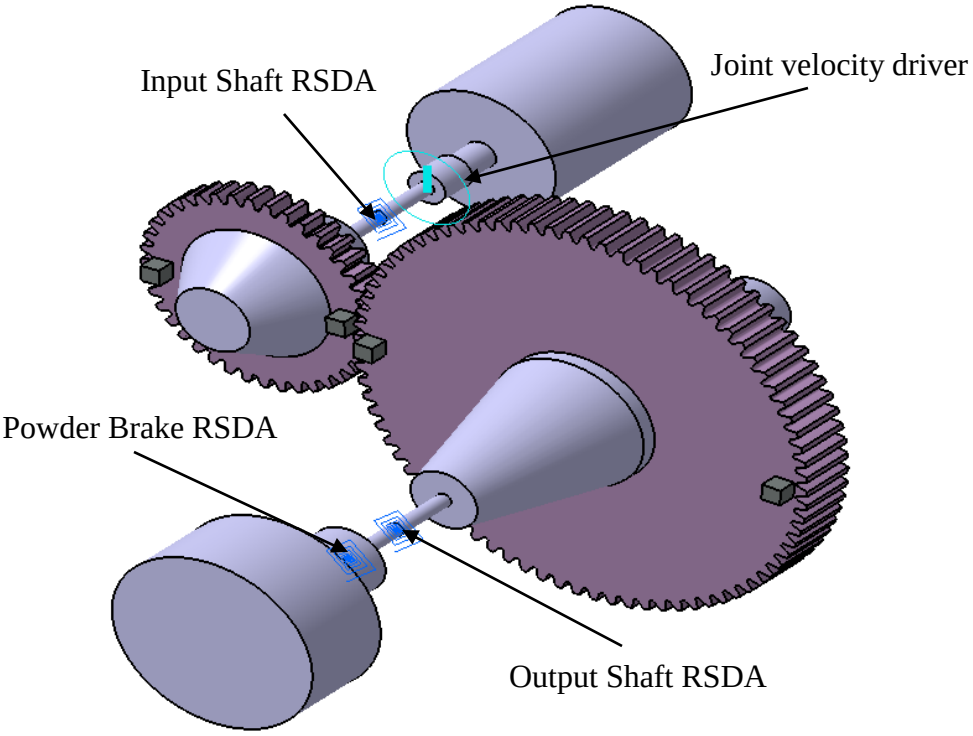

Figure 3-6: Force and driver locations.

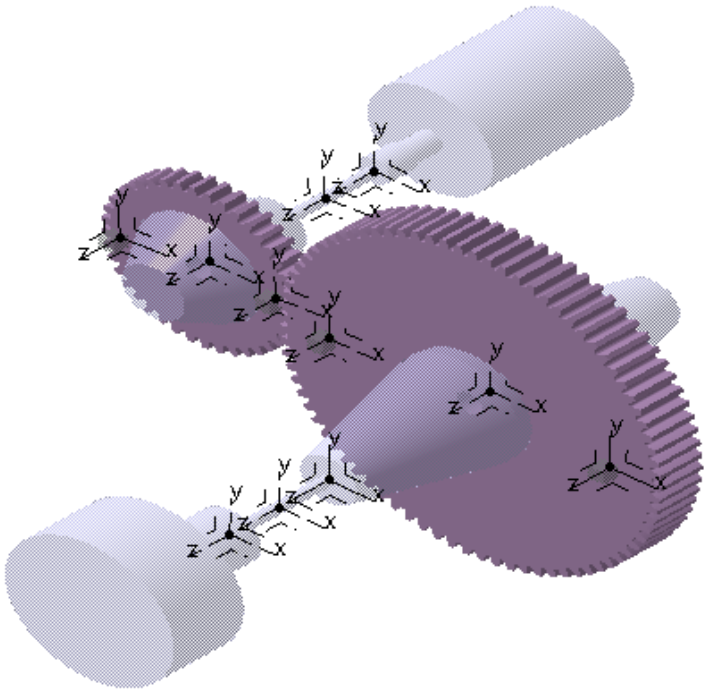

Figure 3-7: Model with axis systems displayed.

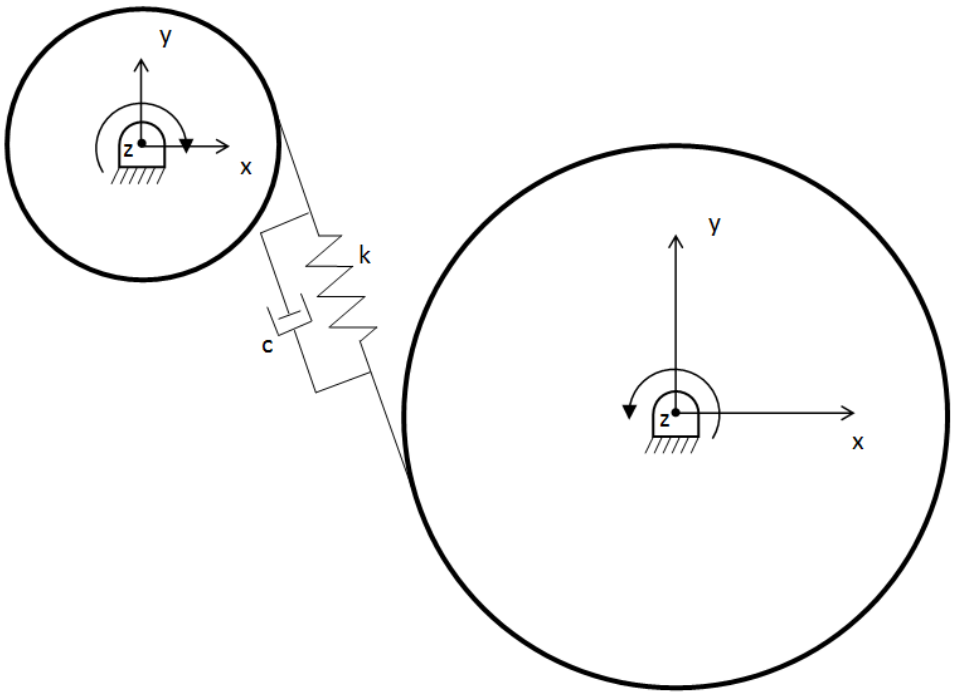

Figure 3-8: Schematic showing the basic theory behind gear contact.

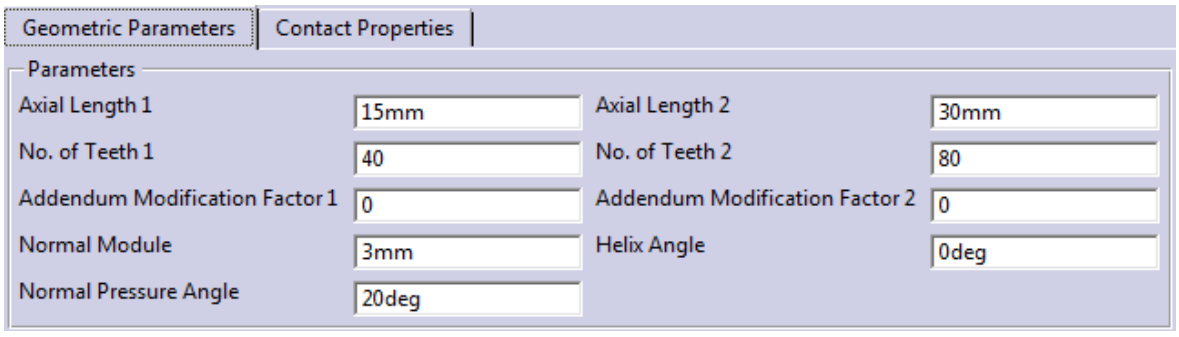

Figure 3-9: Gear Geometric Parameters dialog box in VL.

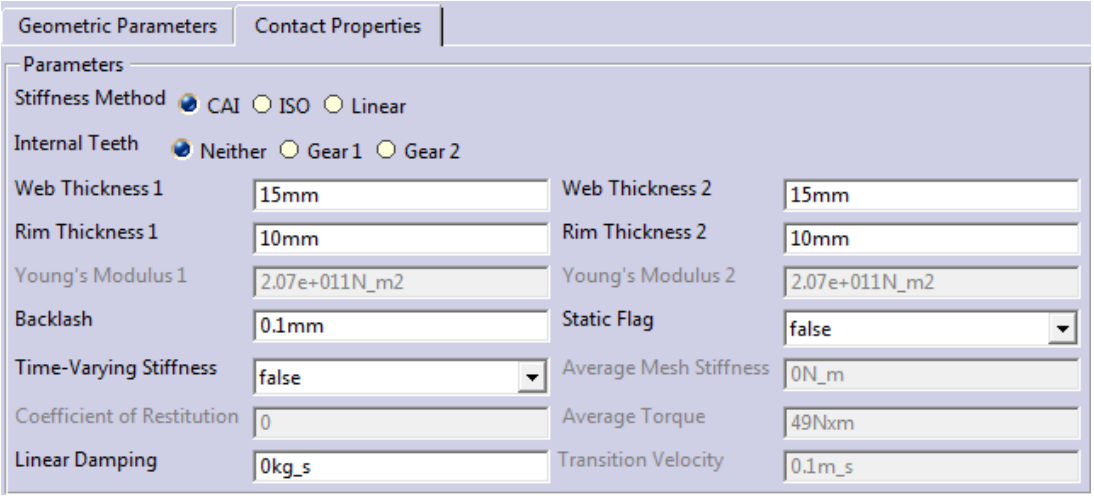

Figure 3-10: Gear Contact Parameters dialog box in VL.

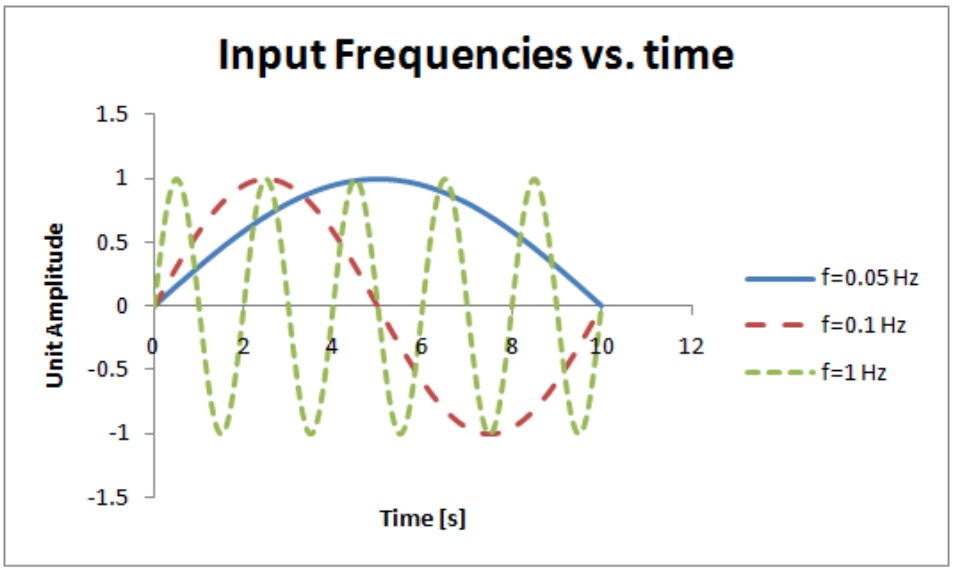

Figure 3-11: Input frequencies vs. time used to drive the quasi-steady model (at unit amplitude).

CHAPTER 4

RESULTS

For all load cases at an applied constant rotational speed of 200 RPM, the simulations were run for 30 s. The 30 s run time was long enough for transients to die out and to reach the steady periodic solution. And, after reviewing the data, an interesting phenomenon was noted. The trend for each load case was similar in that after approximately 17 s, each calculated variable of acceleration, gear contact force, shaft input torque, and shaft output torque, decayed from a higher to a lower magnitude as illustrated in Figures 4-1a through 4-4a. These figures show the system's response subject to application of a constant rotational speed, 200 RPM, but the results are representative to other RPM examined. See Appendix A for plot of each load case.

4.1 Constant Loading Results

For comparison purposes, three quantities were used: percent difference, absolute difference, and RMS values. These were applied to compute the changes in the minimum and maximum values calculated in the simulation. The percent difference was calculated using Equation 4-1

$$\%\, diff = \frac{(\varepsilon_{200} - \varepsilon_{300})}{\varepsilon_{200}} \tag{4.1}$$

where ε is a generic variable for the computed quantities and the subscript refers to the RPM at which the computation was performed, and the absolute difference by Equation 4-2.

$$abs\ diff = |\varepsilon_{200} - \varepsilon_{300}| \tag{4.2}$$

Since the solution is numerical, there could be a discrepancy at the peak values as the time step may have prohibited calculation at the actual peak value. Therefore, the root mean square (RMS) was calculated using Equation 4-3.

$$a_{rms} = \sqrt{\frac{a_1^2 + a_2^2 + \cdots + a_{n_t}^2}{n_t}} \tag{4-3}$$

Since the system is kinematically driven, it should therefore see a significant increase in acceleration, force, and torque with a large increase in RPM as the driver will use the necessary forces and torques to overcome any resistance in the system. But, as the results show in Table 4-1, this was not the case. Looking at the data during steady-state operation, it can be seen that the increase in amplitude did lead to an increase in the measured quantities, but not by a significant amount. The most significant changes occurred in the vibratory acceleration where the absolute differences for the maximum and minimum were 7.7 m/s^2 and 2.0 m/s^2, respectively. This correlates to an increase in RMS of 8.91%. However, given that there is such a large change in the minimum absolute difference and not in the maximum leads to the conclusion that the acceleration amplitude is decreasing as RPM is increased. This is contrary to Cai's publishd results, refer to Figure 2-2.

To show that the model behaved in a similar manner to Cai's experiment, the virtual accelerations were compared to the experimental results and are shown in Figures 4-5 and 4-6. Here the comparison is limited to visual as there are no available data to construct a better comparison. Nonetheless, it can be seen that the magnitudes match at around 100 m/s^2 and the vibration profiles share the similar characteristics of beats, which is most likely as a result of periodic tooth engagement.

The figures were made by plotting the last few seconds of simulation results and making the necessary adjustments. These included measuring the period of vibration, t_z, and normalizing the solution time, t, by dividing it by the period. This then had to be offset by a constant due to the length of the simulation. The linear offset, t_o, is then calculated by Equation 4-4.

$$t_o = \frac{t}{t_z} \tag{4-4}$$

4.2 Quasi-steady Loading Results

As was the case for constant loading, quasi-steady loading varied little as different amplitudes and frequencies were introduced. Regardless of the input, the system responded in a similar manner in that it began at a higher amplitude and damped out to a lower amplitude after about 17 s. This is illustrated in Figure 4-7 but with the addition of the input used to get the generated output. Again, this behavior is what would be expected at an ideal systems level, but not at the component level.

Table 4-2 shows the minimum, maximum, and RMS values for each of the nine runs. As can be seen, there is little difference between each run. But, this is not entirely unexpected as Sheinman points out (Sheinman, 1992) that small variations in gust amplitude for real turbines can be neglected. This is made even more apparent given the results for the constant loading where a variation of 100 RPM gives only a subtle change. Varying the amplitude by less than 15 RPM from the mean of 200 RPM will have minimal effects. When comparing the RMS values for acceleration, force, and torque, the largest differences are less than one unit magnitude (m/s^2, N, or N m). And as before, although there are slightly greater differences in the maximum values, they cannot be used for comparison purposes as they may be skewed by numerical errors or prone to calculation time-steps.

4.3 Further Investigation

Because the system responded as it did, further investigation was necessary. From the modeling standpoint, there are a couple of areas which could have led to the obtained results. Obviously, one or more of the assumptions made to build the model are not correct. Since the system is acting as a filter, negating the semi-transient effects, damping cannot be neglected entirely. A powder brake mechanism is dependent on velocity, adding damping to the RSDA acting as the brake should have an impact.

First, the input driver was changed so that it began and ended at zero, peaking at a value of 1000 RPM halfway through the simulation time. Then four plots were made where both input and output were plotted for the calculated accelerations, gear contact force, and shaft torques and are shown in Figures 4-8 through 4-10. Just as before, the input has little to no affect on the output. Clearly, as the figures show, acceleration is the only variable which saw any change, but is due mainly to the peak amplitude of RPM being so high.

To check if damping has an effect on system behavior, an arbitrary damping constant of 1 $m^2kg/(s\ rad)$ was added to the brake RSDA. Then, the same plots as above were made. The resulting response was that the output does indeed follow the input. However, almost all vibratory response was lost as shown in Figures 4-11 through 4-13. The output responding to the input is an improvement, but the loss of vibration is a setback. The vibratory loss is present even if the damping ratio is diminished in magnitude.

Table 4-1: Constant loading results for each analysis case.

	Acceleration [m/s^2]			Gear Contact Force [N]			Intput Shaft Torque [Nm]			Output Shaft Torque [Nm]		
RPM	**Min**	**Max**	**RMS**	**Min**	**Max**	**RMS**	**Min**	**Max**	**RMS**	**Min**	**Max**	**RMS**
200	2.9	95.9	49.3	0	875.3	518.6	0	72.2	42.8	0	131.3	77.8
300	10.6	97.9	53.7	0	879.7	521.5	0	72.6	43.0	0	132.0	78.2
abs diff	7.7	2.0	4.4	0	4.4	2.9	0	0.4	0.2	0	0.7	0.4
% change	262.02	2.08	8.91	0	0.50	0.55	0	0.50	0.55	0	0.50	0.55

Table 4-2: Quasi-steady loading for nine scenarios.

	Acceleration [m/s^2]			Gear Contact Force [N]			Input Shaft Torque [Nm]			Output Shaft Torque [Nm]		
RUN	**Min**	**Max**	**RMS**	**Min**	**Max**	**RMS**	**Min**	**Max**	**RMS**	**Min**	**Max**	**RMS**
1	3.0	96.8	49.9	0	946.7	524.1	0	78.1	43.2	0	142.0	78.6
2	2.5	96.6	49.7	0	879.3	524.0	0	72.5	43.2	0	131.9	78.6
3	2.7	97.1	49.8	0	1134.4	524.2	0	93.6	43.2	0	170.2	78.6
4	3.0	96.8	49.9	0	878.8	524.0	0	72.5	43.2	0	131.8	78.6
5	2.4	101.3	49.7	0	1281.9	524.6	0	105.8	43.3	0	192.3	78.7
6	2.6	97.0	49.8	0	879.2	523.8	0	72.5	43.2	0	131.9	78.6
7	3.0	96.9	49.9	0	932.1	524.0	0	76.9	43.2	0	139.8	78.6
8	2.3	96.7	49.7	0	1197.9	524.5	0	98.8	43.3	0	179.7	78.7
9	2.5	97.0	49.8	0	880.1	523.9	0	72.6	43.2	0	132.0	78.6

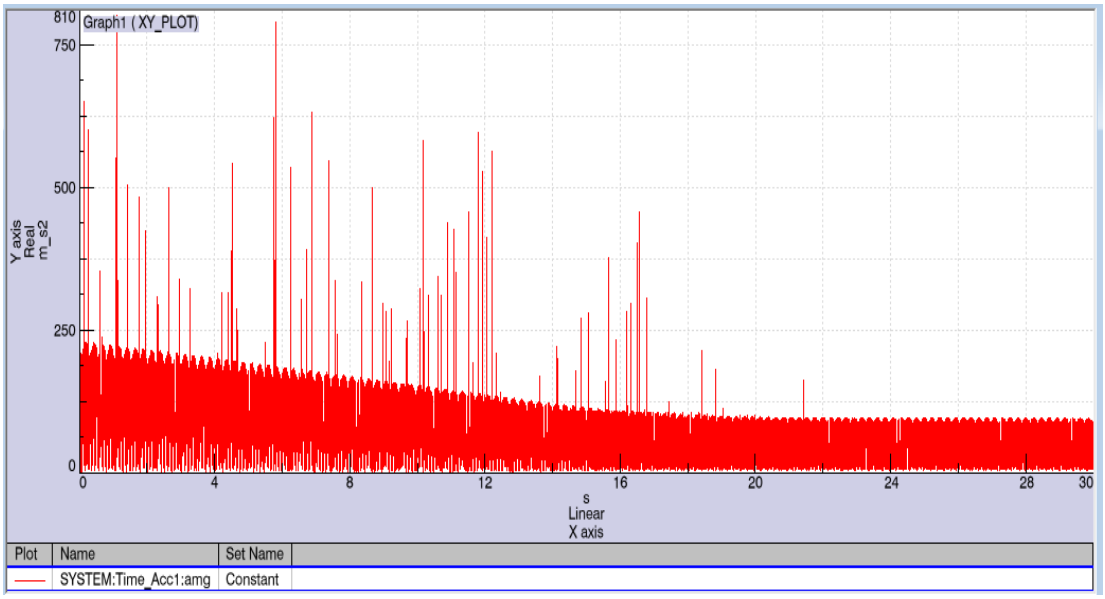

(a)

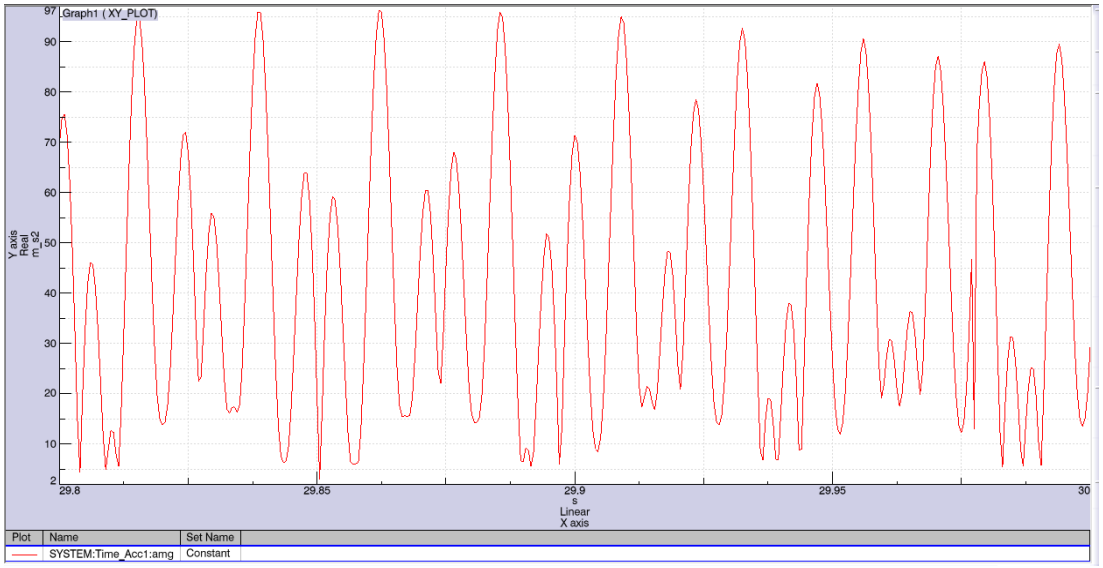

(b)

Figure 4-1: Plot of acceleration at 200 RPM.
(a) Overall, (b) Detailed

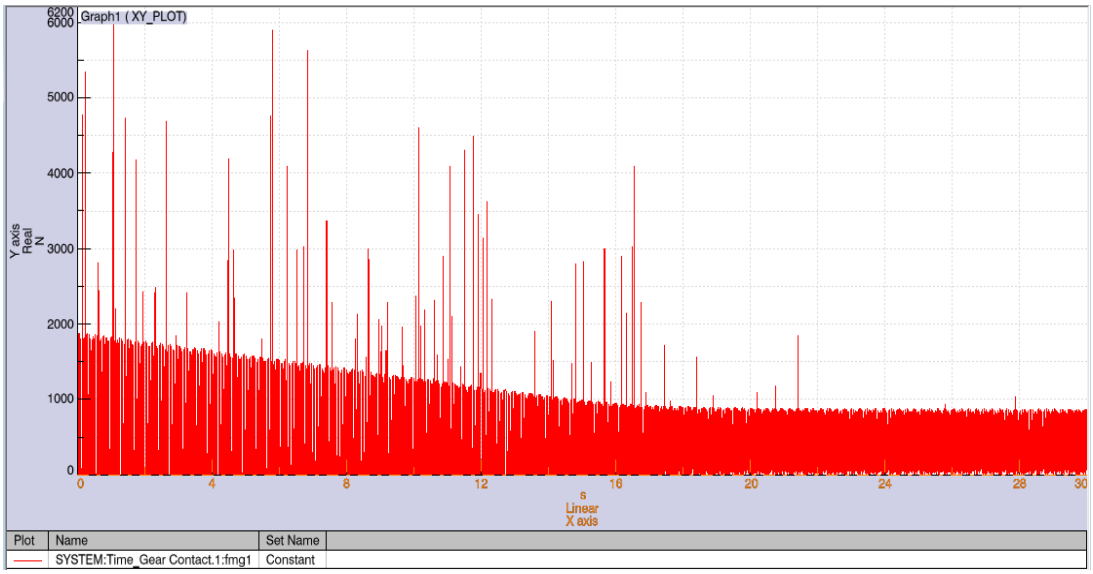

(a)

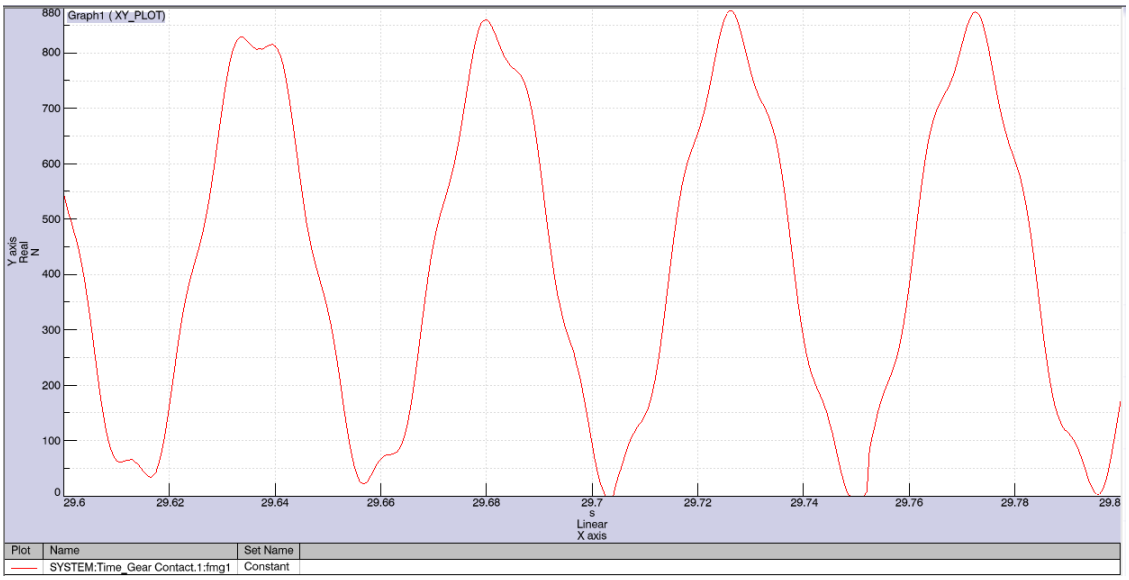

(b)

Figure 4-2: Plot of gear contact force at 200 RPM.
(a) Overall, (b) Detailed

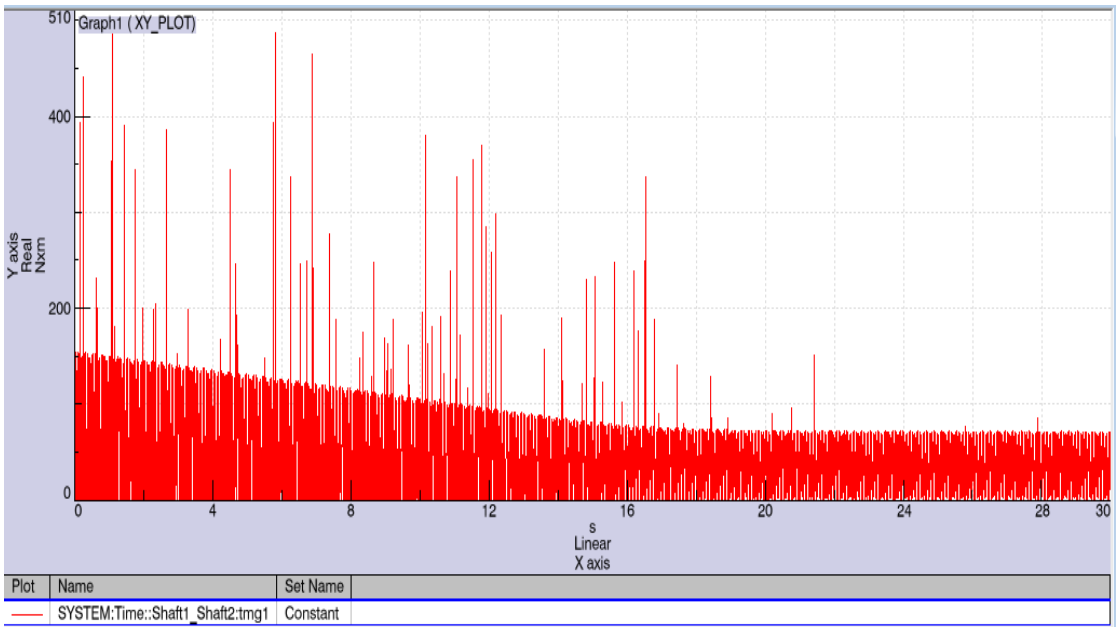

(a)

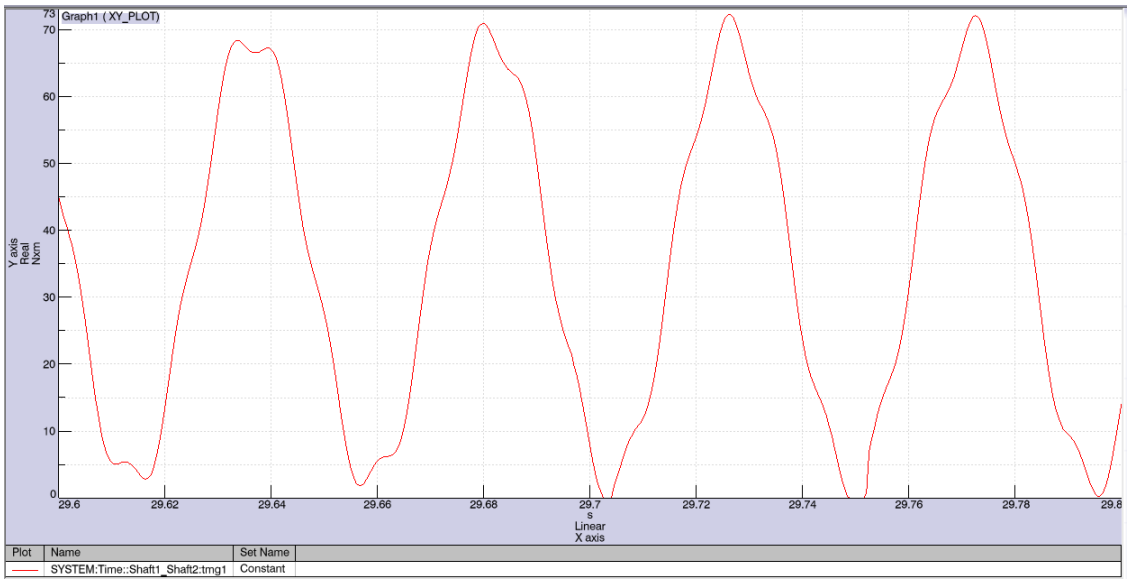

(b)

Figure 4-3: Plot of input shaft torque at 200 RPM.
(a) Overall, (b) Detailed

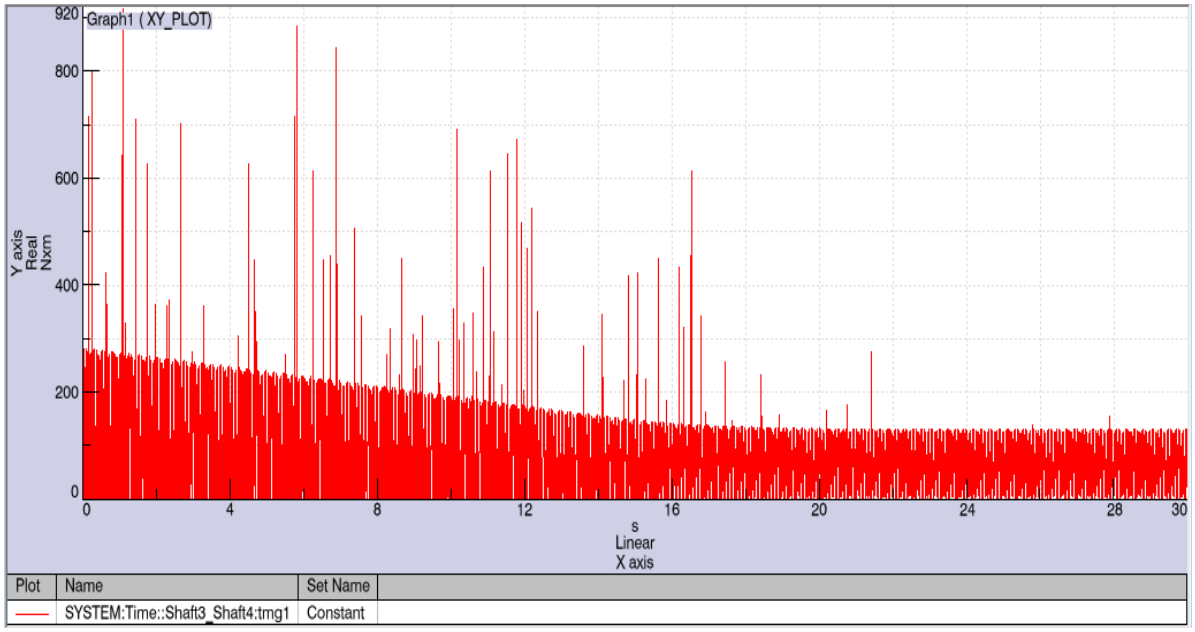

(a)

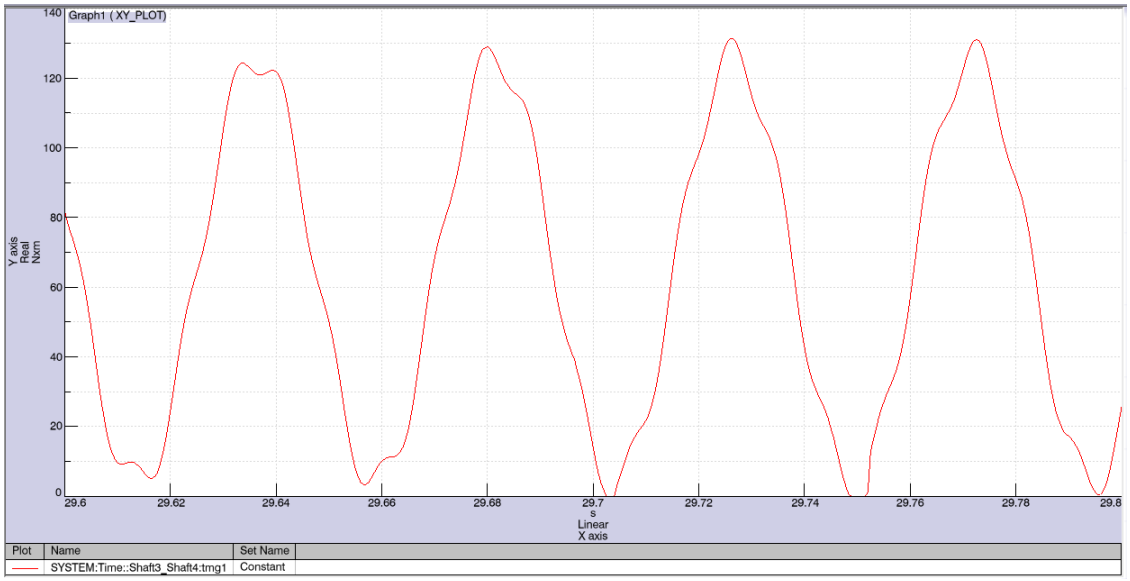

(b)

Figure 4-4: Plot of output shaft torque at 200 RPM.
(a) Overall, (b) Detailed

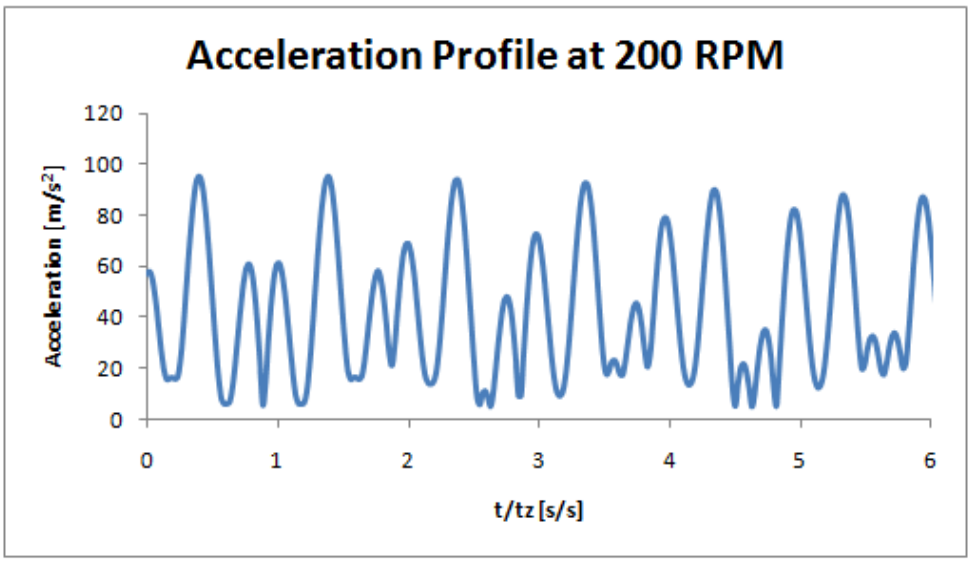

Figure 4-5: Acceleration profile during constant loading at 200 RPM.

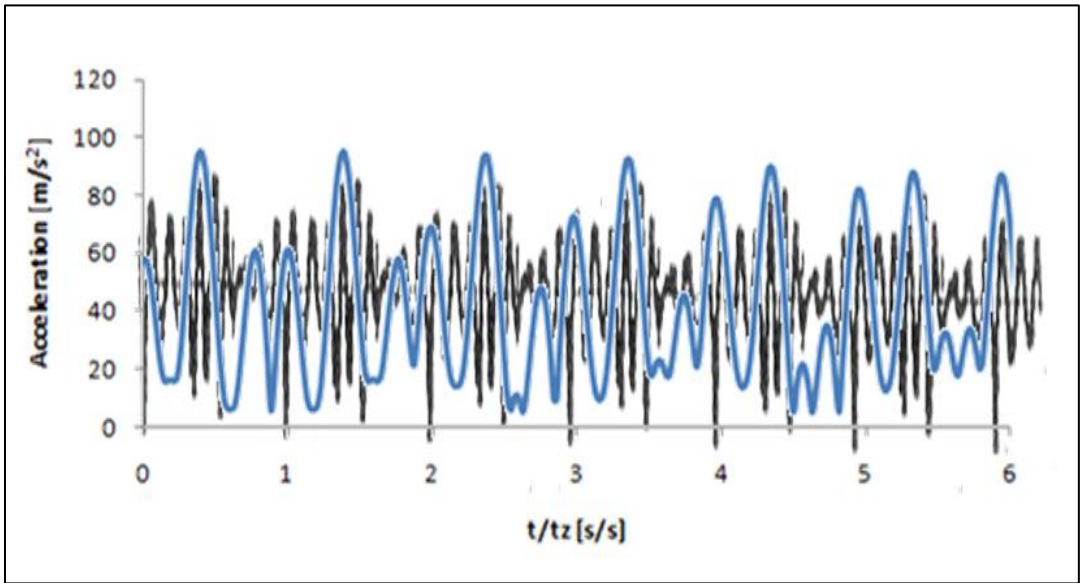

Figure 4-6: Overlay of Cai's experimental results and obtained virtual results for acceleration vibration waveform at 200 RPM.

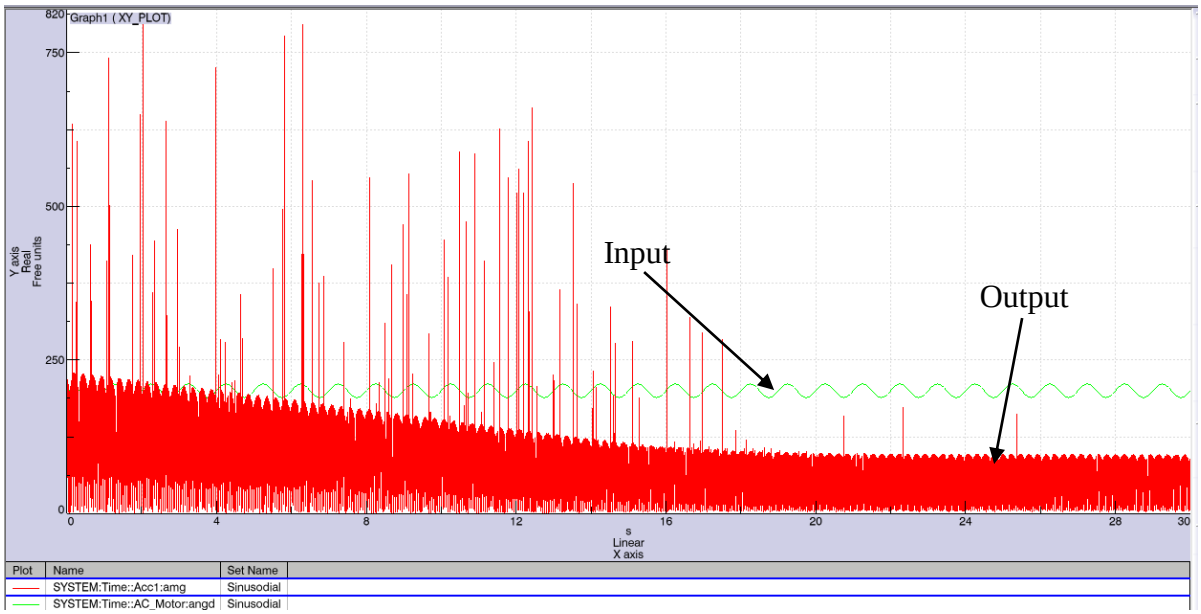

Figure 4-7: Plot of input and output for sinusoidal wave with highest frequency and amplitude.

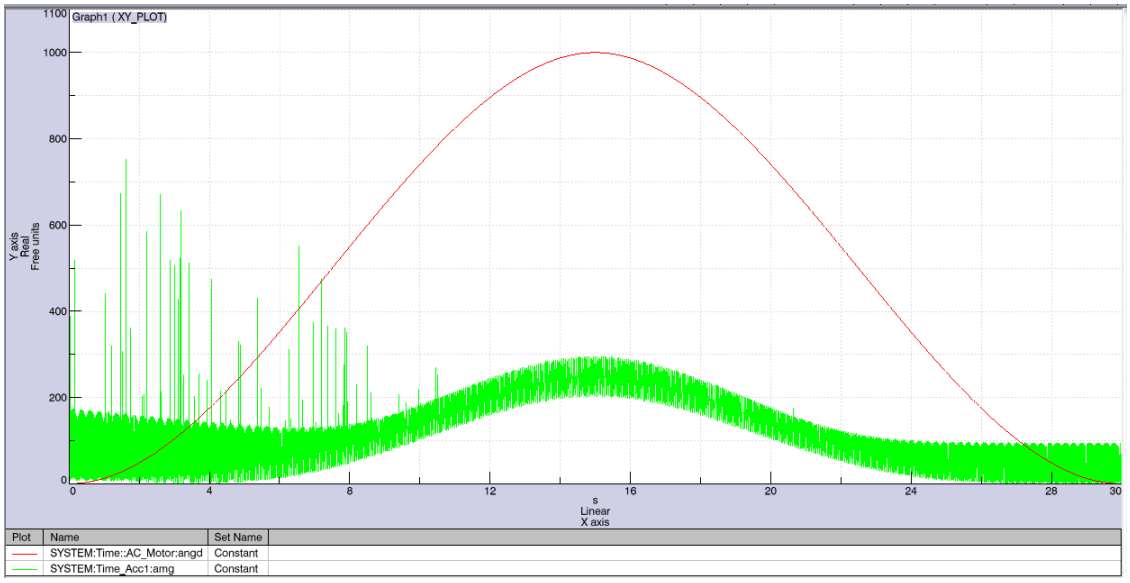

Figure 4-8: Plot of acceleration and driver input at 1000 RPM.

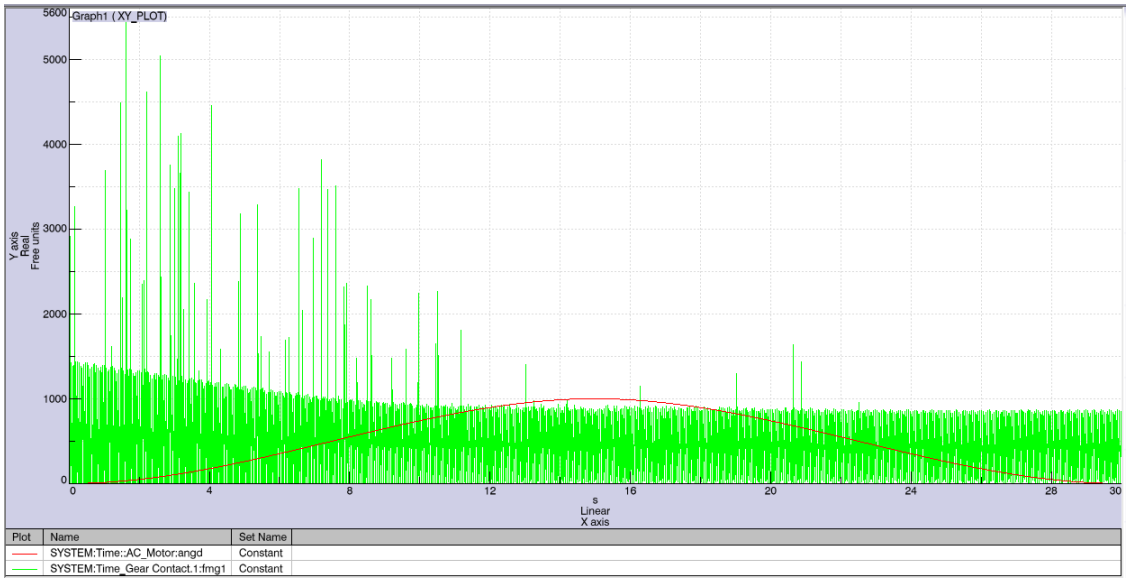

Figure 4-9: Plot of gear contact force and driver input at 1000 RPM.

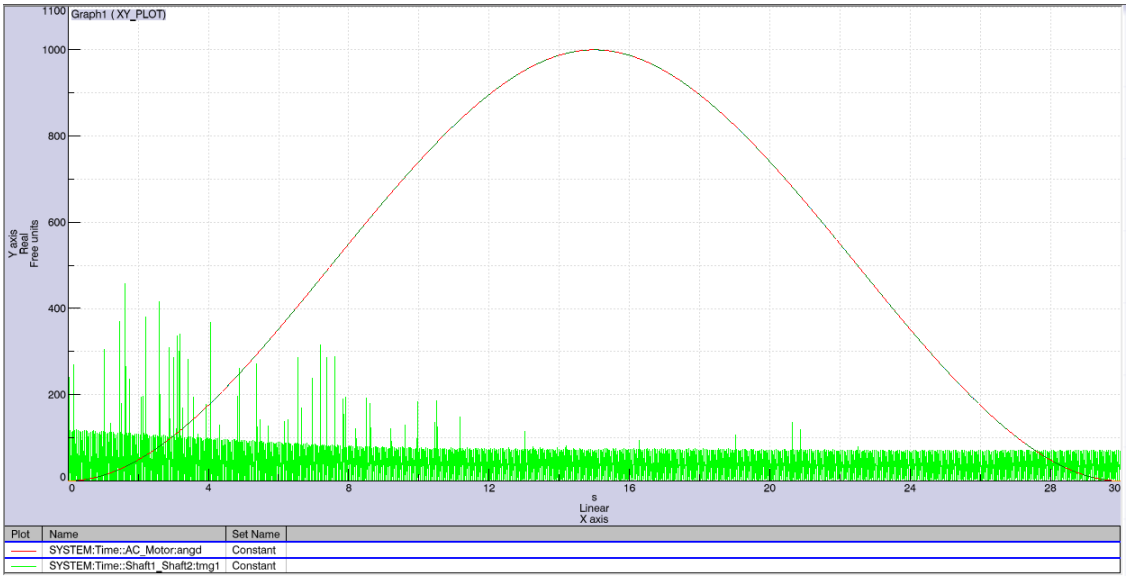

Figure 4-10: Plot of input shaft torque and driver input at 1000 RPM.

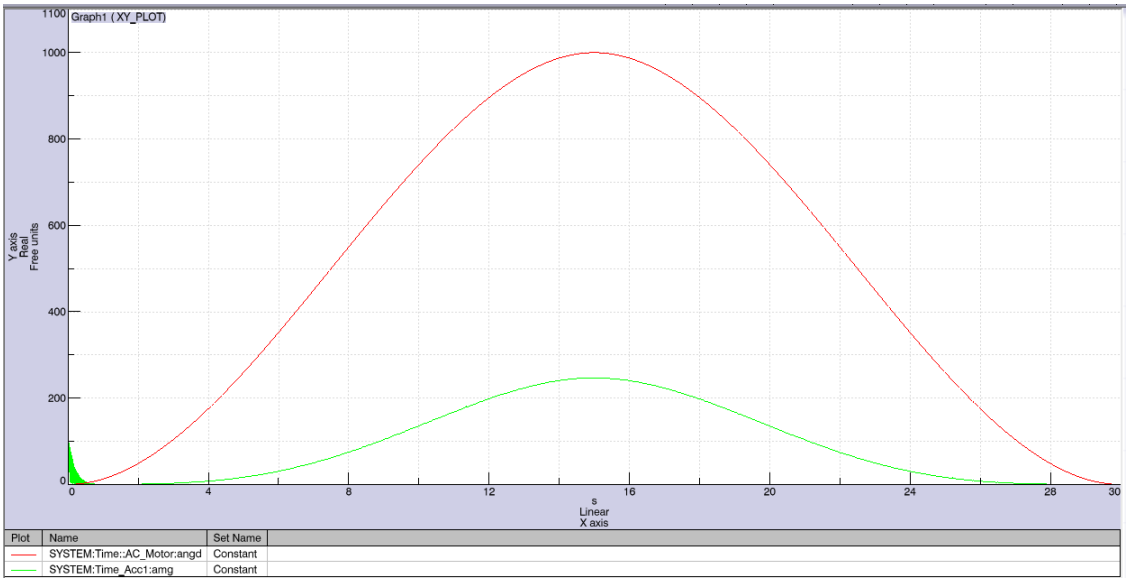

Figure 4-11: Plot of acceleration and driver input at 1000 RPM with damping.

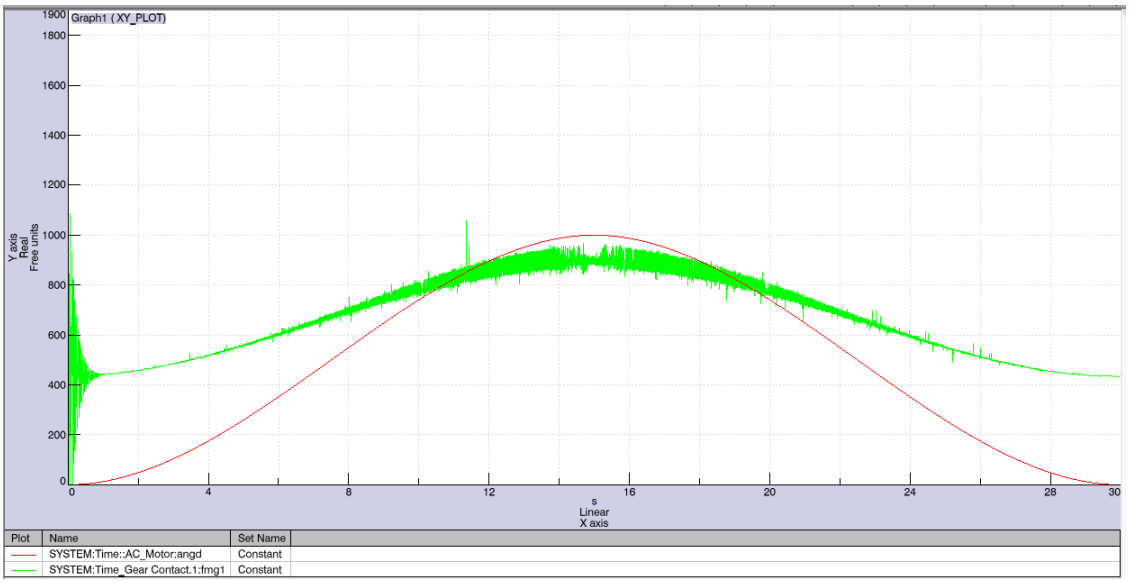

Figure 4-12: Plot of gear contact force and driver input at 1000 RPM with damping.

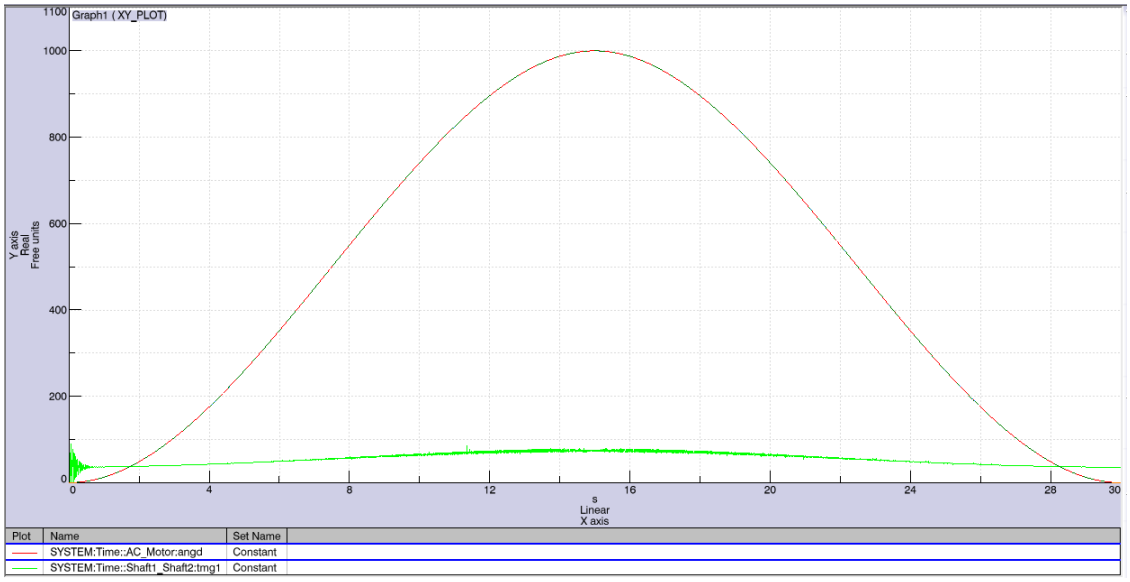

Figure 4-13: Plot of Input shaft torque and driver input at 1000 RPM with damping.

CHAPTER 5

DISCUSSION AND CONCLUSIONS

At the component level, it was expected that the output mimic, to some degree, the input frequencies and amplitudes. However, with the specified parameters, the simulation results suggest that quasi-steady variations at the component level input are washed out at the system level. This is particularly noteworthy for the sinusoidal input load cases as this response was completely unexpected.

From the above analysis, it is clear that the model is behaving in a manner such that the input, either steady or quasi-steady state, has little influence on the overall response of the system. Intuitively, one would assume that the difference in rotational velocity of 100 RPM for the constant load case would have had a greater influence on the system than what was observed. This is chiefly because it is a kinematically driven model, and as such, the driver will use whatever force and torque is necessary to overcome resistance. However, it was found that all of the observed calculated quantities for acceleration, gear contact force, and input and output torque showed no significant changes. This response would be expected, and greatly desired, at a typical systems level, but not at a component level. Since the model is built by from a component level, it was expected that the output would show some variations due to quasi-steady input. And because there were no significant changes, it may be that one or more assumptions made to build the model are insufficient.

Recall that some of the assumptions were made for simplification purposes as some of the necessary data needed were missing and had to be accounted for. These included not only mass, and inertia values, but where to apply them as well. This was not done arbitrarily, but using engineering judgment. For example, these properties were split between the gears and shafts using values calculated form CAD software. The model would no doubt improve if more details were known about the actual properties.

Another restrictive assumption was that damping was neglected altogether as it is difficult to proportion what components receive damping and to what extent. And as was seen, clearly damping had a significant impact on the behavior of the system. For the experiment, the overall damping was found by exciting the system via a hammer and measuring the decay, or damping ratio. However, to distribute the appropriate amounts to each force element in the virtual model is challenging. Perhaps a solution to this would be to set up a design of experiments for the simulation where the design variables are the damping constants in each RSDA and gear contact force element and the cost function is a function of the actual system's damping ratio. The system could then be impacted. After a number of iterations, with the appropriate limits and constraints are set, a solution could be found which would allow the virtual system to oscillate to a resting position just as the experimental model did. This would verify the dynamic response of the virtual model on whether or not it is behaving properly.

Another method to improve verification would have been to compute the fast Fourier transform (FFT), which converts a vibration profile into a series of sine waves and is useful in determining the predominant frequency, at several discrete RPM levels and thus build a frequency range plot. With this information, the predominant frequencies at each of the runs would ideally correlate with the experimental results. This was actually put into practice after the first results were obtained. It was seen that the virtual model corresponded accordingly at low RPM, but not at higher levels. This yet again illustrates that the system is behaving as a low-pass filter.

Therefore, with the above discussion, it may be said that the systems level response is just a coincidence. The data collected offer little usefulness by themselves as they do not describe an accurate system response. With that being said, it is also true that there is no such thing as bad data, only bad assumptions which gave the data. Regardless of the outcome, the data tell engineers information, and it is then up to the engineer to make deductions based on the data. For this study, what has been found is that particular

attention must be given to model parameters, especially damping. Without knowing what the proper parameters are and where to apply them leads to the development of an inaccurate model. Therefore, accurately incorporating these parameters is the first step to improving the virtual model.

CHAPTER 6

RECOMMENDATIONS

It is recommended that this research not cease upon the author's graduation. Rather, more investigation should be undertaken to try and improve the model such that it can more accurately represent Cai's experiments. Some suggested areas for improvement are obviously the gear contact and the braking RSDA elements. It seems that these two elements, although currently are able to describe the system response semi-accurately for low RPM, steady loading, do not allow the system to behave as expected for quasi-steady loading. Another area for improvement is in the parameterization variables. The author took some liberty in assigning values to the bodies which there were no data for. Although it was not arbitrary, there was still some estimation as how to distribute the mass and inertia values appropriately. Finding the actual values and locations would have a tremendous impact. And damping was neglected entirely. Perhaps a method to include the overall system's known damping ratio would have helped eliminate some error. But, as discussed in preceding chapters, damping is usually a system measurement and is difficult to apply to specific areas if the system is even moderately complex.

If the above recommendations are implemented and have the desired effect, the final suggestion is that the model be upgraded and improved on. Currently, it is just a rigid body, kinematic model. Changing the revolute joints to bushing elements would add compliance to the system and make it more realistic. However, the drawback is that more parameters will be needed to do so, but the gain in model performance could well be worth the extra effort.

APPENDIX

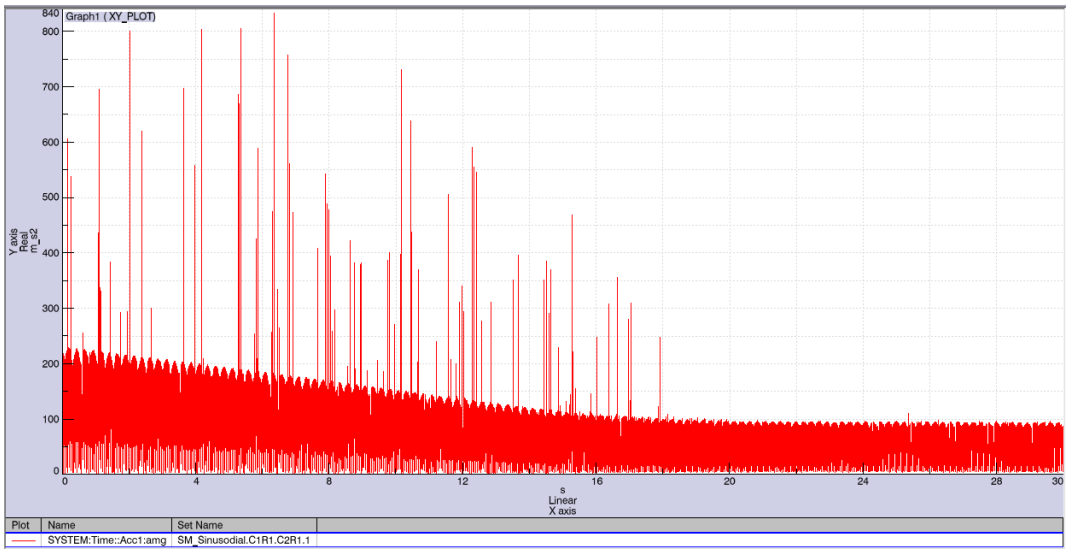

(a)

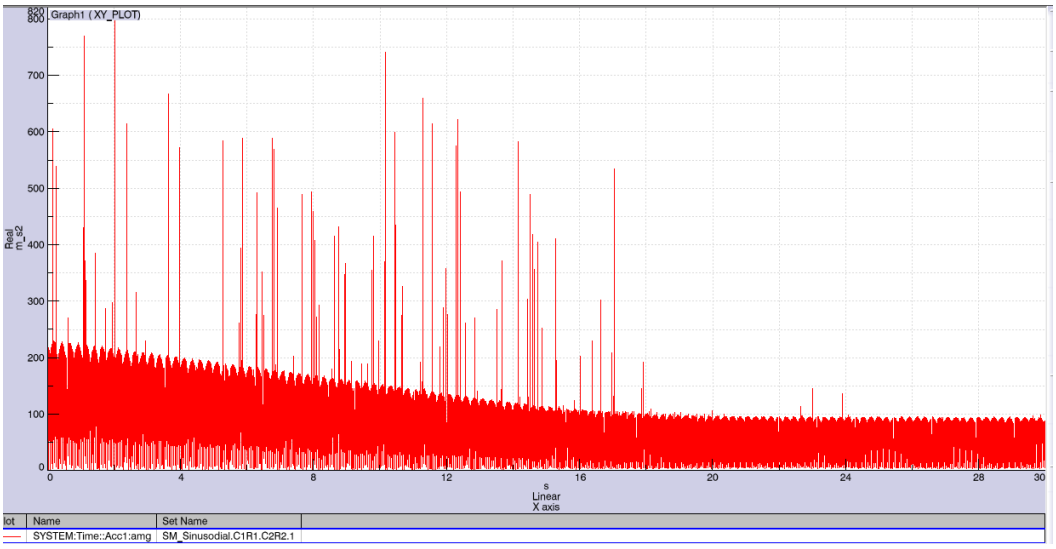

(b)

Figure A-1: Acceleration outputs for sinusoidal runs (m/s^2 vs. time): (a) through (i) are runs 1 through 9, respectively.

Figure A-1 continued

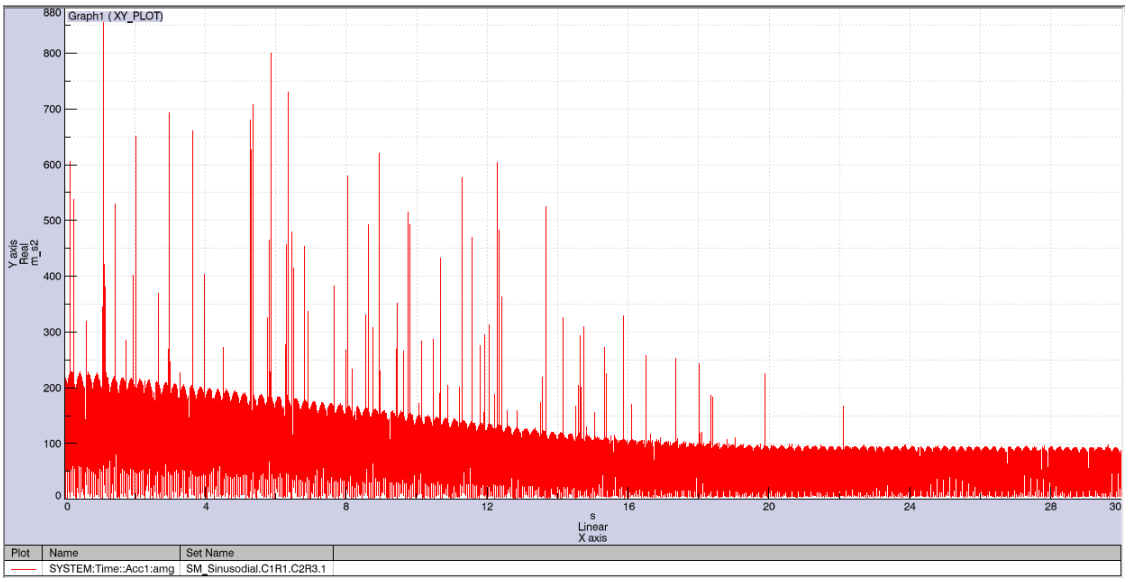

(c)

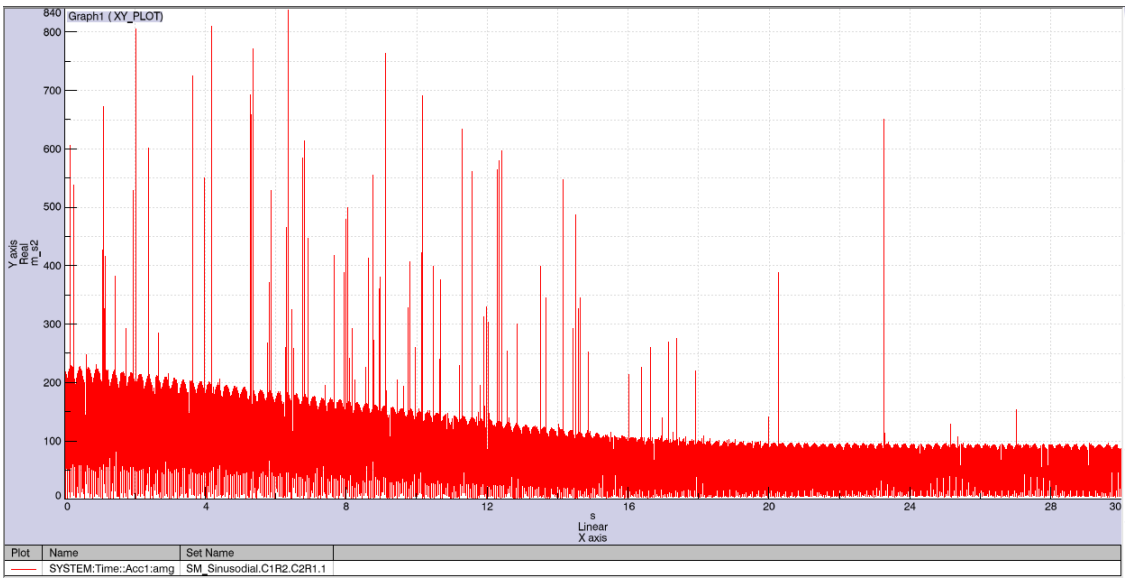

(d)

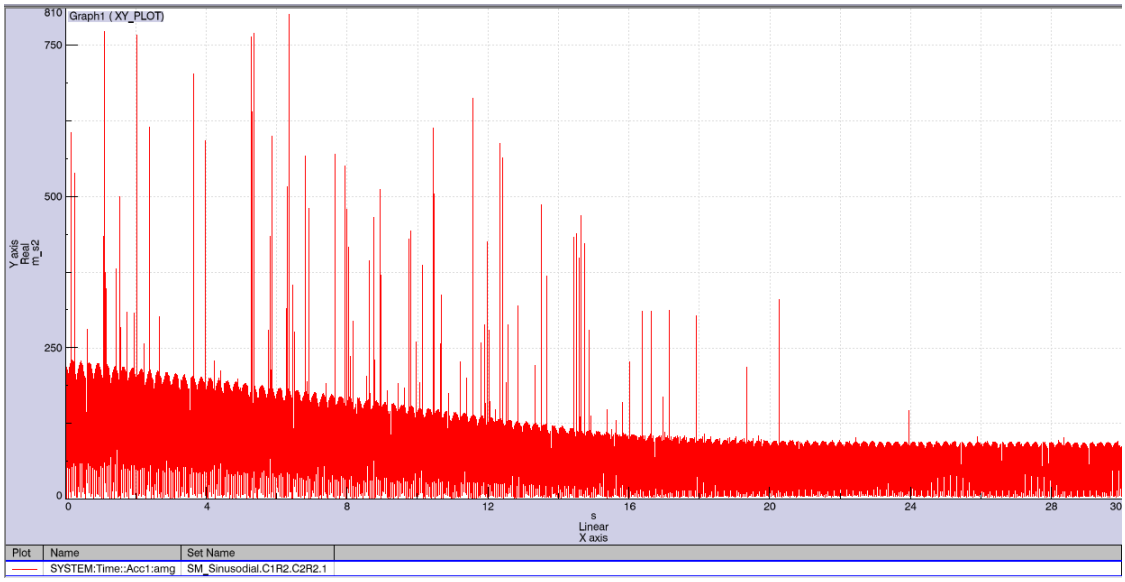

(e)

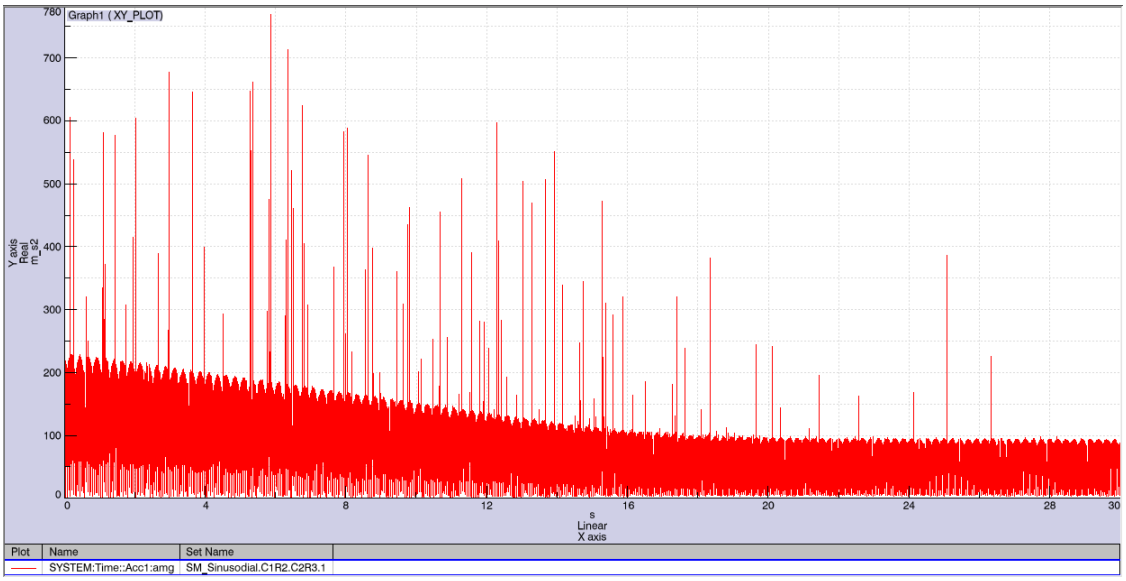

(f)

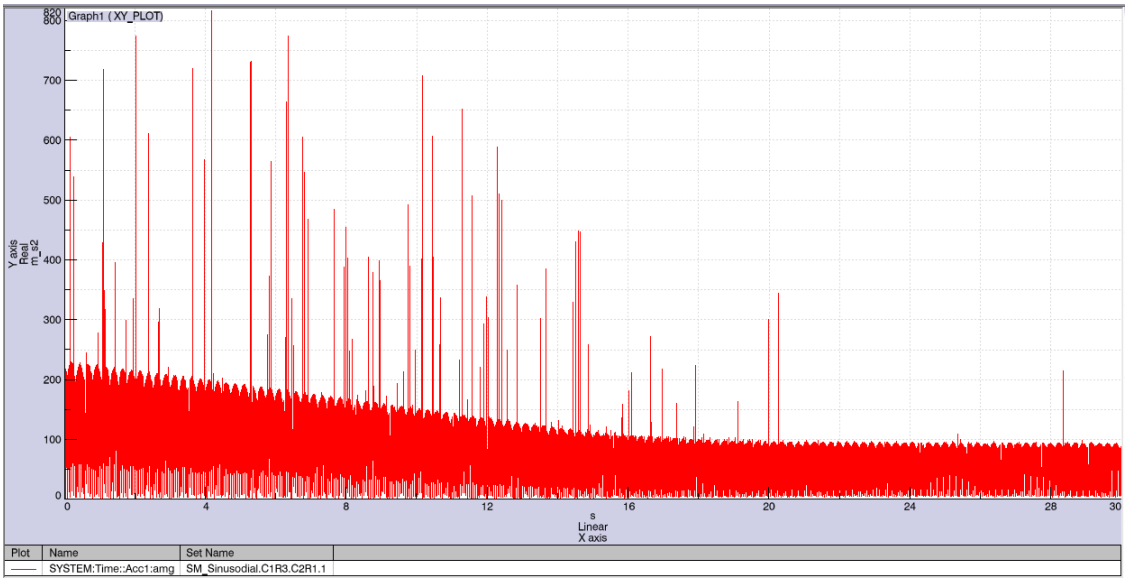

(g)

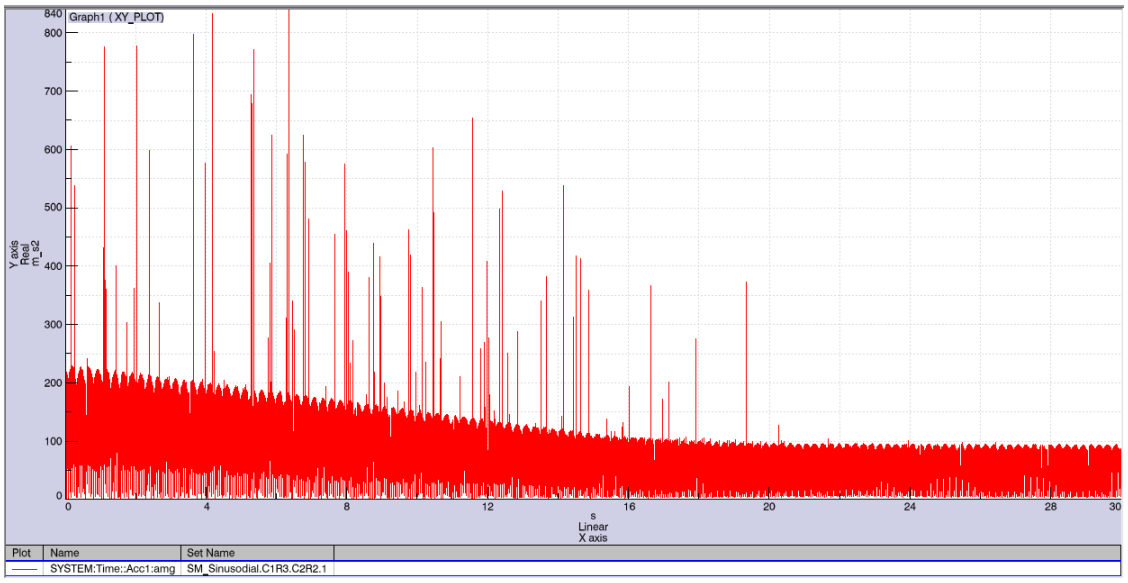

(h)

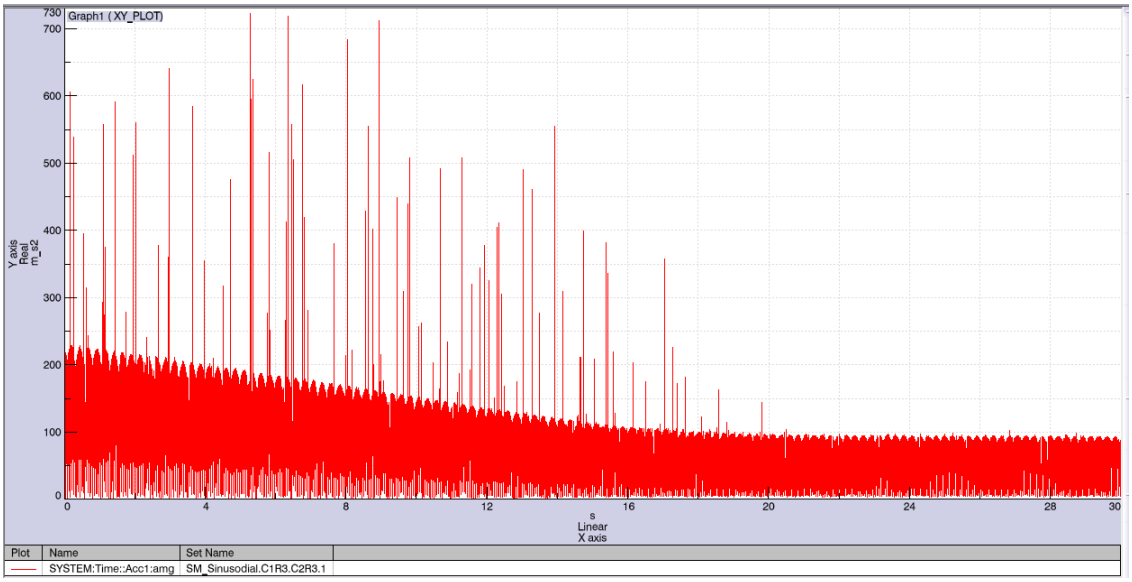

(i)

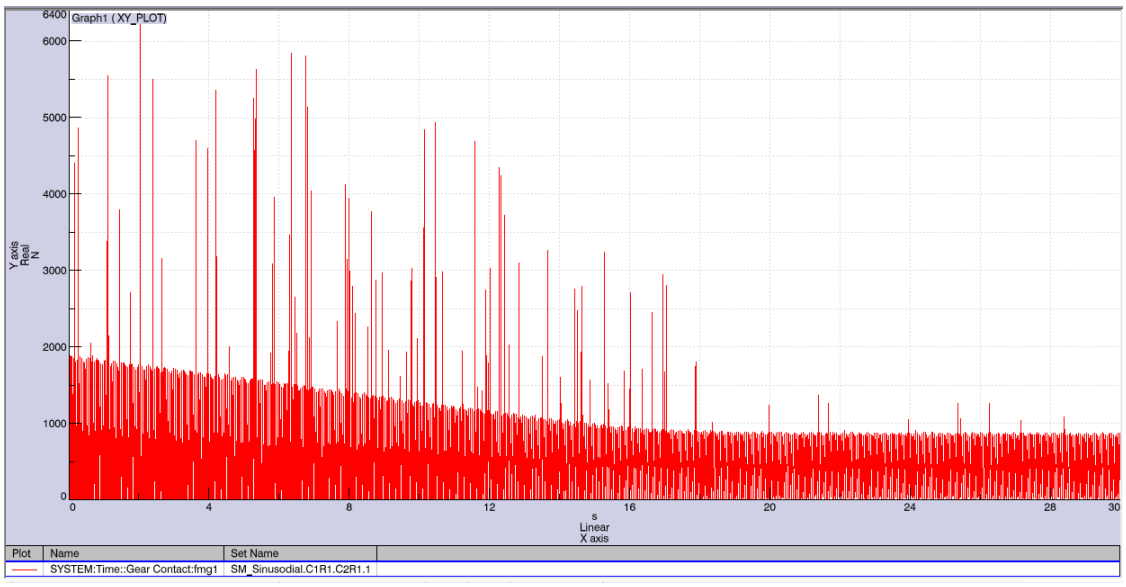

(a)

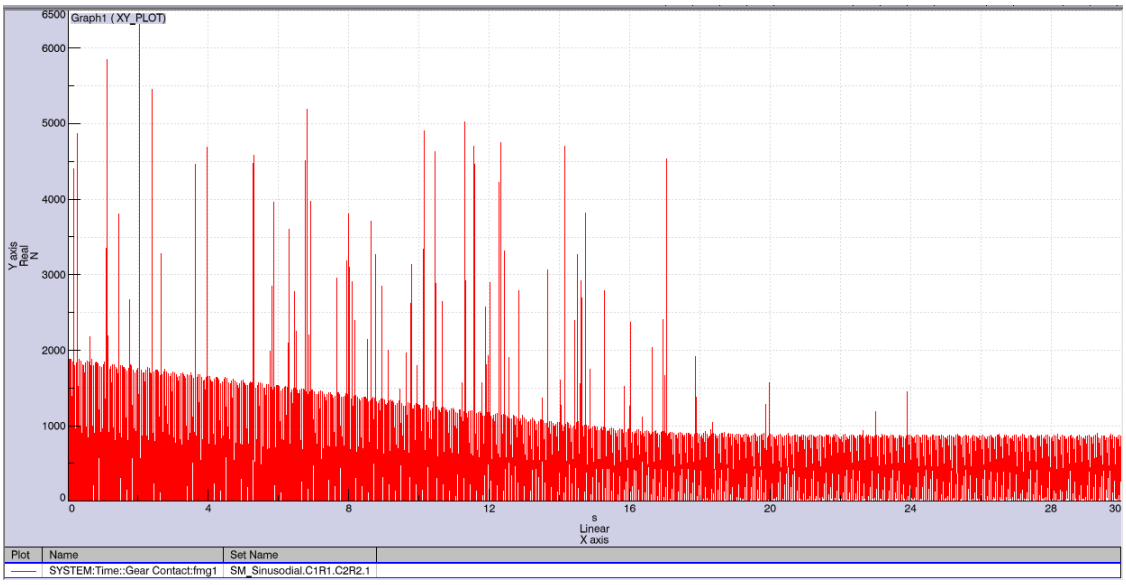

(b)

Figure A-2: Gear contact force outputs for sinusoidal runs (N vs. time): (a) through (i) are runs 1 through 9, respectively.

Figure A-2 continued

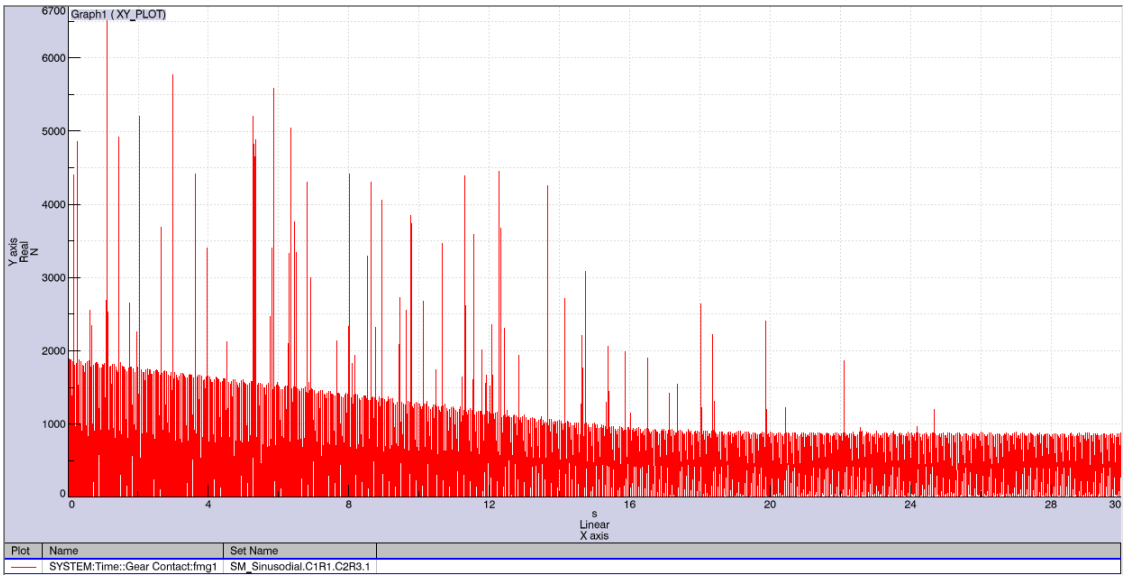

(c)

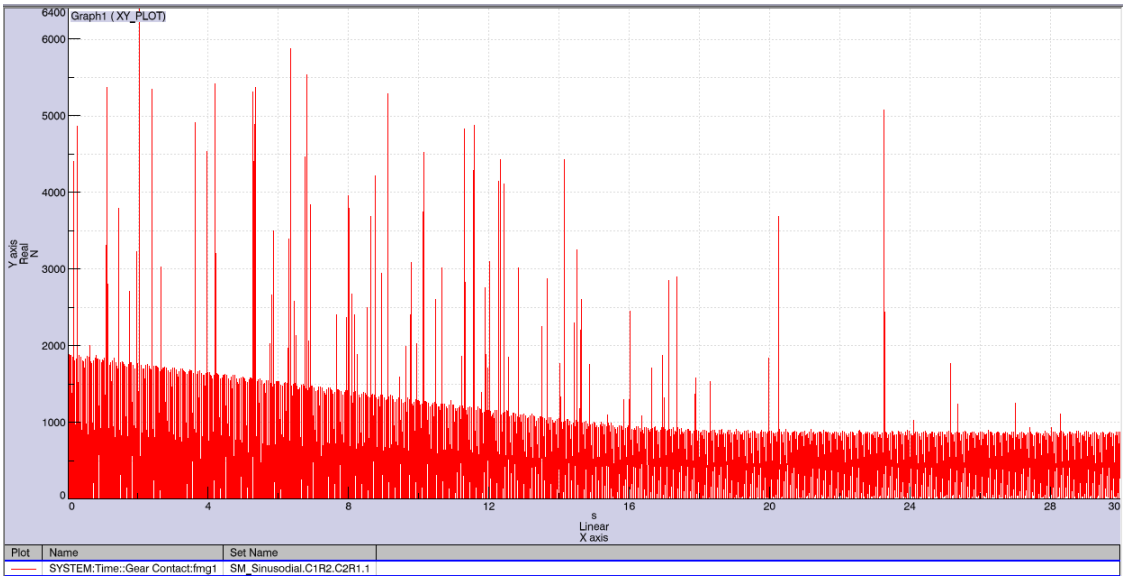

(d)

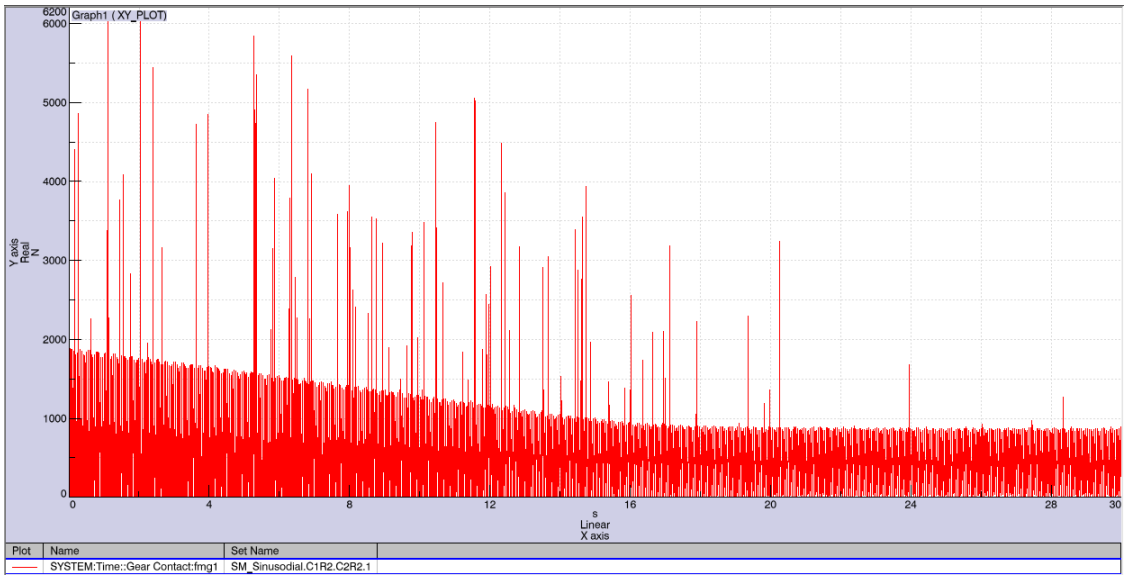

(e)

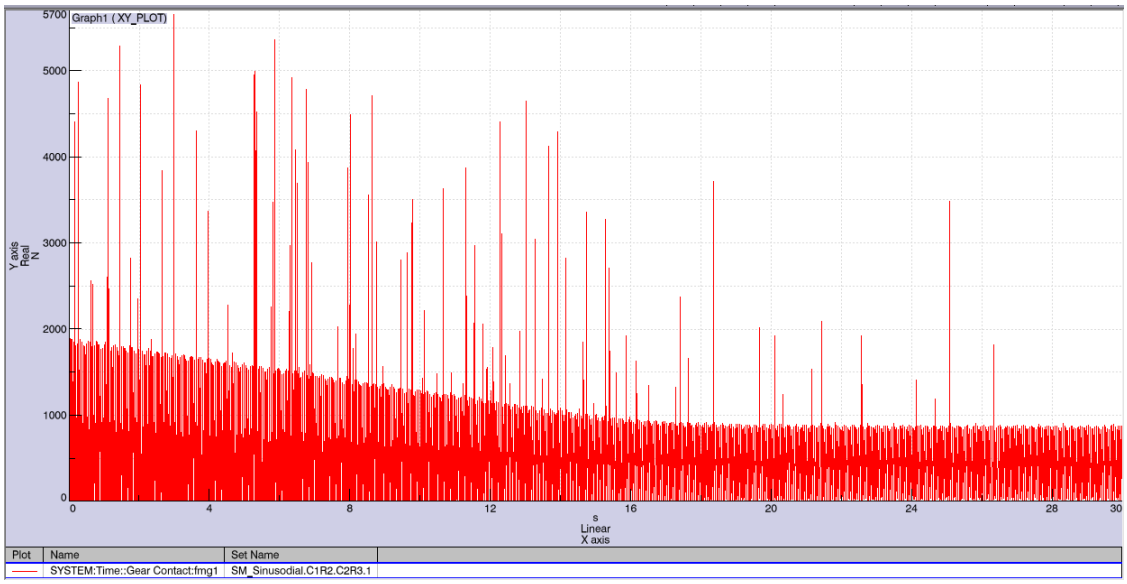

(f)

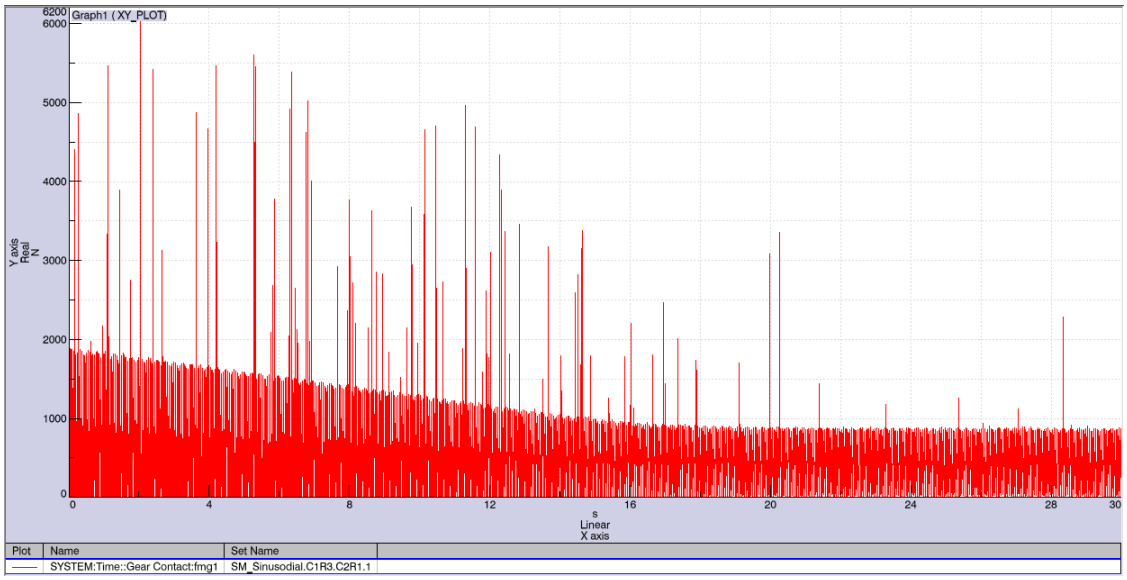

(g)

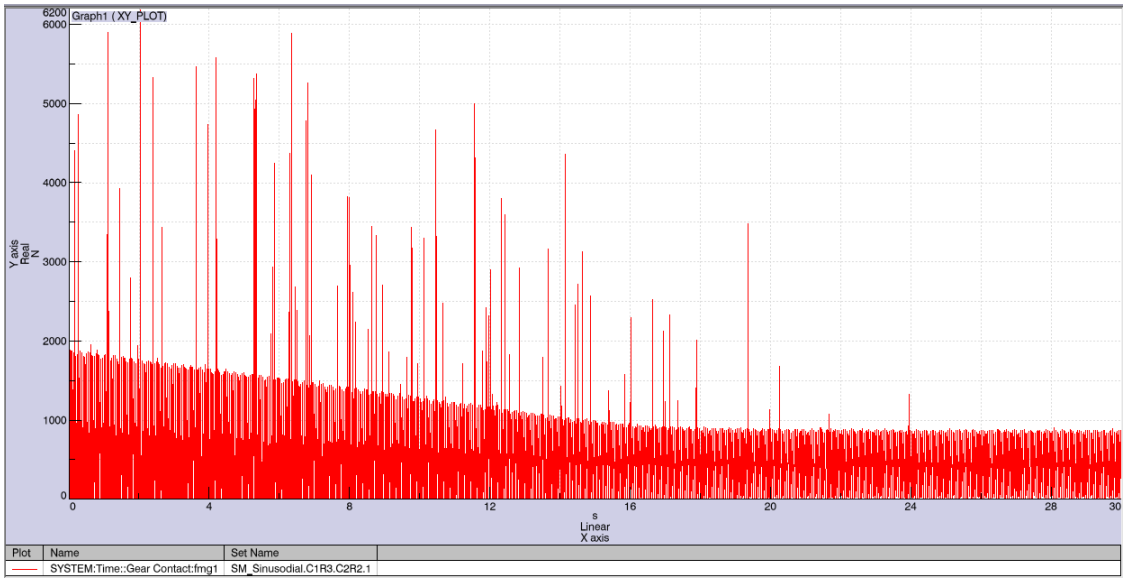

(h)

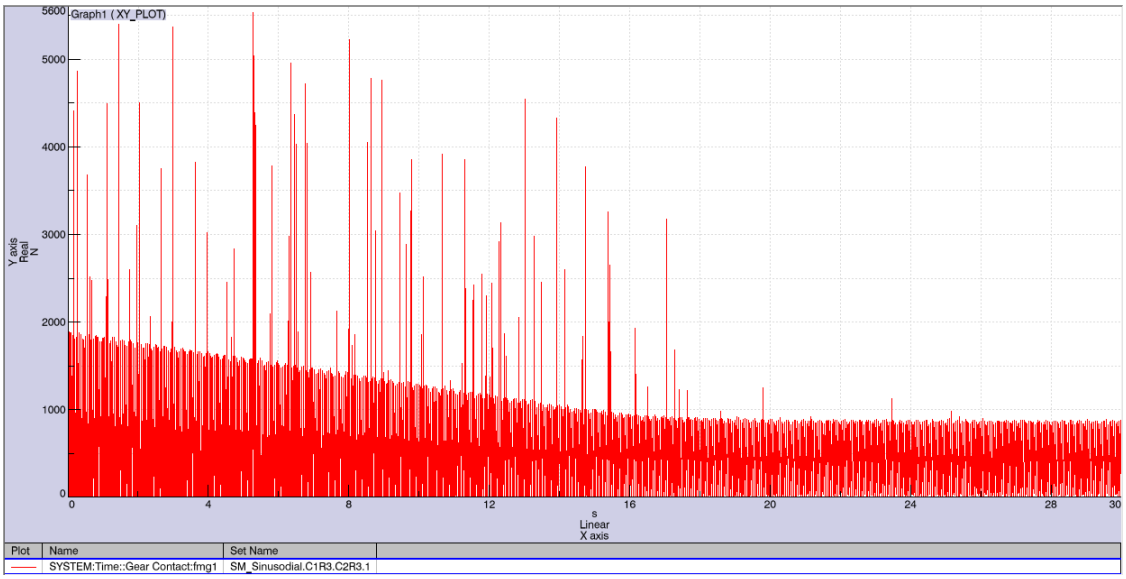

(i)

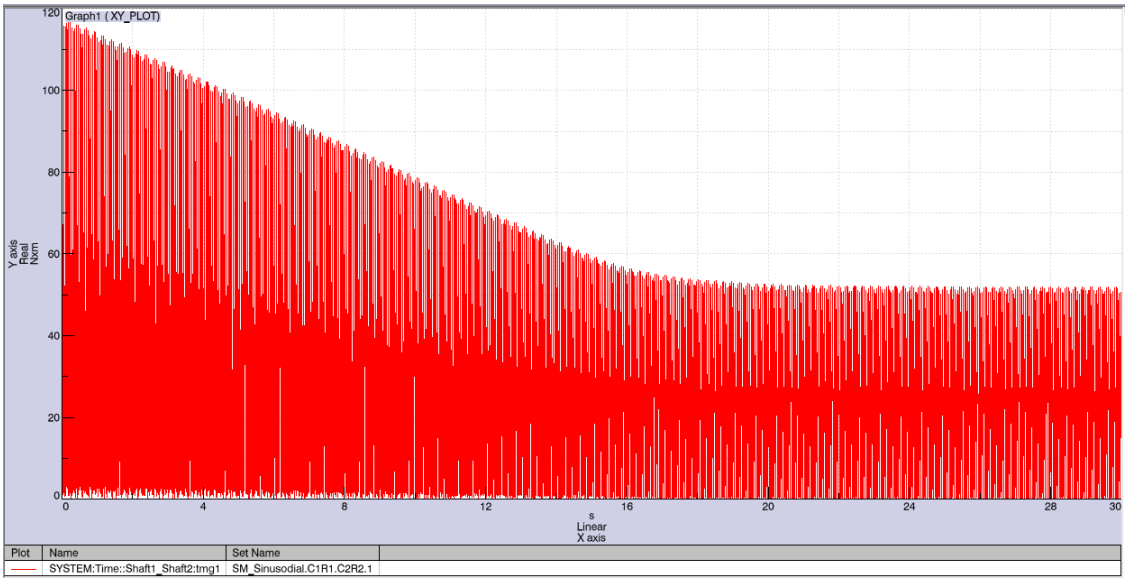

(a)

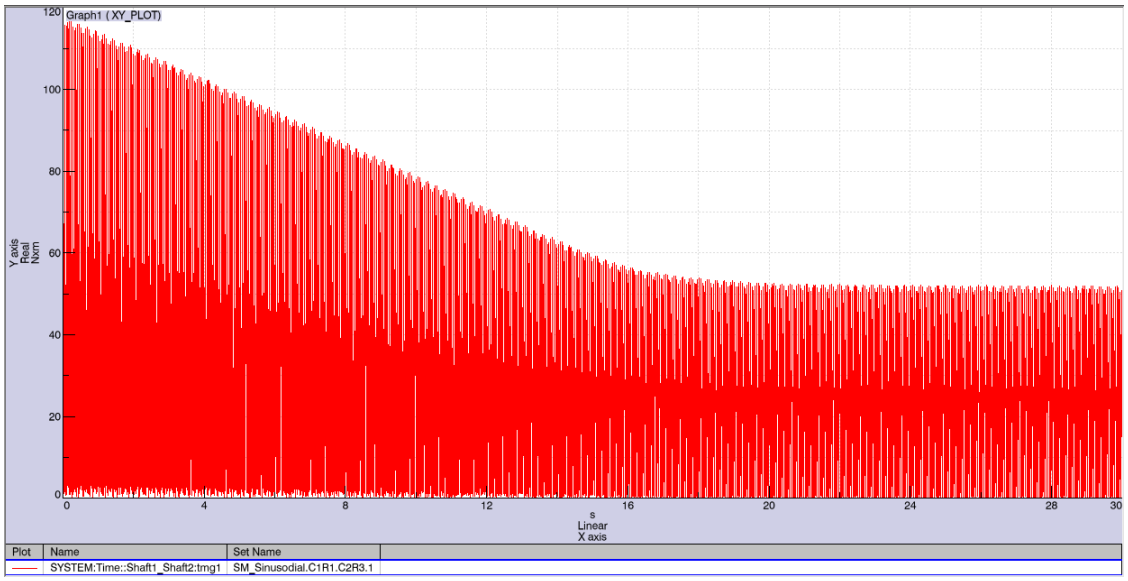

(b)

Figure A-3: Input shaft moments for sinusoidal runs (Nm vs. time):
(a) through (i) are runs 1 through 9, respectively.

Figure A-3 continued

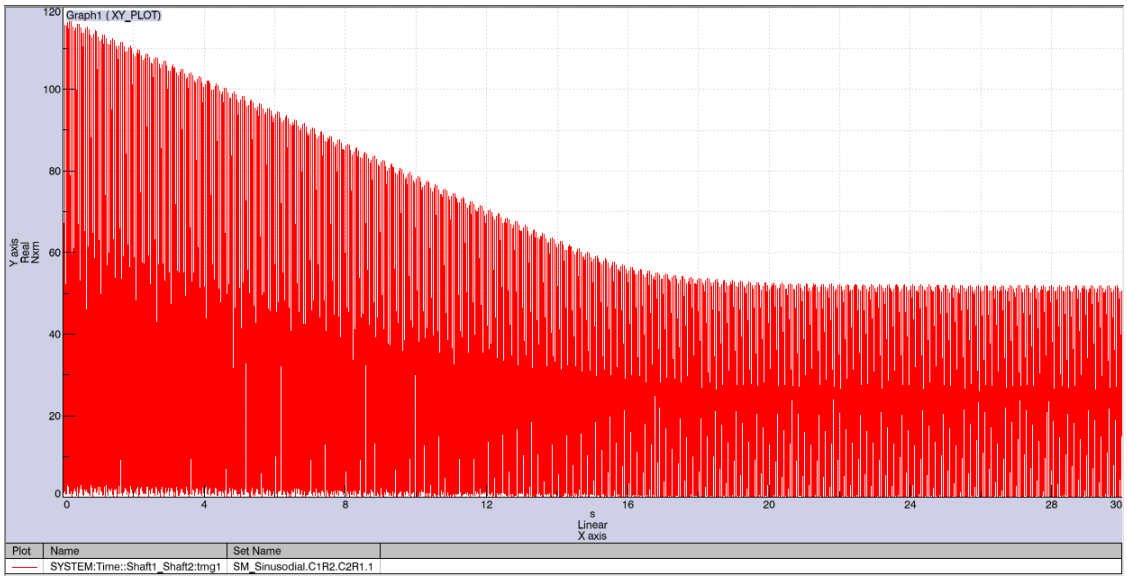

(c)

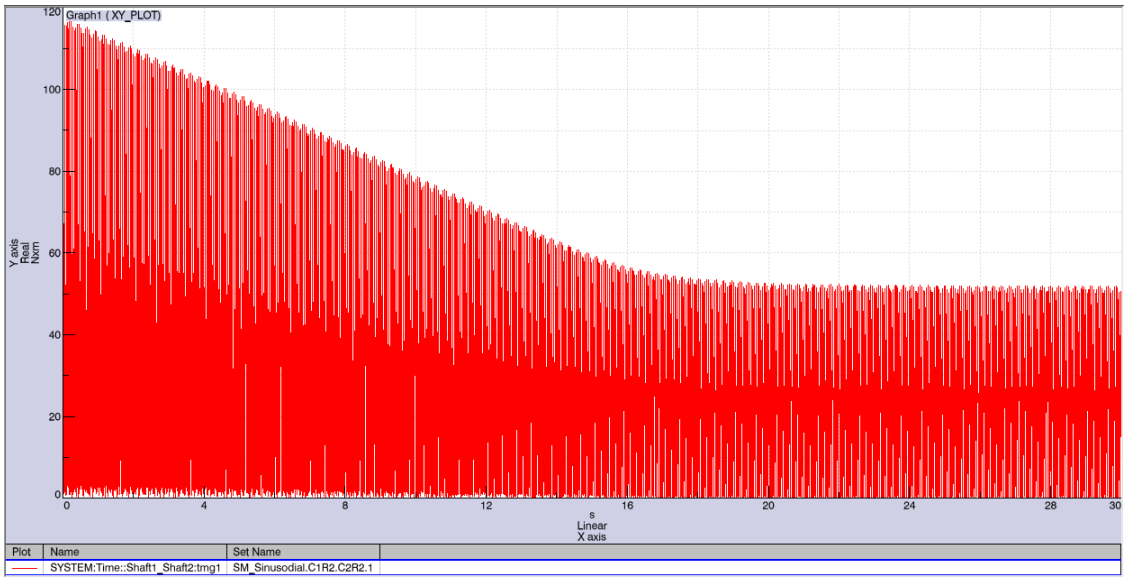

(d)

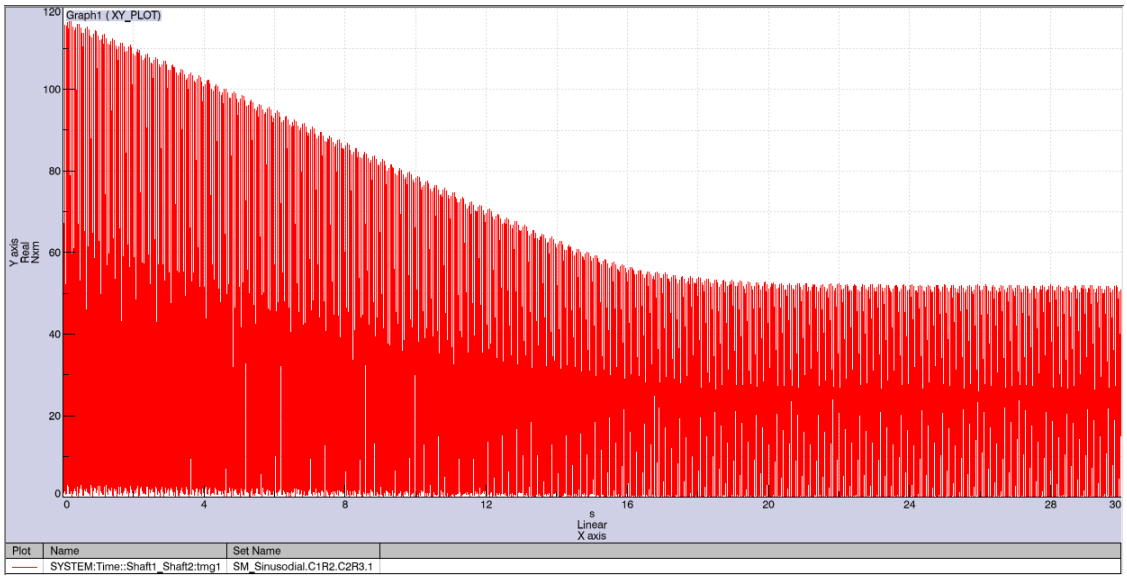

(e)

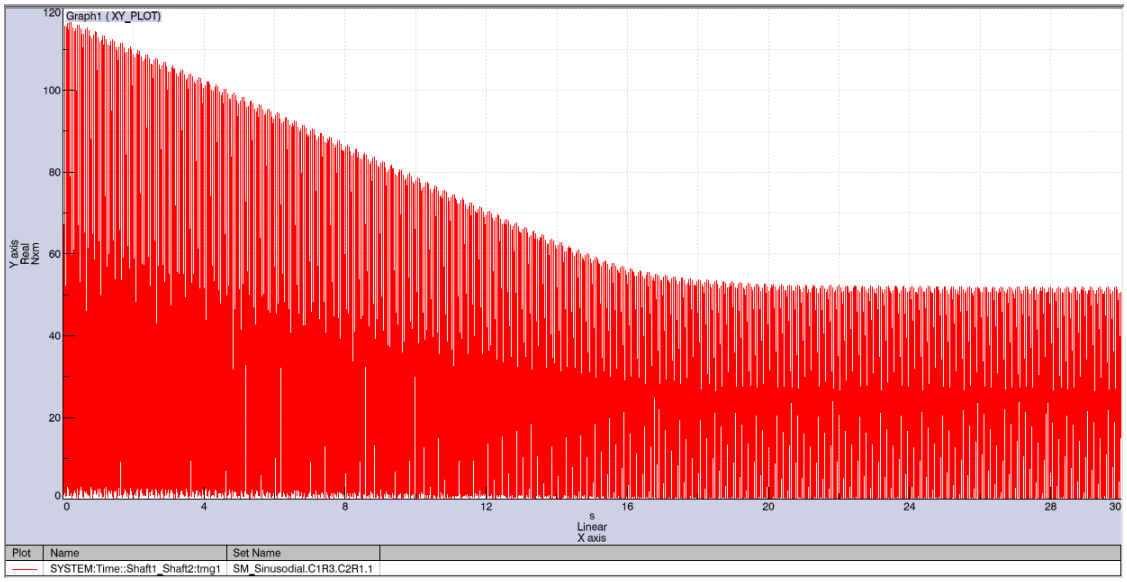

(f)

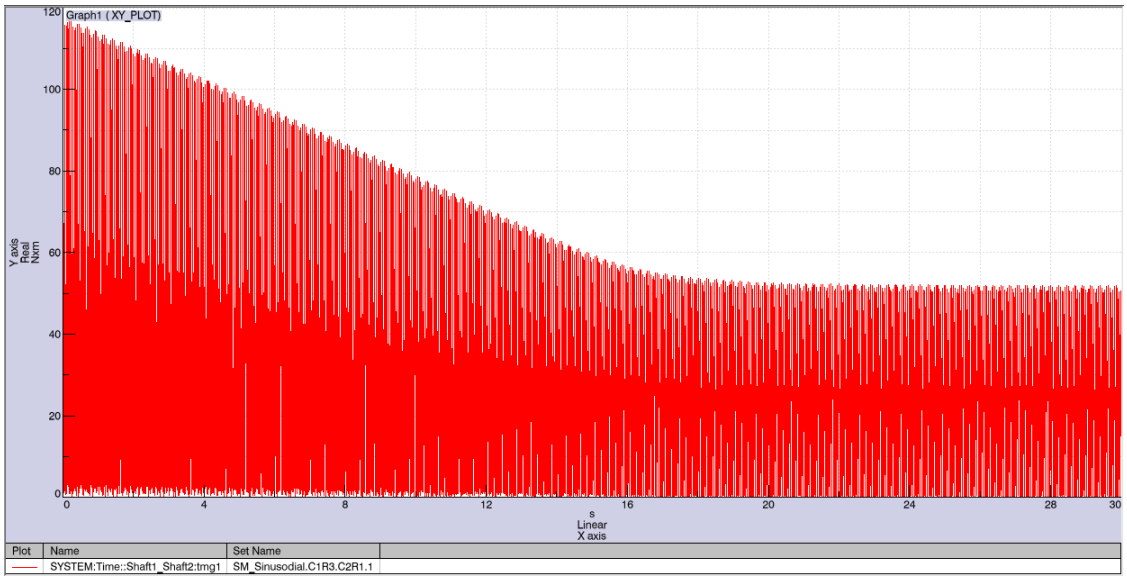

(g)

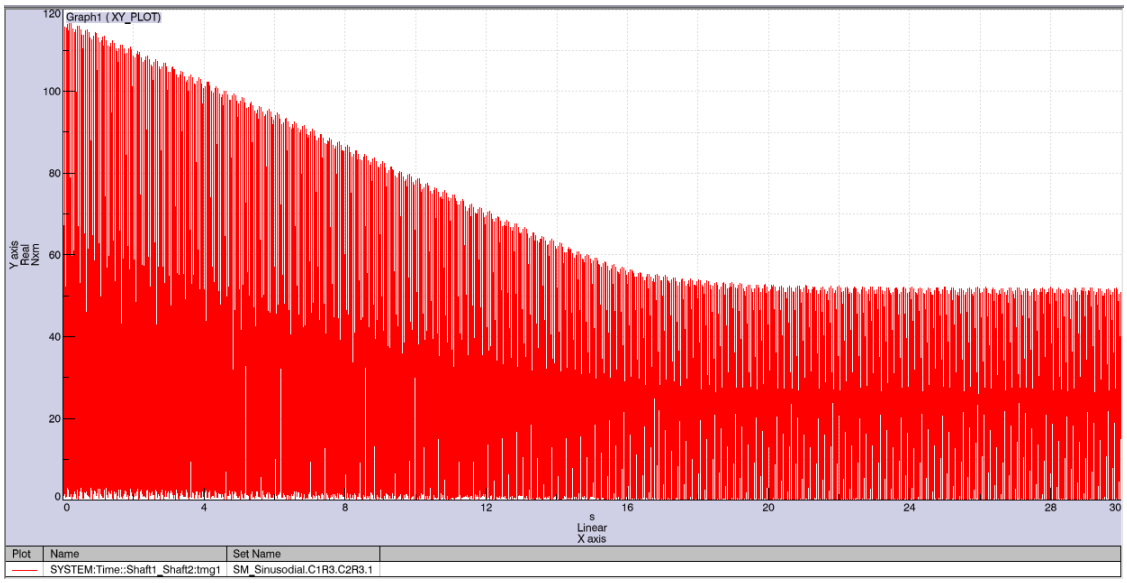

(h)

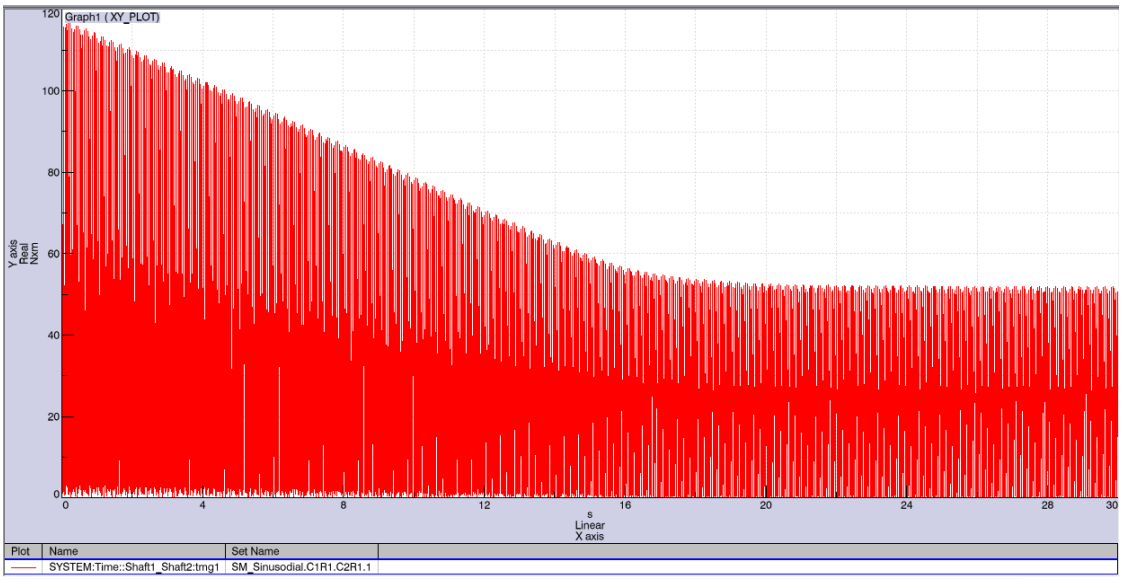

(i)

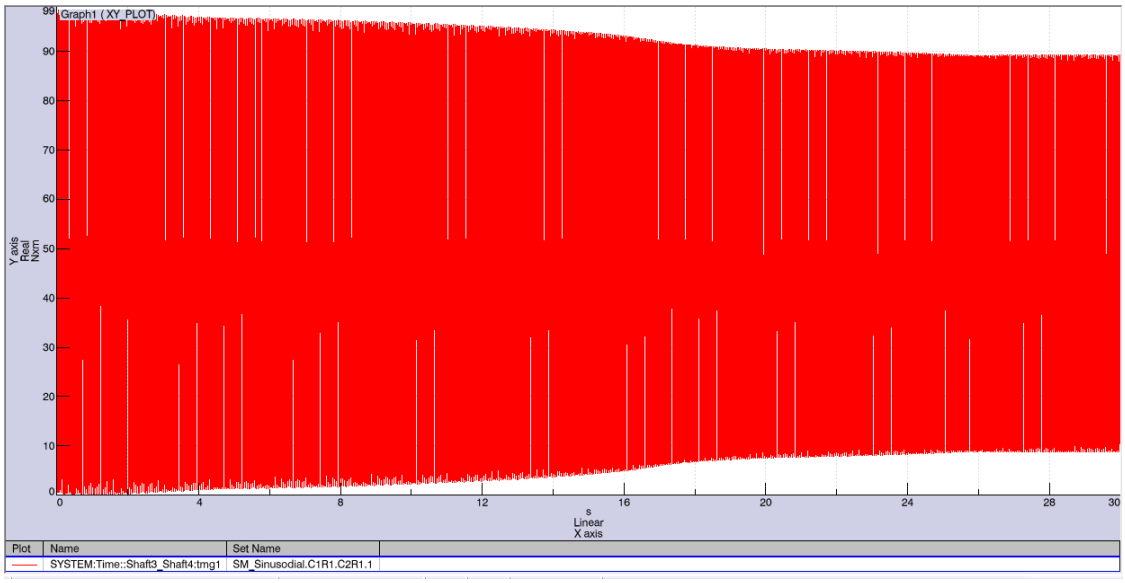

(a)

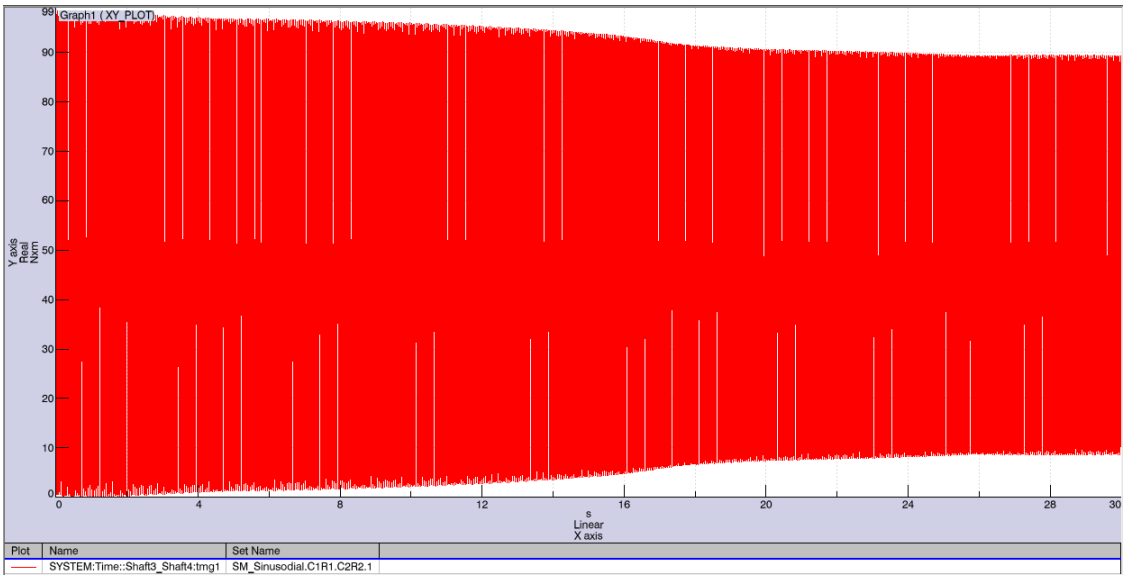

(b)

Figure A-4: Output shaft moments for sinusoidal runs (Nm vs. time): (a) through (i) are runs 1 through 9, respectively.

Figure A-4 continued

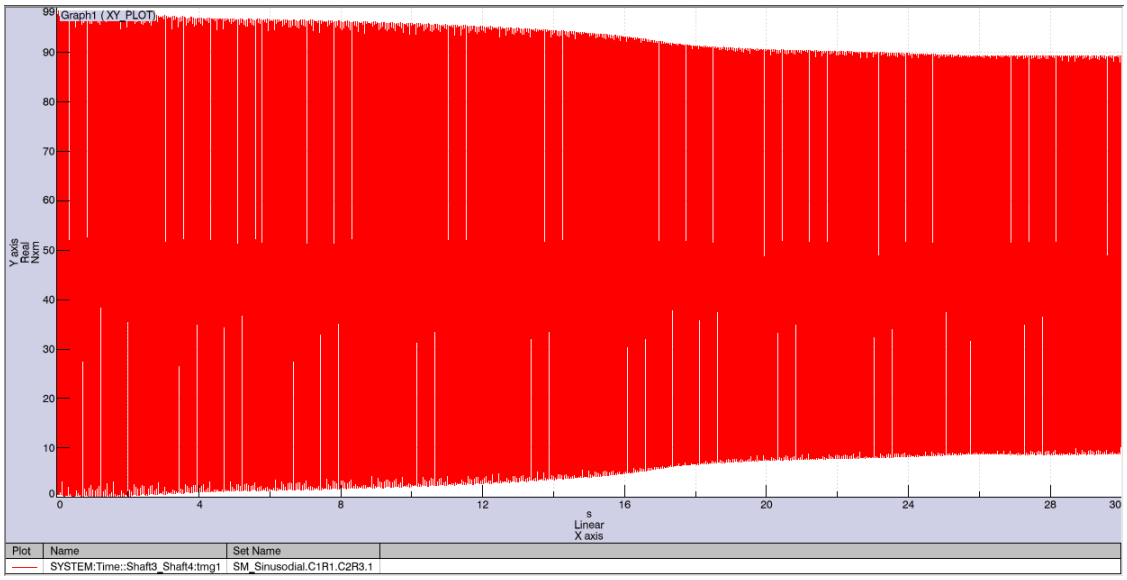

(c)

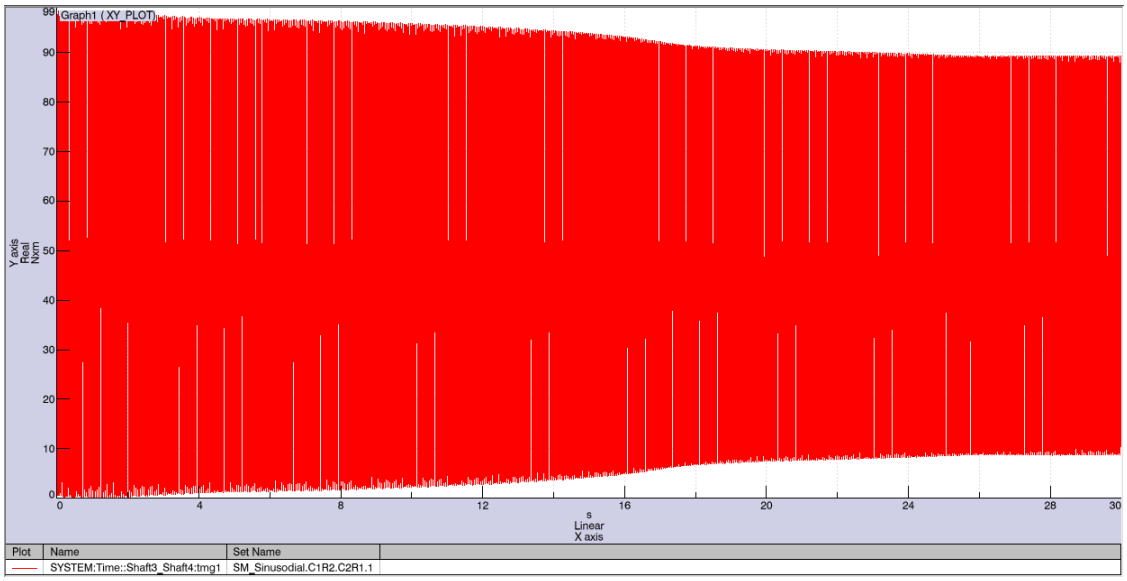

(d)

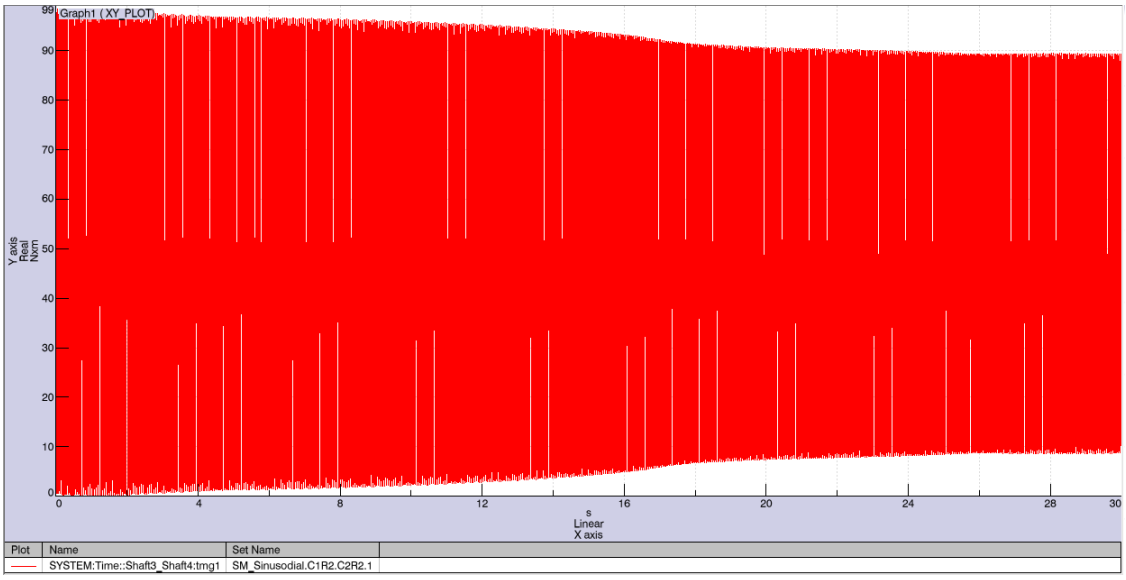

(e)

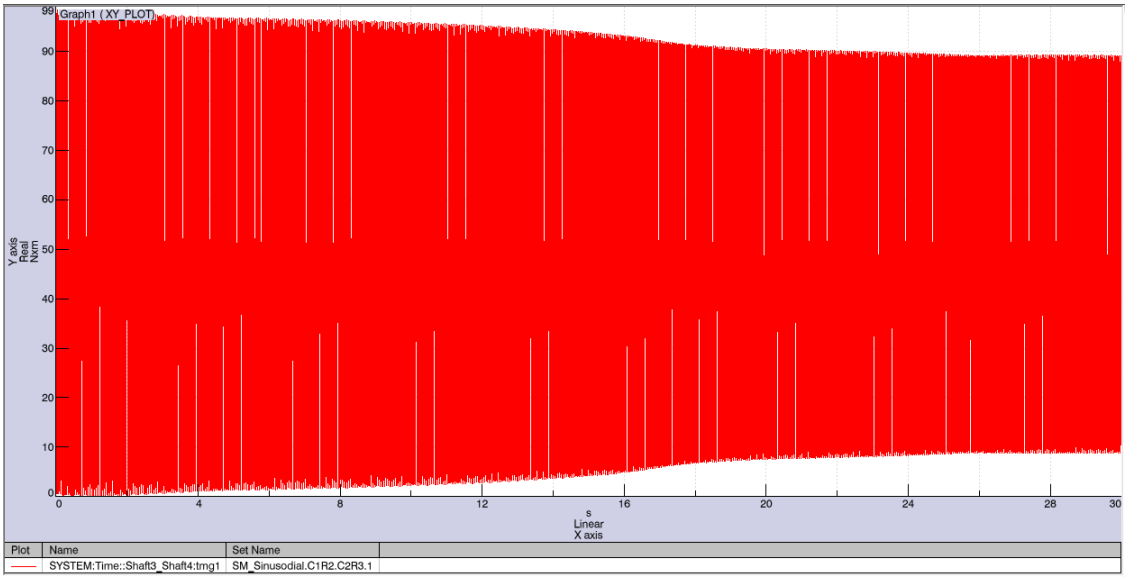

(f)

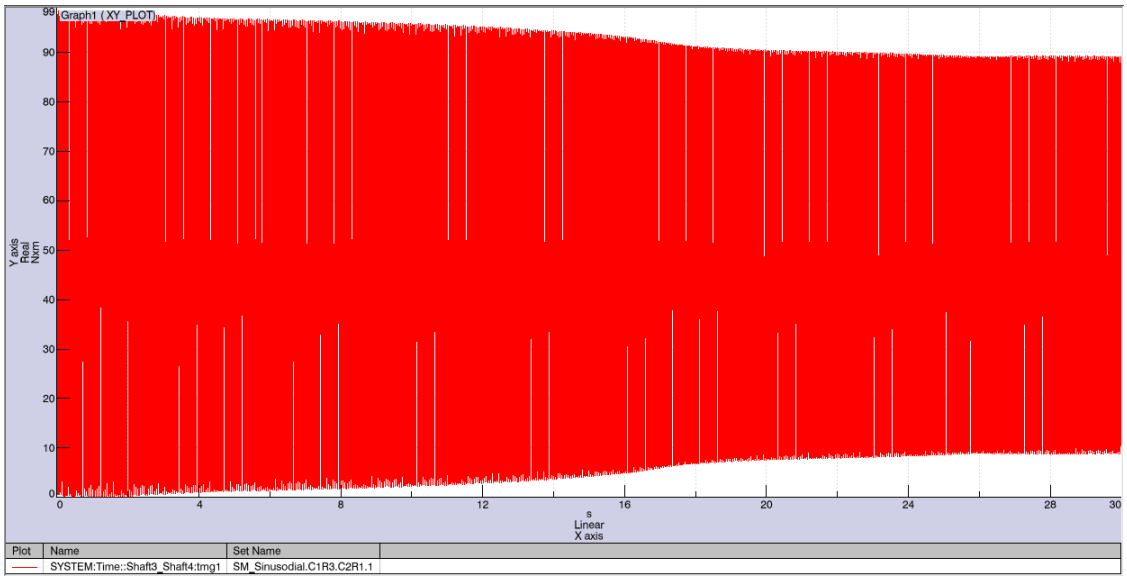

(g)

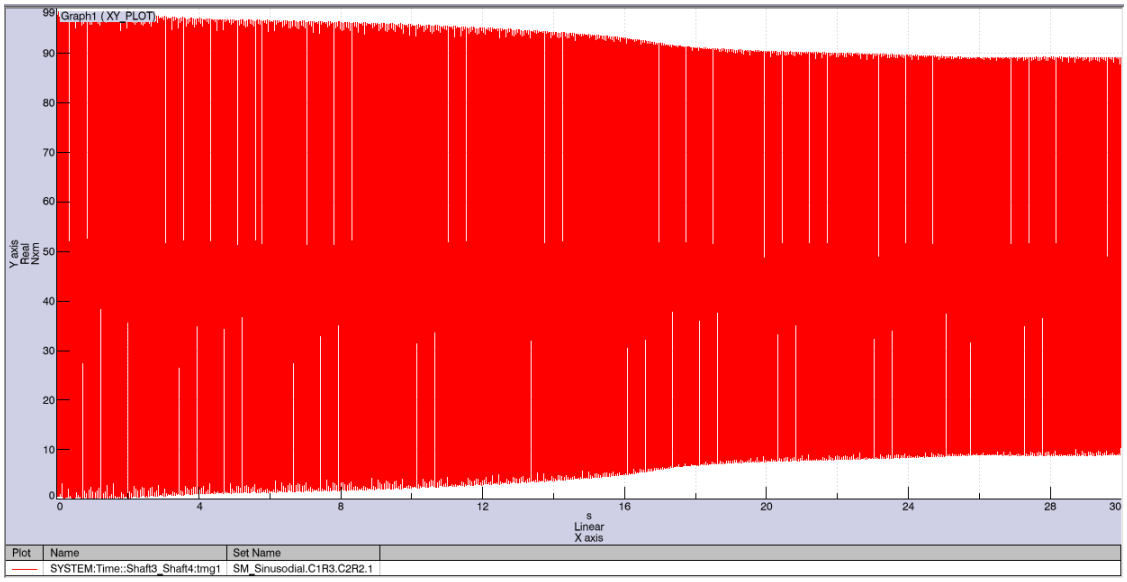

(h)

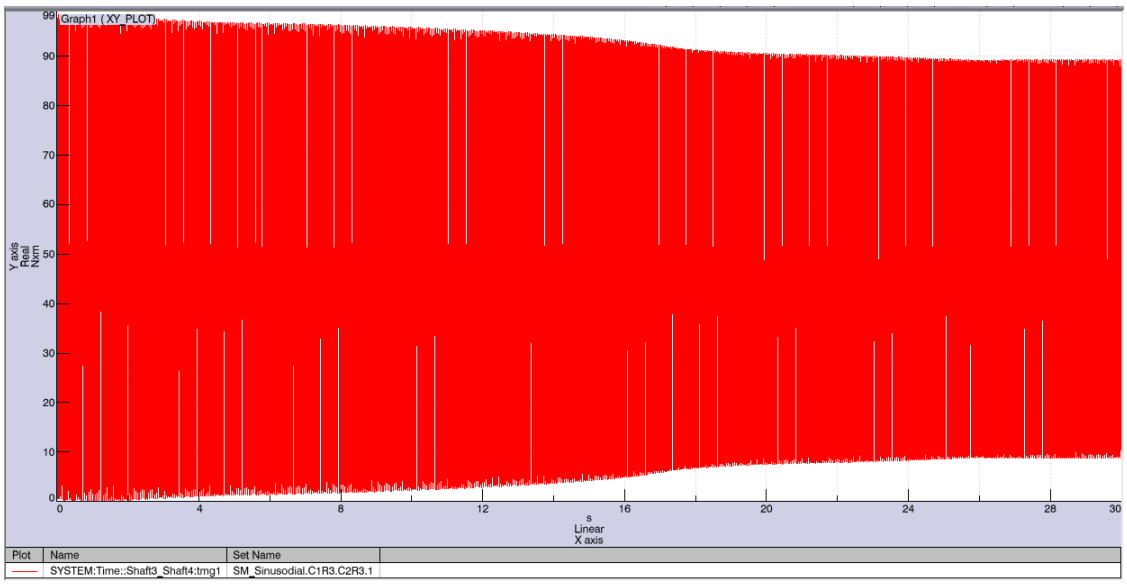

(i)

REFERENCES

Beer, F. P., Johnston, Jr. E. R., (1988) *Vector Mechanics for Engineers: Fifth Edition*. McGraw-Hill Publishing Company. New York, NY.

Bonori, G., Barbieri, M., Pellicano, F. Optimum profile modifications of spur gears by means of genetic algorithms. *Journal of Sound and Vibration*, 2008, v 313, n3-5, p 603-616.

Bosch. (2007). *Bosch Automotive handbook: Seventh Edition* (2007), Robert Bosch GmbH. Plochingen, Germany.

Burton, T., Sharpe, D., Jenkins, N., and Bossanyi, E. (2001) *Fundamentals of Wind Turbines, pp. 17, 19, 21-23, 25-27,161, 428*. John Wiley and Sons Ltd. West Sussex, England.

Cai, Y. The Linear Approximated Equation of Vibration of a Pair of Spur Gears (Theory and Experiment), pp. 15, 26, 27, 29, 273, 521-528, 1992. Ph.D. Dissertation, Precision and Intelligence Laboratory, Tokyo Institute of Technology, Tokyo, Japan, 1991.

Cai, Y., Hayashi, T. "Linear approximated equation of vibration for a pair of spur gears: theory and experiment." *American Society of Mechanical Engineers, Design Engineering Division (Publication) DE*, v 43 pt 2 , *Advancing Power Transmission into the 21st Century*.

Dudley, D. W. (1954) *Practical Gear Design*. McGraw-Hill. York, PA.

Griffiths, D. V., and Smith, I. M. (1991) *Numerical Methods for Engineers*. Blackwell Scientific Publications. Oxford, England.

Haug. E. J., (1989) *Computer-Aided Kinematics of Mechanical Systems, pp. 1, 223*-225. Allyn and Bacon. Boston, MA.

LMS International. (2010). Virtual.Lab R10 User Guide

Mucke, T., Kleinhans, D., Peinke, J. 2011 "Atmospheric turbulence and its influence on the alternating loads on wind turbines." *Wind Energy*, v. 14, (issue) 1, p. 301-316, March.

Munson, B. R., Young, D. F., and Okiishi, T. H., (2006) *Fundamentals of Fluid Mechanics: Fifth Edition.* John Wiley & Sons Inc. Jefferson City.

Musical, W., Butterfield, S., McNiff, B. May 2007. "Improving Wind Turbine Gearbox Reliability." Conference Paper, NREL/CP-500-41548.

Musical, W., McNiff, B. 2000 "Wind Turbine Testing in the NREL Dynamometer Test Bed." NREL Conference Paper, NREL/CP-500-28411, June < http://www.nrel.gov/docs/fy00osti/28411.pdf>

Ohanian, H. C., (1989) *Physics: Second Edition*. Penguin Books Canada Ltd. Markham, Ontario.

Rosenberg, Richard. 1992. Tillers International. "Animal-Driven Shaft Power Revisited."<http://www.tillersinternational.org/farming/resources_techguides/Animal-DrivenShaftPowerRevisitedTechGuide.pdf>

Schobert, H. H., (2002) *Energy and Society: An Introduction*. Tayor & Francis. New York, NY.

Shabana, A. A., (2010) *Computational Dynamics: Third Edition, pp. 1, 112*. John Wiley & Sons Ltd. West Sussex, England.

Sheinman, Y., Rosen, A. "Dynamic model of the influence of turbulence on the power output of a wind turbine". *Journal of Wind Engineering and Industrial Aerodynamics*, 1992, v 39, n 1-3, p. 329-341

Sheng, S., Oyague, F., Butterfield, S. August 2010. "Investigation of Various Wind Turbine Drive Train Condition Monitoring Techniques." Conference Paper, NREL/CP-500-46160.

Ugural, A. C., Fenster, S. K., (2003) *Advanced Strength and Applied Elasticity: Fourth Edition.* Pearson Education Inc. Castleton, New York

U.S. Department of Energy. "US DOE 20% Wind Energy by 2030." July 2008. <http://www1.eere.energy.gov/windandhydro/pdfs/41869.pdf>

U.S. Department of Energy. "Wind Powering America." 31 December 2010. <http://www.windpoweringamerica.gov/wind_installed_capacity.asp>

West Texas A&M University (WTAMU), Killgore Research Center. 2010. Alternative Energy Institute. <http://www.windenergy.org/datasites/>

Williams, R. "Solar One, to International Space Station; Move over I'm coming into Near Orbit." Engineering.com, June 6, <http://www.engineering.com/Library/ArticlesPage/tabid/85/articleType/ArticleView/articleId/704/Solar-One-to-International-Space-Station-Move-over-Im-coming-into-Near-Orbit.aspx>

Zemen J. 2009. "A V-DMAIC Case Study of a High Mobility Multipurpose Wheeled Vehicle Driving on Rough Terrain." Master's Thesis, University of Iowa, pp. 11.